Development, Implementation, and Validation of an Acoustic Emission-based Structural Health Monitoring System

Von der Fakultät für Ingenieurwissenschaften,
Abteilung Maschinenbau und Verfahrenstechnik der
Universität Duisburg-Essen
zur Erlangung des akademischen Grades

einer

Doktorin der Ingenieurwissenschaften

Dr.-Ing.

genehmigte Dissertation

von

Dorra Baccar
aus
Tunis

Gutachter: Univ.-Prof. Dr.-Ing. Dirk Söffker
Univ.-Prof. Dr.-Ing. Claus-Peter Fritzen

Tag der mündlichen Prüfung: 15. Mai 2015

Acknowledgement

Diese Arbeit ist überwiegend während meiner Zeit als Doktorandin am Lehrstuhl Steuerung, Regelung und Systemdynamik (SRS) der Universität Duisburg-Essen entstanden. An dieser Stelle möchte ich meinen besonderen Dank nachstehenden Personen entgegen bringen.

Großer Dank gebührt zuallererst Herrn Univ.-Prof. Dr.-Ing. Dirk Söffker für die Möglichkeit zur Erstellung dieser Arbeit und für alles, was ich während meiner Tätigkeit am Lehrstuhl, sowohl fachlich als auch nichtfachlich, gelernt habe. Die zahlreichen Gespräche auf intellektueller und persönlicher Ebene werden mir immer als bereichernder und konstruktiver Austausch in Erinnerung bleiben.

Der gleiche Dank gilt Herrn Prof. Dr.-Ing. Peter-Claus Fritzen von der Universität Siegen für die Übernahme des Korreferats und die interessanten Gespräche, die wir in diesem Zusammenhang geführt haben.

Besonders danken möchte ich meinen Kolleginnen und Kollegen für die immer sehr angenehme, unterhaltsame und freundschaftliche Atmosphäre, für die vielen interessanten fachlichen und nichtfachlichen Gespräche und für die gute und fruchtbare Zusammenarbeit.

Weiterhin danke ich Yvonne Vengels, Adnan Hasanovic und Herrn Kurt Thelen für die Bewältigung alltäglicher Probleme und zuvorkommende Unterstützung in verwaltungsrelevanten sowie technischen Disziplinen des Lehrstuhls.

Bei meinen Eltern Dr. Moncef Baccar und Kmar Baccar möchte ich mich ganz besonders herzlich bedanken für die uneingeschränkte, liebevolle und vielseitige Unterstützung während meines gesamten Studiums, diese haben in jeglicher Hinsicht die Grundsteine für meinen Weg gelegt.

Meinem Mann Dr. Ahmed Elhaddad danke ich von ganzem Herzen für seine unermüdliche Unterstützung, Geduld, Liebe und Motivation. Er hat mir stets zur Seite gestanden und mich motiviert, meine Dissertation zu vollenden.

Den größten Dank schulde ich meinen beiden Töchtern Hind und Khadija. Sie haben (fast immer) ihre „Fremdbetreuung“ gelassen hingenommen und mich am Computer arbeiten lassen.

Hainburg, im September 2015

Dorra Baccar

Contents

Abstract

In engineering, Structural Health Monitoring (SHM) is an important field of study representing a fundamental process to control the longevity and reliability of structures during service. The objective of an SHM is to detect and quantify the structure degradation at an earlier stage. The acquisition of such information can contribute to prevention of total failure and hence avoiding human and financial losses becomes more possible. With the growing demands for cost-efficient and robust products, SHM is facing particularly high requirements. This thesis focuses on the development, implementation, and experimental validation of an innovative SHM system able to detect, identify, and classify in an extensive way damage mechanisms occurring in different materials. Several techniques can be applied for in situ health monitoring. In this work, Acoustic Emission Technique (AET) is used. Acoustic Emission is a passive nondestructive evaluation technique referring to the elastic waves generated by energy release during microstructural changes in the material. Those changes arise as a result of mechanical and environmental stresses. Monitoring of such a conversion can be continuously done in real-time using suitable hardware and advanced signal processing methods. The performance and reliability of an AE-based damage diagnosis approach are highly dependent on material, structure design and the damage scenarios. Therefore, a Field Programmable Gate Array (FPGA)-based measurement chains developed for sensing and acquiring the generated AE signals. This chain is easily adaptable to different structures and materials. It was therefore kept so far constant as possible throughout all tests conducted. Additionally to the use of highly efficient hardware that enhance the sensing quality and the data acquisition speed, the implementation of advanced filtering techniques with high processing accuracy is of central importance. The main objective of this thesis is to prove the function of the system developed to analyze AE waves under different damage scenarios. For this purpose, three different materials namely wear resistant plates, laminated composite plates, and electrochemical cells are investigated. Owing to the diversity of the studied materials, special attention is paid to the development and implementation of multilevel signal processing approach and pattern recognition methods. The processing chains are capable to detect, quantify and qualify the AE data, whereby AE-based characteristics are identified and correlated with the corresponding AE sources. The designed diagnosis methodology concentrates/focuses on damage detection (feature extraction), damage estimation (feature selection), and damage classification by using time-frequency analysis, multilevel statistical approaches, and supervised classification methods.

The results obtained show a noticeable/remarkable enhancement of the identifica-

tion and classification of damage mechanisms. The efficiency of applying multilevel processing approach is/(could be) thus proved. The methodology presented here, allows an automated structural health monitoring. Hereby, an important step forward in future development of safe and reliable structures is represented.

Kurzfassung

Die Strukturüberwachung *eng.* Structural Health Monitoring (SHM) ist ein grundlegender Prozess für die Kontrolle der Betriebssicherheit und Zuverlässigkeit von Strukturen und Bauteilen während des Betriebs. Ein Überwachungssystem soll die Strukturdegradation in einer frühen Phase erkennen und quantifizieren, um den Totalausfall zu verhindern und somit menschliche und finanzielle Verluste zu vermeiden. Mit der wachsenden Nachfrage nach kosteneffizienten und robusten Produkten ist SHM mit besonders hohen Anforderungen konfrontiert.

Diese Arbeit befasst sich mit der Entwicklung, Implementierung und experimenteller Validierung eines innovativen SHM-Systems, das auf umfassende Weise Schädigungsmechanismen von unterschiedlichen Materialen erkennt, identifiziert und klassifiziert. Für in-situ-Strukturüberwachung können verschiedene Methoden angewendet werden. Hier wird die Schallemissionsanalyse eng. Acoustic Emission Technik (AET) eingesetzt. Acoustic Emission ist eine passive zerstörungsfreie Prüf- und Überwachungsmethode. Sie basiert auf der Analyse elastischer Wellen, die durch freigesetzte Energie während mikrostrukturelle Änderungen wie z. B. Risse, Brüche, und Verschleiß entstehen. Unter Verwendung geeigneter Hardware und fortgeschrittener Signalverarbeitungsverfahren können diese Wellen kontinuierlich und in Echtzeit erfasst und analysiert werden.

Die Leistungsfähigkeit und Zuverlässigkeit einer AE-basierten Schadensdiagnose sind stark abhängig von Material/Werkstoff, Konstruktion und möglichen Schadensszenarien. Der Fokus dieser Arbeit liegt daher auf der Entwicklung einer hocheffizienten und leicht anpassbaren Field Programmable Gate Array (FPGA)–basierten Messkette zum Abtasten und Erfassen der erzeugten AE-Signale. Neben der Verwendung von sehr leistungsfähiger Hardware ist eine zuverlässige Interpretation der AE Signale von zentraler Bedeutung. Deswegen erfordern die Entwicklung und Umsetzung von Multi-Level-Signalverarbeitungsansätzen und Mustererkennungsverfahren eine besondere Beachtung. Die experimentelle Validierung des entwickelten Systems erfolgt durch die Untersuchungen von drei verschiedenen Materialien/Strukturen: Verschleißfeste Metallbleche, Faserverbundwerkstoff Platten und elektrochemische Zelle. Aufgrund der Diversität der untersuchten Strukturen werden drei Verarbeitungsprozesse entwickelt. Die implementierten Algorithmen können AE-Signale erkennen, quantifizieren und qualifizieren, so dass AE-basierte Eigenschaften identifiziert und mit den entsprechenden AE-Quellen korreliert sind. Die Diagnose konzentriert sich hauptsächlich auf die Schadenserkennung (Merkmalsextraktion), Schadensabschätzung (Merkmalsauswahl) und Schadensklassifizierung unter Anwen-

dung von Zeit-Frequenz-Analyse, statistischen Ansätzen und überwachten Klassifikationsverfahren. Die gewonnenen Ergebnisse zeigen eine bemerkbare Verbesserung der Identifizierung und Klassifizierung von Schadensmechanismen und beweisen die Effizienz des angewandten Multi-Level-Verarbeitungsansätze. Die vorgestellte Methodik ermöglicht eine automatisierte Zustandsüberwachung und stellt daher einen wichtigen Schritt in der Entwicklung von sicheren und zuverlässigen Strukturen dar.

List of Figures

List of Tables

List of Acronyms

AE	Acoustic Emission
AET	Acoustic Emission Technique
ANN	Artificial Neural Network
ASNT	American Society For Nondestructive Testing
BPNN	Back Propagation Neural Networks
CC	Coulomb Counting
CFRP	Carbon Fiber Rreinforced Polymer
CWT	Continuous Wavelet Transform
DCB	Double-Cantilever Beam
DFT	Discrete Fourier Transform
DSP	Digital Signal Processing
DWT	Discrete Wavelet Transform
FCM	Fuzzy C-mean
FFT	Fast Fourier Transform
FPGA	Field Programmable Gate Array
FRP	Fiber Reinforced Polymer
GFRP	Glass Fiber-Reinforced Polymer
HDL	Hardware Description Language
HHT	Hilbert Huang Transform
KDE	Kernel Density Estimation
KF	Kalman Filter
LUTs	Look-up tables
MAE	Modal Acoustic Emission
NDE	Non Destructive Evaluation
NDT	Non Destructive Testing
OCV	Open Circuit Voltage
PCA	Principal Component Analysis
PCs	Principal Components
PSD	Power Spectral Density
SEI	Solid Electrolyte Interface
SHM	Structural Health Monitoring
SoC	State of Charge
SoH	State of Health
SOM	Self-organizing Map

STFT	Short Time Fourier Transform
SVM	Support Vector Machine
VHDL	Very High Speed HDL
WT	Wavelet Transform
XSG	Xilinx System Generator

1 Introduction

In children's animated series, speaking vehicles, airplanes, and machines can easily express their suffering from breakage or fatigue. Accordingly, they can determine whether they can still be used or taken out of service because they have reached the end of their lifetime. Over many years, this topic has been researched intensively and still one of the most important focus areas in aerospace, civil, and mechanical engineering. Also with regard to industrial investors, it attracts a lot of attention since it first and foremost concerns human safety. Using today's available technologies, monitoring the integrity of a structure in real-time and an autonomous permanent way during its use is approaching reality through the integration of advanced diagnosis and prognosis approaches.

All structures undergo degradation of their mechanical properties during service or even at rest. Indeed, a material crack of only a few micrometers can contribute to a reduction of the performance and can lead to complete system failure causing economic loss and sometimes personal injury. Therefore, the development of reliable techniques for online damage monitoring represents an indisputable interest for more and more researcher and is of increasing demand reflecting an enhanced awareness of the importance of early-stage damage diagnosis. Such systems have to satisfy the maintenance requirements related to product quality over time.

The majority of complex systems need to be maintained at regular time intervals for safety and environmental reasons. Maintenance frequency depends on many factors such as application field, probability of defects, structure complexity, material, and age of structure. How and when the structure has to be inspected is generally determined by the manufacturer. Here, experience plays a decisive role. However, maintenance and inspection are, usually, associated with downtime and resulting in high costs and labor requirement. Therefore, during the last years, many maintenance methods based on Non-Destructive Testing and Evaluation (NDT/NDE) have been developed aiming to save costs and time and most importantly to ensure user safety.

Non-Destructive Testing methods are applied for in-service damage inspections in order to evaluate the structural integrity without destroying it. Non-Destructive Testing includes all methods of detecting and evaluating defects in materials. The most applied NDT methods are visual inspection, radiography, eddy current, ultrasonic, penetrant testing, magnetic particle, vibration monitoring techniques, and Acoustic Emission (AE). However, using conventional NDE, the system or device has to be taken out of service. In addition, in the case of radiography, it is necessary

to disassemble the structure, to have direct access to components out of reach without making sure of the presence of damage. Moreover, visual inspection, which is the oldest and most common inspection method, is time consuming, expensive, and very often limited when dealing with the detection and characterization of damage that could compromise the integrity and reliability of complex structures. Recent years have shown an increasing use of Acoustic Emission to overcome the constraints of traditional NDT methods. Based on sensor technology, AE allows continuous monitoring of large parts of structure, such as bridges and aircraft components, in real time. In fact, NDT focuses mainly on the equipment. Technology integrating NDT, diagnostic and prognostic approaches is called (SHM). Using SHM, structural reliability can be maintained over the service life without increasing the maintenance costs [Bal06]. Hence, maintenance strategy can be improved and changed from Planned Maintenance (maintenance timing and tasks are scheduled [NL10]) to Condition-based Maintenance (assets health condition is continuously monitored in order to perform maintenance only when it is necessary [Tsa95]). Subsequently, downtime due to inspection can be kept to a minimum and thereby, maintenance costs can potentially be reduced.

In order to contribute to a common understanding of relevant terms related to SHM, the definitions of the most important terms are given as follow:

Health monitoring: "The scientific process of non-destructively identifying characteristics related to the fitness of an engineered component (or system as it operates)," [Ada07].

Damage: "Changes to the material and/or geometric properties of a system, including changes to the boundary conditions and system connectivity, which adversely affect the current or future performance of these systems," [FW07].

Failure: "The termination of the ability of a component or system to perform a required function," [VDE94].

Maintenance: "The combination of all technical and corresponding administrative actions intended to retain an item in, or restore it to, a state in which it can perform its required function," [VDE94].

Reliability: "The ability of a component or system to perform required functions under stated conditions for a stated period of time," [VDE94].

Safety: "The absence of conditions that can cause death, injury, occupational illness, or damage to or loss of equipment or property, or damage to the environment," [VDE94].

Damage diagnosis: "The process of identifying damage in structural material and systems," [Ada07].

Damage prognosis: "The process of predicting the future probable capability of a structure, material, or system in an online manner, taking into account the effects of damage accumulation and estimated future loading," [Ada07].

1.1 Motivation for Structural Health Monitoring

Structural health monitoring refers to the process of real-time monitoring of the actual state of a structure during operation. Over the years, many definitions have been attributed to SHM. In [HBC+97] SHM is defined as “the use of in-situ, nondestructive sensing and analysis of structural characteristics, including the structural response, for detecting changes that may indicate damage or degradation”. While NASA describes it as "the operational capability of a system to contain, prevent, detect, diagnose, respond to, and recover from conditions that may interfere with nominal mission operations" [JGK+11].

The main objective of SHM is to ensure the health of structures, extend lifetime, anticipate failure, enhance performance, and guarantee safety while reducing maintenance costs. Accordingly, SHM involves economic, commercial and safety aspects. Structural health monitoring approach is the interaction of a set of processes and control strategies aiming to monitor continuously or periodically the integrity of a structure by detecting cracks or defects. In addition to NDT methods, SHM technology involves sensor networks and signal processing systems. Hence, development of reliable and robust SHM system requires extended knowledge and understanding of materials science, structural mechanics, sensor technology, embedded electronics, and signal processing [SUS13].

Depending on the embedded NDE and sensor system, SHM can be applied as global method as well as local method. Furthermore, SHM systems provide two approaches allowing the continuous assessment of the state of health of structures, namely passive methods and active methods. Active approaches involve the use of actuators or piezoelectric wafer active sensors (PWAS). These approaches require knowledge of the physical properties of the material as well as the different phenomena related to wave propagation characteristics in material [SUS13]. These methods are in an early stage of development and are strongly influenced by environmental and operational conditions such as temperature, pressure, humidity, and structural boundaries. In contrast, passive approaches are based on sensing the structure dynamic response to mechanical and environmental stress applied in service. The detected possible waves or vibration could be interpreted as caused by the damage [RBMK14]. Under mechanical, thermal, or chemical load, materials emit energy in the form of high frequent mechanical vibration. These emissions propagate throughout the surface of the material and are detected by very sensitive sensors. Acoustic Emission is the most commonly used passive method and is one of the few SHM approaches having a successful industrial application in aircraft.

Industrial applications of SHM are include mainly the sectors of civil engineering (bridges and dams), machinery, energy (oil and gas pipelines, wind turbines), and aeronautics. However, effective SHM applications to in-service structure are still limited. Structural integrity assessment and continuous health monitoring of metallic and composite structures represent the most important concerns in structural engineering.

In summary, SHM systems have greatly improved the maintenance of innovative and complex structures. Using SHM, enormous benefits regarding safety, costs, and structure design aspects could be gained [Ada07, Sta02].

1.2 Scope and Objectives of the Thesis

Growing demands for cost-efficient and environment-friendly products have led to a relatively widespread implementation of newly developed materials, components, and devices that possess better properties fulfilling customer specific requirements.

A good example is composite material, which, due to its particular properties, is becoming more and more attractive for aerospace applications. Within a few years, its usage rate in new civil aircraft has exceeded 50% allowing the production of lightweight structures and thereby reducing fuel consume and emissions. For the same goals, the urban transport sector has shown an increasing development through integration of electrochemical components in vehicles. In 2013, the percentage of electrified vehicles compared to all vehicles has reached 6% in some European countries (Norway) [VTFF14]. Nevertheless, the history of operation of these components is unknown, and damage scenarios are complex and cannot be detected with traditional inspection methods. Additionally, the severity of damage effects on performance and lifetime cannot be accurately predicted yet. Therefore, in order to guarantee safety and reliability of these newly designed devices, new generation of SHM systems is needed [Ada07].

Typical SHM systems comprise a measurement chain and a signal processing chain. A measurement chain, including sensors, instrumentation, and data acquisition systems, depends on the NDT method. Whereas a signal processing chain includes several filtering techniques and algorithms used for damage diagnosis and prognosis. Accordingly, to develop robust and efficient SHM systems, appropriate NDT technique should be selected. Furthermore, in order to ameliorate the sensing quality and the processing accuracy, both chains have to be improved regarding high-performance/high-speed hardware and suitable signal processing tools.

The main objective of this thesis is to develop, implement, and evaluate an Acoustic Emission-based SHM system and to prove its effectiveness when dealing with detection, identification, and classification of damage dependently of the material/component to be monitored. This will be demonstrated based on three different applications.

This thesis is essentially focused on the analysis of AE waves and resulting diagnosis. For this purpose, different test rigs were used, series of tests were carried out, and signal processing techniques, as well as pattern recognition approaches, were developed and implemented. It will be demonstrated that through the integration of high-speed electronic devices, continuous and real-time damage identification can

be realized. In addition, it will be shown that acquisition, processing, and interpretation of data are the core of an SHM system determining its efficiency and reliability.

The main objectives and research activities of this thesis are as follows:

- Building a solid knowledge base of AE technique and understanding the fundamental mechanisms generating AE waves in wear resistant plates, Carbon Fiber-Reinforced Polymer (CFRP)-based structure, and lithium-based batteries.
- Enhancement and development of measurement chain by implementing several filtering techniques in Field Programmable Gate Array (FPGA) board.
- Testing the newly realized hardware with respect to real time processing of AE signals
- Development and experimental validation of reliable and efficient AE-based condition monitoring system for online detection and automated classification of wear state of interacting metal surfaces in relative motion
- Development and experimental validation of frequency-based procedure for identification, characterization, and classification of damage occurring in CFRP laminate during indentation tests by means of AE and advanced signal processing approaches
- Invention of AE-based methodology to monitor the actual State of Health (SoH) of lithium-based batteries

1.3 Thesis Outline

In Chapter 2, the theory and the principle of Acoustic Emission including AE wave propagation and AE data analysis are presented. This chapter is divided into three main parts. First, a brief introduction to wear mechanisms is given, followed by a comprehensive literature review on AE examination of wear resistant plates. The second part begins with a short overview of composite materials and their failure modes. Subsequently, an extensive literature review dealing with AE application for damage identification and characterization in CFRP plates focusing on the used signal processing and pattern recognition approaches is provided. In the third part, the main aging mechanisms in lithium-based batteries and the available methods for estimation of state of health and state of charge are introduced.

In Chapter 3, the development process of AE based SHM system is depicted. Based on a generalized description of SHM strategy, the general concept is explained. Measurement chain including sensor and FPGA-based data acquisition system and signal processing chain comprising theory and design of advanced filtering techniques developed for damage detection are presented. Special attention is paid to the

performance of FPGA-board, which is illustrated by design and implementation of filtering modules that allow an online analysis of AE data.

In Chapter 4, the work described in [Det11] is extended and an application of the developed SHM system to tribological system is presented. Beginning with the presentation of the test rig used and experimental setup, this chapter presents a methodology based on different time-frequency analyses for examination and classification of AE data. The developed approach describes quantitatively and qualitatively the wear progression process by establishing a direct correlation between the state-of-wear and the measured AE data.

In Chapter 5, AE monitoring of CFRP structures is investigated. First, the experimental apparatus including specimen properties are introduced. Next the developed multilevel processing approach combining time-frequency analysis, multivariate statistical analysis, and classification procedure is presented. Furthermore, a study of waveform and frequency content of AE signals generated in CFRP subjected to indentation tests is presented and compared with fundamental assumptions reported in this field. Subsequently, experimental results are discussed focusing on advantages of the multilevel processing approach when leading with failure mode identification and classification.

In Chapter 6, a brand new technology namely AE monitoring of lithium-polymer batteries is introduced. The measurement chain and the signal processing strategy detailed in Chapter 4 are used for online battery diagnostic. Results of the estimation of deterioration level and its automated classification are highlighted, and benefits gained from this new methodology are discussed.

In Chapter 7, the research results are summarized, the main contributions to the current state of the art are presented, and recommendations for future works are given.

2 Literature Review and Theoretical Background

This chapter provides an overview of Acoustic Emission (AE), and a detailed literature review of experimental results obtained using the AE Technique (AET) for damage identification in different materials.

In the first section, theoretical background and principle of AET are introduced. Here, special attention is given to wave propagation and AE data analysis. In Section 2.2, AE examination of sliding wear, starting with an introduction to wear mechanisms, is discussed. Then, previous works to date of AE monitoring of sliding contact with focus on relationship between sliding wear and AE are reviewed and implications for this study are discussed. In section 2.3 the basic theories of Fiber Reinforced Polymer (FRP) composites are presented along with a description of the different damage mechanisms. Furthermore, an extended review on the use of AET to identify failure modes in FRP is provided. In addition, the relevance of review findings to this work is discussed. Finally, section 2.4 introduces the application of AET to electrochemical cells focusing on lithium-based batteries and highlights the challenges of this new application field.

2.1 Acoustic Emission Technique

A large number of studies have been conducted on the use of NDT to identify and discriminate damage and failures in a structure. Nondestructive testing methods "examine a part, material, or system without impairing its future usefulness" [MHM05]. These include vibration techniques, eddy current testing, ultrasonic, radiographic, magnetic testing, and Acoustic Emission. Since the seventies Acoustic Emission is classified as NDT method and has been considered as the prime approach for the detection, micro-structural characterization, and monitoring of damage processes [SBWDM00].

Acoustic Emission is defined in American Society of Testing and Materials Terminology for Nondestructive Examinations [AST90], as

"the class of phenomena whereby transient elastic waves are generated by the rapid release of energy from localized sources within a material."

Compared to other NDT methods, AET is usually realized during loading while most other methods are applied before or after the loading of the structure. Acoustic Emission Technique is classified as passive NDT because it is performed by the energy released by the object and does not require an artificial excitation. Another advantage of the AET is that the dynamic processes or changes, in a material can continuously be monitored in real-time using suitable hardware [Val02]. Acoustic Emission Technique also has the ability to determine the location of damage source. These benefits make AET one of the most appropriate NDT methods for *in-situ* health monitoring applications and especially when it is related to examination of dynamic failures [FLK$^+$03].

Nondestructive Testing includes all methods of detecting and evaluating defects in materials. Nondestructive evaluation is important in operation reliability and in quality control. It is widely applied in diagnosis and prognosis.

Under mechanical, thermal, or chemical load, materials emit energy in the form of high frequent mechanical vibration. These emissions propagate throughout the surface of the material as Rayleigh waves with frequency bandwidth in the range 100 kHz to 1 MHz [EM08]. These waves can be detected with very sensitive AE sensor. The sensor converts the released energy into electrical signal, which is transferred to electronic equipment for further processing. A graphical illustration of the basic principle of AET is shown in Fig. 2.1. Acoustic Emission is caused by sudden structural changes which are due to different mechanisms of deformation and fracture such as cracking, plastic deformation, and wear. These mechanisms also include phase transformations, boiling, and electrical discharges [MP99]. In composites, AE is affected by matrix cracking, fiber breakage, and debonding. The AE vibration is called AE activity and it depends on type and properties of the material [MHM05]. With rapid developments in computational, data processing capabilities, and smart sensors, the application field of AET has seen an increase and involves many materials such as metals, ceramics, polymers, composites, wood, concrete, and geologic materials. Various successful applications of AET were observed in laboratory testing of small structures. Nevertheless, actual industrial applications of AET are restricted to pressure vessel and pipelines.

2.1.1 Historical Background

The Acoustic Emission Technique has long been known in its audible form. The earliest AE practical use is associated with pottery. Quality of ceramics was assessed based on the sound produced by vessels cooling [Shu02]. Around 3,700 BC, tin smelters in Asia Minor made first observations of Acoustic Emission in metals during mechanical twinning of pure tin. The audible emissions were caused by plastic deformation and are known as “tin cry” [MHM05]. According to [MHM05], the

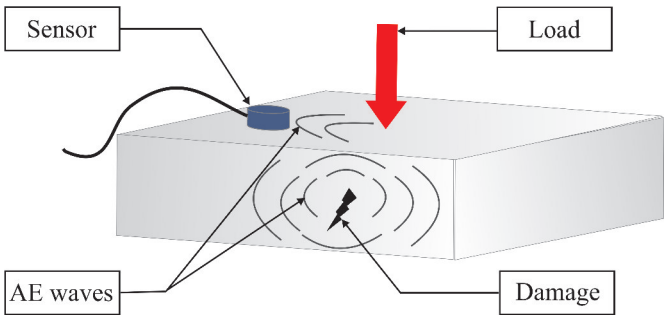

Figure 2.1: Basic principle of Acoustic Emission Technique

Arab alchemist Geber was the first documenting AE observations in the 8th century. Geber reported that during forging, tin emits a louder, cracking sound than iron. Around 1820, Brunel had observed that workers, during tunnel construction work, chose larch wood planks for ceiling support because they give a clearly audible (warning) signal before failure [DC84]. However, electronic transducers were used for the first time in the thirties to study AE. The first scientific contribution of AE instrumentation was carried out by the seismologist Kishinouye in 1933. Here, the generated AE during wood breaking were examined [GO08]. In 1936 in Germany, Forster and Scheil conducted the first experiments by means of piezoelectric sensors for the detection of AE caused by martensitic transformations in steel [SAS03]. In 1950, Josef Kaiser published an early study concerning AE data interpretation. In his work titled "Results and Conclusions from Measurements of Sound in Metallic Materials under Tensile Stress", Kaiser investigated AE and the noise levels generated from various metals subjected to tensile load [Kai50]. Two effects of particular importance in AE application were discovered. The first observation is that all materials tested under load emit AE [Ten04]. The second observation is the phenomena of irreversibility that is nowadays known as Kaiser Effect. This effect is defined as "absence of detectable Acoustic Emission until the previous maximum applied, stress level has been exceeded" (ASNT 1987). The Kaiser Effect reveals information about the previous maximum applied load and has been used to determine a relationship between AE activity and stress-strain curve. Thus began the modern application of AE.

2.1.2 Wave Propagation

Acoustic Emission waves are elastic stress waves propagating in materials in various modes. Acoustic Emission waves are strongly dependent on the nature and geometry of the medium and are affected by numerous factors. The main effects that influence the AE wave propagation include attenuation, propagation velocities, dispersion, diffraction, and reflection [Shu02]. The wave velocity is often used to determine AE source location and depends on wave types, material properties (isotropic or anisotropic), and frequency (in case of guided waves).

Different wave propagation modes are identified when AE travels from source to sensor through the material. In following a short overview of the three main modes is introduced.

Bulk (body) waves: These waves occur in homogeneous, isotropic solids; they travel inside the structure as longitudinal or shear waves. In longitudinal waves (P-waves), the particle displacement occurs in the direction of the wave propagation while in shear waves (S-waves) the particle displacement occurs transverse (perpendicular) to the direction of the wave propagation [Har05]. The longitudinal wave travels with a higher velocity and consequently, it is chronologically the first measured AE signal. The velocities of P- and S-waves are defined as [Pie89]

$$\upsilon_l = \sqrt{\frac{\lambda + 2\mu}{\rho}} \tag{2.1}$$

and

$$\upsilon_s = \sqrt{\frac{\mu}{\rho}}, \tag{2.2}$$

where ρ denotes the material density, λ and μ the elastic constants.

Rayleigh (surface) waves: This type of waves is generated by the reflection of bulk mode at the material surface. The particle's displacement of Rayleigh wave is elliptical, normal to the surface, and parallel to the direction of the wave propagation. Rayleigh waves travel along the surface with an amplitude less than that of bulk waves that decreases with depth. The velocity of surface waves is slightly smaller than that of S-waves and is given by

$$\upsilon_R = \upsilon_s \left(\frac{0.87 + 1.12\nu}{1 + \nu} \right). \tag{2.3}$$

Lamb (plate) waves: Lamb waves are probably the most commonly used guided waves. This type of waves occurs in double bounded medium that have two parallel surfaces, e.g. laminated composites, when the thickness of the plate is negligible in comparison to the wavelength. Lamb waves travel parallel to the surface in two fundamental modes, namely extensional/symmetric mode and flexural/antisymmetric mode. The number of propagation modes increases with increasing frequency. In symmetric modes ($S_0, S_1, \ldots$), particles are characterized by a large in–plane displacement while in antisymmetric modes ($A_0, A_1 \ldots$) the large particles displacement is out-of-plane [LX01]. Generally, extensional modes travel faster and are less (or not) dispersive than flexural mode. The velocities of Lamb waves depend on the

plate thickness and oscillation frequency and are defined as [Ach73]

$$v_e = \sqrt{\frac{E}{\rho(1-\nu^2)}} \tag{2.4}$$

and

$$v_f = \sqrt{\omega\sqrt{\frac{D}{\rho h}}}, \tag{2.5}$$

where D denotes the plate bending stiffness and h the plate thickness.

Based on plate wave theory and on the fact that the different modes involve different frequency components, Gorman and Prosser [GP91] introduced in 1991 the Modal Acoustic Emission (MAE) technique also known as waveform analysis. Extensional mode and flexural mode were investigated with respect to shape, frequency, and energy. Since, MAE is considered as a promising method that offers a better theoretical background of AE.

Lamb waves method has been successfully used, as active method, for damage diagnosis and especially for source location since it has been found that the propagating waves already interact with very small structural damage.

Wave types

Two main types of Acoustic Emission are usually observed. They depend on the nature of energy released. Burst or transient AE signals are individual discrete micro-mechanical events well separated in time [Rao13]. They can clearly be distinguished from noise. Burst signals are characterized by short duration and high amplitude noticeably larger than the background [GO08, Rao13]. Transient AE are caused by phase transformations, crack initiation and propagation in a brittle material [GO08]. Continuous AE signals are closely spaced in time characterized by low amplitude and appear on initial observation similar to electronic noise. Continuous signals are time-overlapped signals caused by plastic deformation, diffusion, and controlled phase transformations [KKB$^+$09]. A continuous AE signal can be defined as "one in which the average time between emissions of similar amplitude is less than the duration of the emission" [MSS02].

2.1.3 Acoustic Emission Data Analysis

Since the first application of Acoustic Emission technique, it has been proved that AE activity is directly related to damage. Consequently, many studies have been

carried out with the aim to find the best method that provides most useful information, which leads to accurate damage identification and classification. In general, three approaches are used to analyze the AE signals received from the transducer.

Parameter-based analysis

The parameter-based method is based on extraction of significant certain time-domain-based parameters and waveform features from one isolated and separated AE hit. Using this method, the signal stored in a "distorted version of the source waveform" is compared to a threshold. The threshold is positive predefined in function of the background noise and can be fixed or floating [Unn08]. If the signal exceeds the threshold, a hit is detected. Parameters characterizing a single AE hit are illustrated in Fig. 2.2. These parameters are defined by [AST90] as

- Event: local material change giving rise to Acoustic Emission. Event rate is the number of events/hits per time.
- Signal amplitude: absolute value of peak voltage of the waveform of one or more AE events given by

$$A[dB] = 20\log(\frac{V}{V_{ref}}). \tag{2.6}$$

  Generally, V_{ref} is chosen equal to $1\mu V$, referred to the voltage generated by $1mbar$ pressure on the sensor's surface. This parameter is a term of interest because it is closely associated with the magnitude of the AE source [GO08].
- Arrival time: time of the first threshold crossing.
- Rise time: time interval between first threshold crossing and the peak amplitude.
- Count: number of times a hit crosses the threshold.
- Duration: time difference between first and last threshold crossing.
- Energy: integral of the squared amplitude over the duration of the AE hit. The energy, like the amplitude, is considered as an important parameter that provides information about the strength of the AE source.

Typically, a single parameter is used for damage identification in composite materials. In many cases, the amplitude is correlated to the damage severity by attributing specific amplitude ranges to different damage mechanisms. However, the amplitude is strongly affected by the attenuation. Signals close to the sensor are more intensive than those located further away. It was also observed that frequencies situated some kilohertz apart the resonance frequency of the transducer are transmitted differently [Unn08]. Consequently, it is accepted that one parameter, such as amplitude or hits count, does not convey the requisite information about the AE source.

This problem leads many researchers to study various parameters simultaneous (multivariate analysis) and /or to perform a correlation analysis by plotting one parameter as a function of another [Unn08]. The use of the multiparameter analysis has been highly improved due to the rapid development of signal processing tools. Generally, the method is used in combination with statistical approaches such as Principal Component Analysis (PCA), k-mean, or Artificial Neural Network (ANN) in order to obtain clusters of signals with similar properties.

Other investigations have showed that, when the study is related to the fatigue behavior of materials, it is more useful to use the cumulative counts distribution, cumulative amplitude distribution, and cumulative energy distribution [HCP87]. In conclusion, the parameter-based analysis can determine the damage evolution and distinguish between different failure modes.

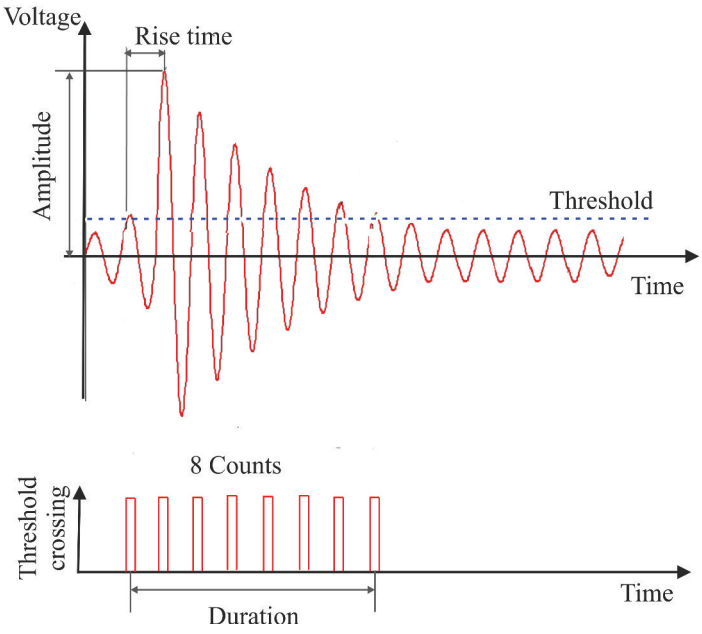

Figure 2.2: Illustration of commonly used AE parameters

(Time-)frequency- analysis

Frequency-based analysis involves features extracted from AE signal in frequency domain. Frequency-based features include power spectrum, peak frequency, dominant frequency band, frequency centroid, and energy defined as the area under the energy density spectrum [CV05]. The frequency spectrum is most often calculated using Fast Fourier Transform (FFT); FFT decomposes the signal into harmonic waves of different frequencies which can be assigned to specific damage mechanisms. However, the FFT results provide information about frequencies contained in the signal only and do not reveal how they change with time. Since the AE signal is

mainly non-stationary transient waves, time-frequency methods are applied to analyze both frequency and time-varying behavior. The most used methods for this purpose are Short Time Fourier Transform (STFT), Wavelet Transform (WT), and Hilbert Huang Transform (HHT). Using time-frequency methods more accurate failure mode identification, qualitative distinction between different damage states, and enhanced noise discrimination could be achieved [Pro02].

Modal analysis

Modal analysis, also called waveform analysis, is a quantitative method that takes into consideration the shape and the propagation modes generated by AE source [SBWDM00]. To use this technique, the AE signal has to be stored in its source waveform. This offers a large number of possibilities in which the signal has to be processed in a way to extract the most relevant information about the damage mechanisms. The modal analysis consists of studying the flexural and the extensional modes with respect to amplitude, frequency, and duration ratio [BB06]. An example of AE waveform illustrating the extensional and the flexural modes is depicted in Fig. 2.3. In the last years, the modal analysis has proved to be capable of distinguishing between different damage failures and has known an increasing success when leading with AE source location [ZG91, SW99].

An extensive literature review on the use of the above mentioned AE analysis methods, with a focus on the advantages and drawback of each method, for metallic as well as composite structure is given in the next two sections respectively.

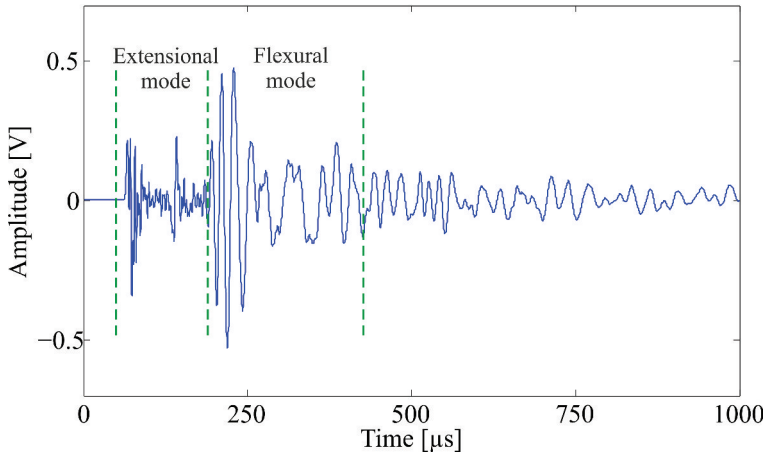

Figure 2.3: AE waveform illustrating the extensional mode and the flexural mode

2.2 Signal Processing for Damage Detection

In this section, theoretical background and definition of the signal processing techniques used in this thesis to analyze AE signals are introduced. In addition, statistical approaches applied for clustering of AE data measured during tests on CFRP are proposed. Subsequently, an approach used for automated classification of identified failure modes is described. A detailed description of the signal processing chains utilized in each experiment will be introduced later.

2.2.1 Signal Processing Techniques

To detect, assess, and classify damage using AET, AE signals need to be processed by means of appropriate processing methods. Over the years and with the rapid development of Digital Signal Processing (DSP) hardware, many techniques including time-frequency analysis, clustering, pattern recognition, statistical approaches, and classification approaches have been developed in order to build a new generation of monitoring systems, able to identify, evaluate, and classify the damage automatically. In the cases studied in this thesis, such systems should contain following processing steps:

- Pre-processing of measured AE data (denoising)
- Feature extraction (damage detection)
- Feature selection (damage identification / severity estimation)
- Pattern recognition / clustering (distinction between different types of damage)
- Classification (automated classification of damage)

An overview of general steps used for processing of AE signals and the commonly signal processing tools used for damage identification and classification are shown in Fig. 2.4 respectively.

Time-frequency analysis

In general, Fast Fourier Transform is the most applied frequency-analysis method in engineering. It decomposes a signal into single harmonic sinusoid functions and transforms it from time domain into frequency domain. The FFT reveals information about the frequency content of the signal, information about time of occurrence of this content are lost; this limits the application of FFT to stationary and periodic signals [GDSK03].

The recorded AE signals are non-stationary and appear as transient signals with undefined waveform. According to [LHL$^+$12], the meaningful AE characteristics, occurring due to instantaneously physical character, vary in time and frequency. Hence, it is highly useful to extract information about the spectral components

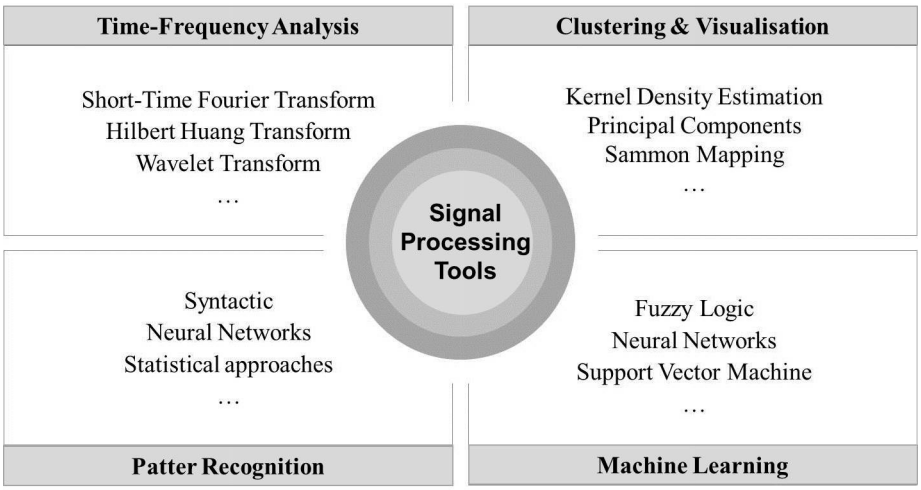

Figure 2.4: Signal processing tools

contained in the signal and assign them to specific points in time. A representation in which the signal components are plotted both over time and over frequency is needed. The Fourier Transform does not solve this problem because it does not use the time related information.

To overcome this limitation, analysis providing the possibility to evaluate the time-variant character of the frequency components and allowing a 3D representation should be applied. The time-frequency analysis methods commonly used to study AE signals are STFT, Continuous Wavelet Transform (CWT), Discrete Wavelet Transform (DWT), and Hilbert Huang Transform (HHT). Here the focus is on STFT and CWT, which are applied, depending on the experiment, separately or in combination. In the processing steps of AE signals, STFT and CWT are used as feature extraction methods allowing the detection of specific frequencies related to different damages and failure modes.

Short-Time Fourier Transform (STFT)

The Short-Time Fourier Transform is the classical method of time-frequency analysis approach. The principle of STFT is to multiply a signal $x(t)$ by a window function $g(t-\tau)$ and then to calculate the FFT of the windowed signal. Afterward, the sliding window moves along the time axis, and the procedure is repeated until the end of the signal. Mathematically, the STFT is described by [GY10]

$$STFT(\tau, f) = \int x(t)g(t-\tau)e^{j2\pi ft}dt. \tag{2.7}$$

Over the last years, many types of window functions were developed such as Gaussian, Hamming, and Hanning windows. The width of the window in which the signal

is assumed to be stationary has a major influence on the quality of the resolution. The use of a large window ensures high frequency resolution and low time resolution and vice versa. To study AE signals, a good frequency resolution is required. Consequently, broad analysis window is often used [Coh92]. A judicious choice of the window width needs a priori knowledge of the signal to be analyzed. The window function must be fixed at the beginning of the analysis and is still constant for all frequencies. The major limitation of this method for the analysis of non-stationary signals is substantially achieved [Hog07].

The influence of the width of the window on STFT results is depicted in Fig. 2.5.

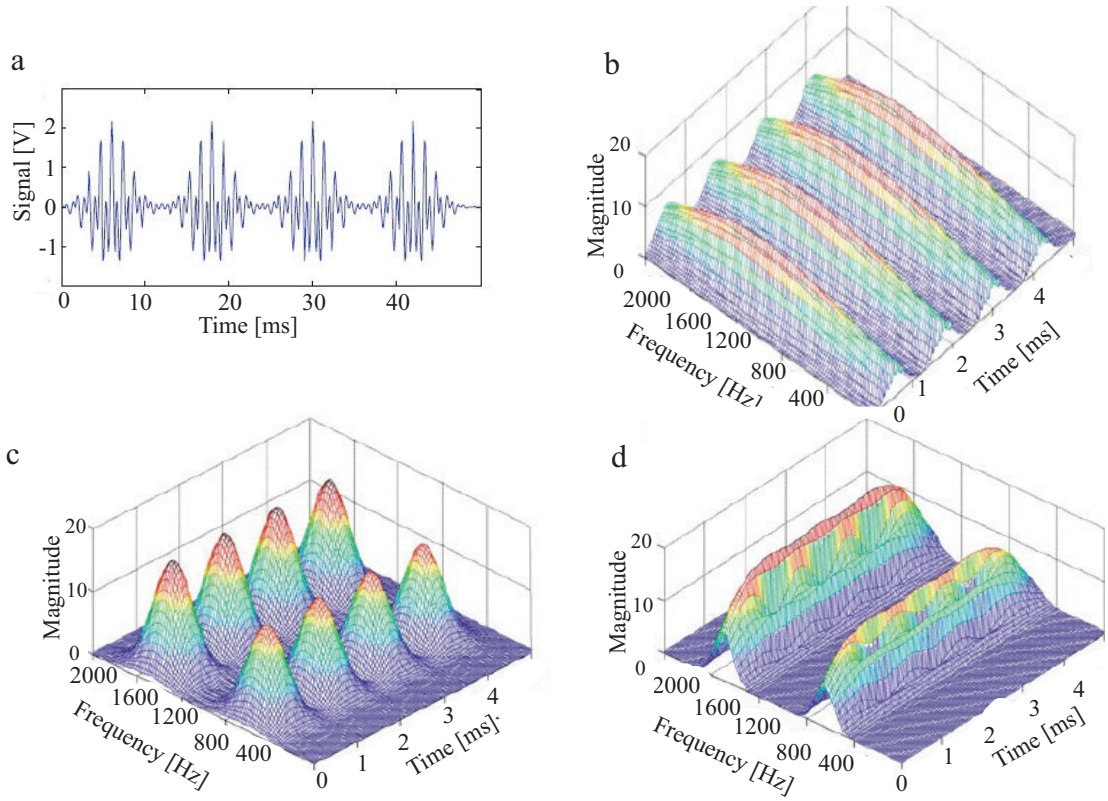

Figure 2.5: Short-Time Fourier Transform result of a non stationary signal (a) using three different window sizes. (b) Window size 1.6 ms, (c) window size 25.6 ms, and (d) window size 6.4 ms *[GY10]*

Short-Time Fourier Transform provides information about the specific frequency characteristics of the occurring events and allows a representation in the time-frequency domain [Lee13]. This information is, therefore, limited in precision when the size of the selected window does not correspond to the changing of these signals.

In addition to STFT, WT has been used for analysis of transient AE signals. Compared to FFT that deals with sinusoidal functions of infinite duration, WT uses wavelets of limited duration as basic functions [Mal08]. Wavelet transform provides suitable time-frequency localized information, which is analyzed simultaneously with

high resolution at different frequency ranges [Add10]. The superiority of the wavelets is more denotative in the case of non-stationary measurements, sudden changes in time direction, discontinuities in higher derivatives, and breakdown points [SIA09]. Wavelet transform (WT) is also applied to compress or denoising a signal without noticeable attenuation [ABSC11]. In the last years, WT was widely used in field of fault detection and identification. The majority of studies carried out within the last decade concerning Acoustic Emission and time-frequency analysis involved the wavelet transform in its several form [BTI+11, QBHK97, KFO10].

Continuous Wavelet Transform (CWT)

The Continuous Wavelet Transform (CWT) is defined as

"*the sum over all time of the signal multiplied by scaled, shifted versions of the wavelet function*" [DS14].

The CWT is a time-frequency representation of a time series using wavelets as basis function. The application of CWT involves the detection of hidden transients and short-time events, multi-resolution features extraction, and data compression. During the last decade, CWT has been widely used in field of AE analysis particularly since it is applied in the field of multi-resolution features extraction and also as pattern recognition approach.

To implement CWT a mother wavelet $\psi(t) \in L^2(\mathbb{R})$ with a zero average and an effectively limited duration is required. According to [Tan00], the mother wavelet $\psi(t)$ must satisfy the following properties:

- The function integrates to zero

$$\int_{-\infty}^{\infty} \psi(t)\, dt = 0, \tag{2.8}$$

- The Fourier Transform $\psi(\omega)$ satisfies the admissibility condition as

$$\int_{-\infty}^{\infty} \frac{|\psi(\omega)|^2}{\omega} d\omega < \infty. \tag{2.9}$$

Once the mother wavelet is chosen, the CWT of the function $f(t) \in L^2(\mathbb{R})$ is defined by the equation [Tan00]

$$CWT\left(a,b\right)=\left(f,\psi_{a,b}\right)=\frac{1}{\sqrt{s}}\int_{-\infty}^{\infty}f\left(t\right)\psi^{*}\left(\frac{t-\tau}{s}\right)dt. \tag{2.10}$$

The variable $s \neq 0, \in \mathbb{R}$ represents the scale and determines the stretching and compressing of the wavelet, parameter $\tau, \in \mathbb{R}$ indicates the translation, and $\psi * (t)$ is its complex conjugate.

Equations 2.8 and 2.9 assure the perfect reconstruction of the signal $f\left(t\right)$ from the coefficients $CWT(s,\tau)$ by means of the inverse CWT, which is described in [Tan00] as

$$f(t)=\frac{1}{C}\int_{-\infty}^{\infty}\int_{-\infty}^{\infty}\frac{1}{|s^{2}|}CWT(s,\tau)\psi\left(t\right)dsd\tau, \tag{2.11}$$

$$C=\int_{0}^{\infty}\frac{|\psi\left(\omega\right)^{2}|}{\omega}d\omega. \tag{2.12}$$

The principle of CWT with respect to scale and translation is illustrated in Fig. 2.6.

Numerous types of mother wavelets such as Daubechies, Haar, and Morlet wavelets have found use in many diverse applications and especially in analyzing of AE behavior. The choice of the mother wavelet depends on the type of the signal to be analyzed and on the application field [Add10].

In this work, the Morlet wavelet is chosen as mother wavelet to analyze the AE data measured during different processes. According to [Li02], Morlet wavelet achieves a very good compromise between time- and frequency-resolution. It is widely used for detection and identification of transient events with hidden information. The Morlet wavelet is defined in [GY10] as

$$\psi_{M}\left(t\right)=\frac{1}{\sqrt{\pi f_{b}}}e^{j2\pi f_{c}t}e^{\frac{t^{2}}{f_{b}}}, \tag{2.13}$$

where f_c is the wavelet center frequency and f_b denotes the bandwidth. Morlet wavelet and its magnitude spectrum are illustrated in Fig. 2.7.

An example of raw AE signal and its CWT result using the Morlet wavelet is depicted in Fig. 2.8.

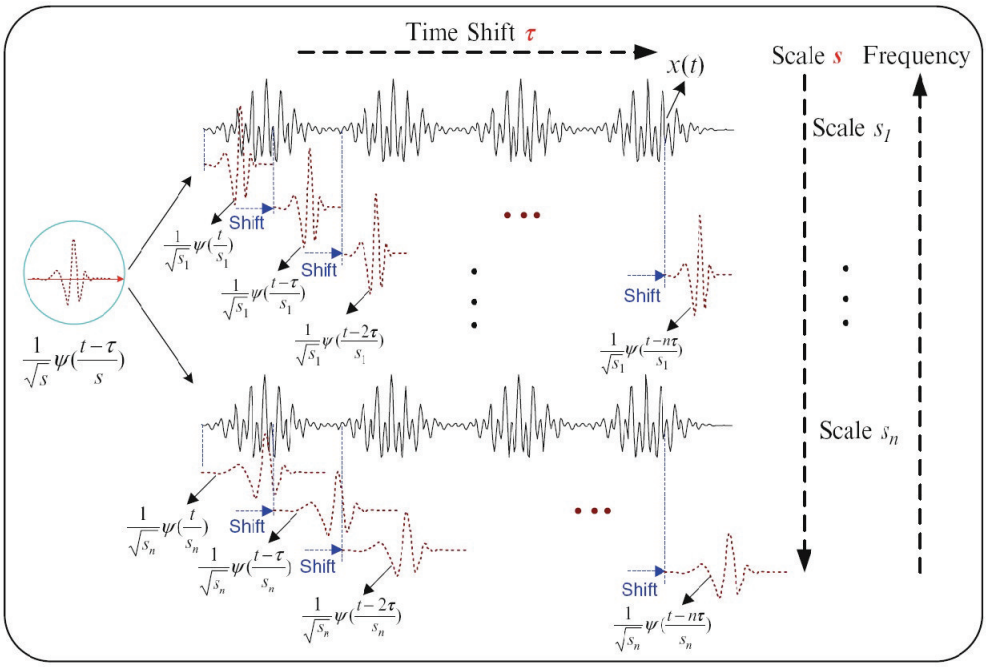

Figure 2.6: Principle of Continuous Wavelet Transform *[GY10]*

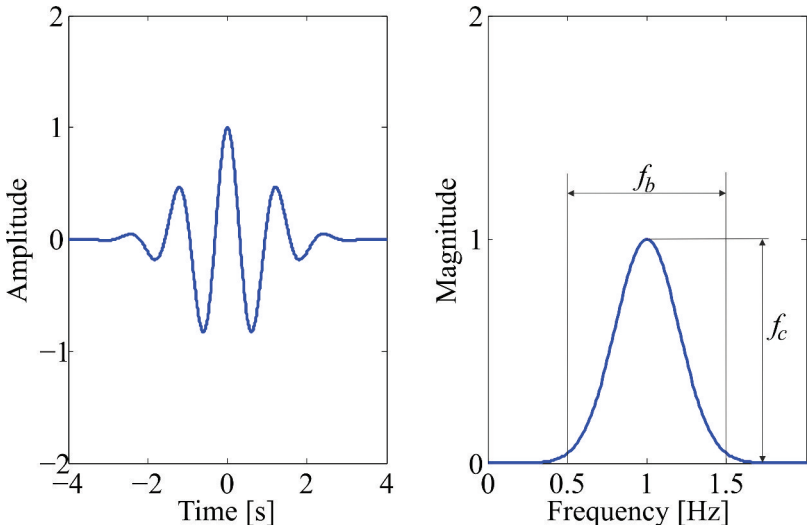

Figure 2.7: Morlet wavelet and its magnitude spectrum

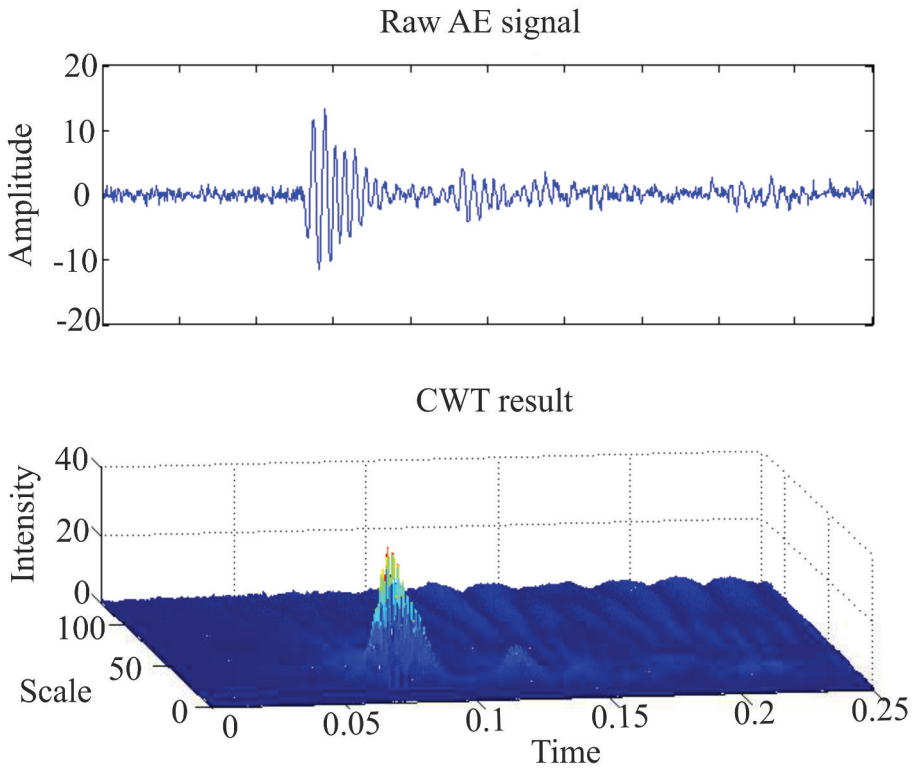

Figure 2.8: Raw AE signal and its CWT result using Morlet wavelet

2.3 Pattern Recognition and Clustering Approaches

2.3.1 Multivariate Statistical approaches

Principal component analysis

A feature set extracted from AE data is in its original form often improper for a direct analysis due to high degree of correlation, large data sets, and redundancy. Principal component analysis (PCA) is a method that is used to deal with this problem.

Principal Component Analysis (PCA) is one of the most popular multivariate statistical analyses [Jol02]. It is commonly used to reduce the dimension of multidimensional interrelated data set and to project them into a reduced space with a minimal loss of information allowing a better visualization [AAF11, KL97a, Gor07, CCC+03, Jol02]. Principal Component Analysis was first introduced by Pearson in 1901 as linear regression and was further developed by Hotelling in 1933 based on eigenvalue decomposition [DK96].

Principal Component Analysis is an orthogonal linear transformation that generates new orthogonal and uncorrelated variables called Principal Components (PCs),

which are normalized eigenvectors of the covariance matrix of the original variable [Jol02, SW04]. According to [Gor07, Jol02] the PCs have to satisfy the properties

- linear combination of the original variables,
- orthogonal to each other, and
- retaining the maximum variance in the data.

The PC's are ordered descending with respect to the variance. The first component denotes the direction in which the data set has the largest variation. The second component describes the direction of maximum remaining variance and so on.

Given the data vector $X = (x_1, x_2, ...x_m)$, the PCA transforms it in a new vector defined as [MK95]

$$X = TP^T = t_1 p_1^T + t_2 p_2^T + ... + t_m p_m^T = \sum_{t=1}^{m} t_i p_i^T, \tag{2.14}$$

where p_i are eigenvectors of Σ the covariance matrix of X which is defined as

$$\Sigma = cov(X) = \frac{X^t X}{m-1}, \tag{2.15}$$

where the matrix T represents the score matrix of PCs. The matrix T provides information about relationship between samples. The matrix P defines the PC's loading matrix. It contains information about the relationship between the variables. Principal component analysis (PCA) is often used in combination with other statistical techniques and also has some other applications including blind source separation, denoising, and data compression [KL97a, SZNR10, BP06]. In some applications, such as process monitoring, the maximum variance dominates the high-order PCs because the original variables have a low influence on the first few PCs [BCBK01].

Principal Component Analysis has found numerous applications in fault detection and identification [CLL+05] and damage discrimination in composite materials based on AE data [CCP13, SMHH12, SGR+12, Joh02]], however the selected features are mainly restricted to those extracted from AE signals in time-domain.

Kernel Density Estimation

Kernel Density Estimation (KDE) is an unsupervised learning method and probably the most common non-parametric statistical procedure [Sil86]. Using KDE empirical distribution density function can be calculated from data samples.

Considering a random sample $S = \{X_1, X_2, ..., X_N\}$ from a distribution density function $p(x)$, the d dimensional multivariate kernel density estimator $\hat{p}(x)$ at x is defined in [WJ94] as

$$\hat{p}(x; H) = \frac{1}{n} \sum K_H(x - X_i), \tag{2.16}$$

with $x = (x_1, x_2, ..., x_d)^T$and $X_i = (X_{i1}, X_{i2}, ..., X_{id})^T$. The kernel function K_H determines the shape of the bumps [PLI09] and is expressed as

$$K_H(x) = |H|^{-\frac{1}{2}} K(H^{\frac{1}{2}} x). \tag{2.17}$$

The kernel function has to meet the following criteria:

- symmetric around zero,
- integrating to one, and
- non-negative.

The matrix H is a dxd matrix containing smoothing parameters which defines the kernel bandwidth [Sil86]. The bandwidth matrix is:

- positive definite,
- non-random, and
- symmetric.

Suitable bandwidth choice is required because it determines the amount of smoothing of the density function and has strong influence on the KDE result.

Many studies have been conducted discussing the application of KDE in monitoring of multivariate processes [CWGS00], classification [GCS06], and pattern recognition [EPH13, LZ12].

2.3.2 Support Vector Machine

Support Vector Machine (SVM) is a supervised machine learning algorithm developed by Corinna Cortes and Vladimir Vapnik [CV95] in 1995 for classification approaches and was extended to solve regression problems. Based on the concept of large margin classification, SVM separates a set of points using the optimal separating hyperplane between two or more classes by maximizing the distance between the plane and the set of points. The Support Vector Machine can be applied to both linearly and non-linearly separable data. For a linearly separable n-dimensional data

set, SVM can find an infinite number of hyperplanes that separate the classes; the goal is to obtain the decision boundary with the optimal hyperplane. An example of two possible hyperplanes is shown in Fig. 2.9.

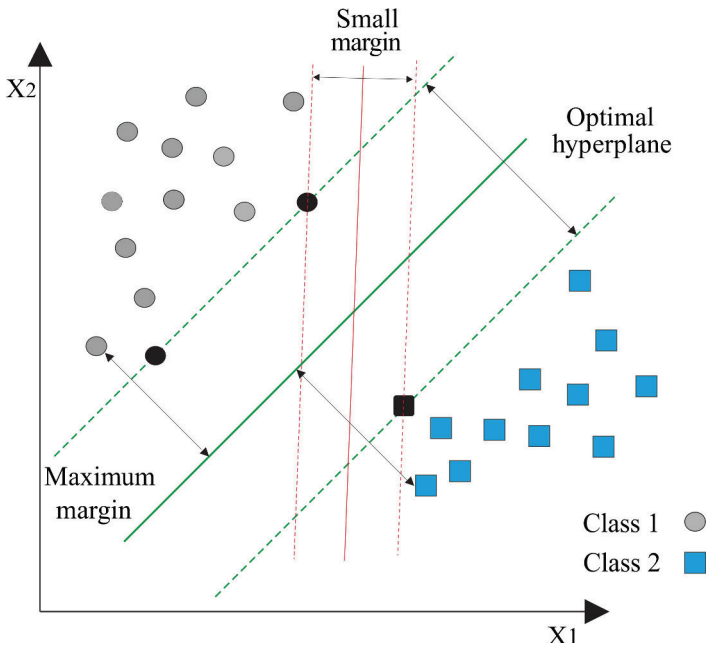

Figure 2.9: Maximum margin hyperplane and small margin of a SVM trained with samples from two classes. Samples on the margin (black samples) are called Support Vectors.

A decision boundary of a linearly separable data set $\mathbf{x}_i = (x_{i1,}x_{i2}, ..., x_{id})^T$ with class label $y_i \in \{-1, 1\}$ can be mathematically written as [Abe10]

$$\mathbf{w}.\mathbf{x} + b = 0, \tag{2.18}$$

where $\mathbf{w} = (\mathbf{w_1}, \mathbf{w_2}, ..., \mathbf{x_d})$ is a d dimensional vector, that represents the orientation of the hyperplane in space, b is a scalar which fixes the parallel shift of the hyperplane, and $x_i = (x_{1,}x_2, ..., x_d)$ is the training attributes vector.

The parameters $\mathbf{w}$ and b are estimated during the training phase and must fulfill the following two conditions

$$\mathbf{w}.\mathbf{x}_i + b \geq 1, \text{ if } y_i = 1 \tag{2.19}$$

and

$$\mathbf{w}.\mathbf{x}_i + b \leq 1, \text{ if } y_i = -1. \tag{2.20}$$

Equation 2.19 and equation 2.20 can then be combined into the equation

$$y_i(\mathbf{w}.\mathbf{x}_i + b - 1) \geq 0 \text{ for } i = 1, 2, ..., d. \tag{2.21}$$

Unfortunately, many real-word data such as AE data are non-linear so that no adequate hyperline can be found. To classify non-linearly separable data, transformation should be applied to the above introduced process. Using a non-linear mapping, the original data can be transformed from their current coordinate space into a new space with high dimension. The features are then linearly separated [Bur98].

In recent years, SVM was effectively extended to solve multiclass problems. There are two ways to classify more than two classes using SVM.

The first method is the *one-against-all* method [CS02]. It builds N binary classifiers (SVM models) to classify N classes. The i^{th} classifier is trained to classify the i^{th}class with positive label and all the rest with negative label. The second method is the *one-against-one* method [HL02]. In this method $N(N-1)/2$ classifiers are built, and each one is trained on data from two classes. It is important to note that to obtain a good classification rate, data set (features) have to be scaled into a common range so that all dimensions have the same influence. A successful application of SVM in conjunction with the AE technique in fault diagnosis can be found in [HZZ+13, WKS+09, KL14, FMM+14]

2.4 Acoustic Emission Examination of Wear Resistant Plates

This section introduces a review of achievements to date regarding AE examination of metallic structure. Primarily, this involves AE applications in wear processes, but also includes studies investigating AE signals during crack initiation and crack propagation. For a deep understanding of the outcomes, an overview about wear mechanism is firstly presented.

2.4.1 Wear Mechanisms

Wear is a type of surface damage that occurs due to contact and periodically repeating relative motions between solid surfaces. It involves progressive loss of materials

that leads to loss of mechanical performance. Wear depends on surface properties, material properties, operating conditions, stresses, lubricants, and geometry [FLK+03]. Wear is defined in [VDE94] as

"*progressive loss of substance from the operating surface of a body occurring as a result of relative motion at the surface.*"

The material removal rate is generally slow, but continuous and steady and after a certain period, leads to system failure.

Wear mechanisms may occur separately, overlapping, or consequently in more than one form causing physical and chemical transformations. Wear mechanisms, dominated by mechanical behavior of materials, are fundamentally divided into three groups namely adhesive wear, abrasive wear, and surface fatigue.

Abrasive wear arises when the sharp materials produce loose grains in form of surface asperities that have higher hardness than that of the surface. During sliding motion, hard debris move under pressure along solid surface causing abrasion [MF82].

Adhesive wear often called galling or scuffing. Adhesive wear generally appears in form of wear elements generated by adhesion and tearing off of material from the sliding surface [RCNR84]. Most of surfaces are rough and show irregularities or asperities. In consequence, cold welded junctions are formed due to surface contact at single asperities and "the subsequent shearing of the junctions from softer material causes adhesive wear particle" [Hur72].

Surface fatigue occurs as cracks and fractures caused by high plastic deformations [FK01]. Depending on the stresses applied in or below the surfaces, surface fatigue causes a noticeable decrease of functional properties of damaged structure and may lead to an unsafe machine operation [ZMP06]. An illustration of the main wear mechanisms is shown in Fig. 2.10.

Wear phenomena also include asperity fraction, crack initiation, crack propagation, and plastic deformation [BM91]. Along with the different wear phenomena, the produced atomic rearrangement in materials emits energy in the form of high frequency mechanical vibrations. Waves propagate throughout the surface as elastic waves within the frequencies range of 100 kHz to 1 MHz [EM08] and are defined as AE. Acoustic Emission technique have been widely used for crack detection, microstructural characterization, and monitoring of wear processes.

2.4.2 Wear Detection and Identification

During the progress of this work, this subsection has been partly published/ demonstrated in [BDS11, BS12a, BS13, BSS14, BS15].

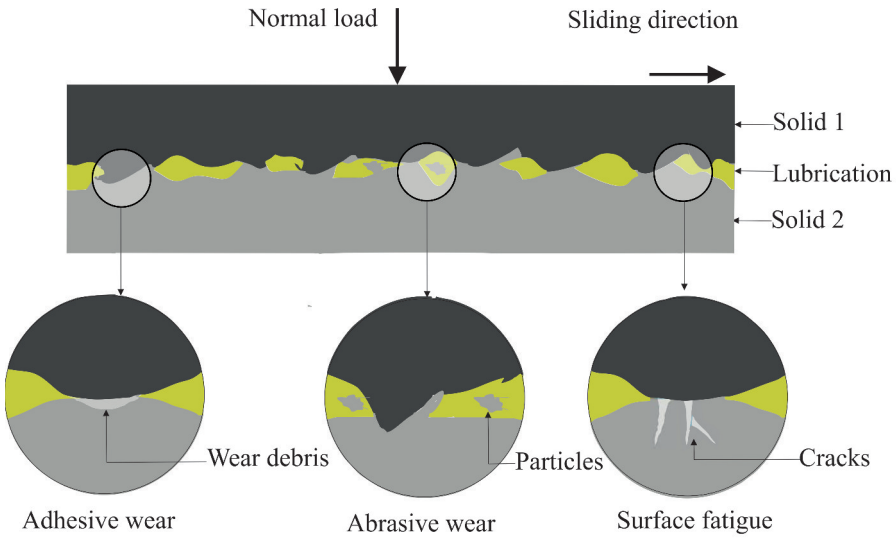

Figure 2.10: Graphical illustration of the main wear mechanisms

One of the primary objectives of this work is to establish a direct correlation between state-of-wear generated in a tribological system and emitted AE. To provide a starting point, relevant literature covering the application of AE to wear detection have been reviewed and summarized as follow.

The contemplation of changes in the contact surface of material structures is of high importance especially for rotating and sliding machinery. Contact damage of at least two bodies is generated by periodically repeating processes. Surface fatigue causes a noticeable decrease of functional properties of damaged structure and may lead to an unsafe operation of machine [ZMP06]. The literature on this topic, such as [HLCW11, BKSS11, AKM11] shows that AE is a suitable method to detect the damage state and to give information about the quality of contact surface [MDP11]. In this context AE is caused by the interaction of two surfaces in relative motion. Due to friction, AE is generated by impact of friction surfaces, surface damage, and formation of adhesive junctions [BKSS11].

Since the late eighties, many studies investigating the relationship between AE behavior and mechanical wear mechanisms have been carried out. The first group of authors used the parameter-based method to analyze AE signals. This method is based on the extraction of relevant and important AE features from the AE raw signal measured in time domain. In general, AE counts, cumulative AE energy, cumulative AE hits, and AE energy distribution are generated and correlated with the damage evolution.

Han et al. [HLCW11] examined the AE characteristics during fatigue crack propagation. The AE behavior exhibits the existence of three phases corresponding to fatigue crack initiation denoted by a rapid growth of AE counts, stable crack propagation specified by a decrease of AE counts, and unstable fatigue crack propagation

identified by an increase of the AE counts until the end of the experiment.

In [AKM11] the sensitivity of AE to damage process during fatigue crack test is discussed and examined, it was concluded that the accumulated AE activities increases when damage increases.

Zykova et al. [ZMP06] analyzed the measured AE activity with the counts rate method and the cumulative AE counts method. The authors identified three contact fatigue stages. At the beginning of the test an increase of AE activity was observed. This was assigned as running-in phase (self-accommodation). The end of the run-in phase is clearly indicated by a reduction of AE events which stayed constant. This stable phase ends when a strong pitting appears, and the AE activity begins to increase rapidly up to failure of the system. This correlation of the AE parameters with contact damage degradation was also recognized by [BKKK06, FMK11, MDP11].

In [EM08] and [LKSK08], it was stated that in rotating machinery the sources of AE are due to impacting, asperities contact, cyclic fatigue, friction, turbulence, material loss, cavitation and leakage. It has also been found that in sliding machinery AE activity is caused by cold-welding, scuffing, scouring abrasion, and surface fatigue [BB10].

Experiments realized by [YJK$^+$00] exhibits that, with the application of the AE parameter analysis, a correlation between AE signals activity and the characteristics of fatigue crack initiation and propagation (crack growth) has been found. The cumulative AE counts measured in real time during fatigue cycle loading test was supposed to be one of the effective parameters to estimate the evaluation of damage accumulation.

Heiple, et al. [HC83] explain that the AE output increases when the plastic strain increases. The authors demonstrated that AE activity has a Weibull distribution function behavior. This observation has also been detected by [KDA92].

In [CHWK09, ELH$^+$04, MZ08] a different position was pointed out. Here, the process was subdivided in more than three phases. Muravev et al. [MZ08] examined the deformation behavior of Low-carbon steel. The obtained result, displayed in Fig. 5 allows the subdivision of the AE activity in four phases. Phase I describes the elastic stage. During this phase, AE signals with high peak amplitudes are detected. They are generated from the contact friction of between the boundary surface of the sample and the testing machine. Phase II identify a 'yield plateau' in which the measured AE are related to "a moving source whose position coincides with a Lüders Band". Phase III represents a pause that is called "silence zone", in this phase, no AE events are detected because of the Kaiser effect. The silence zone denotes the end of the yielding, and it predicts the beginning of stage of parabolic strain hardening.

In recent years, the frequency-based AE analysis has become a promising alternative to the parameter-based AE analysis. Frequency-based method allows the investigation of the complete transient data (raw data), which involve more details and

information about the damage process and the moving path of the emitted waves. This method is mainly based on power spectral analysis. The frequency components of AE signals are examined by means of Fast Fourier Transform (FFT) and several time-frequency analysis methods like STFT and WT. The peak amplitude of the spectrum and dominant frequencies were used as features to study the characteristics of Acoustic Emission signals.

Hase et al. [HMW12] examined AE signals during adhesive wear and abrasive wear by means of FFT. Here, adhesive wear was characterized by a frequency peak at 1.1 MHz which was physically correlated to transfer particles and quantities of wear elements, while abrasive wear such cutting and plastic deformation was denoted by frequency components in the range of 250 kHz to 1 MHz. Similar results were observed in [WMS90].

Asamene et al. [AS12] performed studies on two sliding flat steel surfaces to investigate the relationship between sliding friction and AE signals. Frequency components about 700 kHz were detected and assigned to friction. Kolubaev et al. [KKS10] observed the presence of high frequency components related to formation of a damage surface layer during sliding friction tests.

Chang et al. [CHWK09] in investigated the crack closure of physical short and long cracks of LY12CZ aluminum alloy during fatigue process. Results showed that emissions with frequency components in the range of 200-400 kHz are referred to friction of the surfaces and do not depend on the length of the crack.

As stated in [MSS02] AE signals occurring during sliding wear between a steel ball and a sapphire disc show frequency components in the range of 100-500 kHz. The results reveal that there is a "strong dependence on the lubrication conditions". This conclusion has also been noted in [SRB01]. Here, the wavelet transform was used for early damage detection of highly stressed rotating components. The experimental results indicate that frequency components of 200-250 kHz correspond to crack initiation, while crack propagation is characterized by AE signals with frequency components up to 400 kHz. Regarding the mentioned review, it is obvious that using only the parameter-based or the frequency-based AE method no agreement on the wear mechanism, resulting wear state, the corresponding AE parameters, and AE frequency components can be realized.

2.4.3 Summary and Discussion

In this section, an overview of the main wear mechanisms occurring during sliding motion is provided. From literature review, it has been shown that AE has a great potential in SHM application and can reveal significant information about the tribological behavior of sliding contact. The wear mechanism could be identified from amplitude and frequency peaks of the detected AE signals. It has also been concluded that AE activity increases with increasing damage severity [HLCW11, MDP11, AKM11, EM08, FMK11]. However, amplitude and frequency

peak values change from application to another, depending on material properties and geometry. Typically, time-domain based AE parameters such as energy and count rate were used to characterize the AE activity and to describe the damage/wear evolution. The parameter-based approach is very computationally intensive and time consuming when it is related to test of long duration due to the high sampling rate and the large volume of generated data. The main objectives of this thesis is to develop a processing method to (i) manage the great volume of data in order to extract more relevant information., (ii) calculate the frequency-based AE energy by developing a new signal processing method, and (iii) establish a direct correlation between state-of-wear and emitted AE. In detail, the effects of the damage progression process have to be described quantitatively and qualitatively. The potential benefit of this work in terms of SHM is the possibility to judge the actual wear state based on related individual measurement without any manual engagement.

2.5 Acoustic Emission Examination of Composites

A composite material is defined in [Cam10] as

> *"a combination of two or more materials that results in better properties than those of the individual components used alone. In contrast to metallic alloys, each material retains its separate chemical, physical, and mechanical properties."*

Based on this definition, a wide range of new products possessing unique properties can be manufactured for several engineering purposes. Composite materials can be designed to obtain particular properties, that cannot be fulfilled anymore by already known materials, by combining optimum components. The main reason for increasing interest in composite materials is the rising need for material with high strength and low weight. In addition to their structural properties, composites exhibits electrical, thermal, tribological, and environmental qualities, that makes them more attractive for various applications [MD01].

Fiber Reinforced Composite is a material consisting of stiff and strong fibers embedded in a matrix. The matrix makes the structure rigid and determines many important properties; it binds the fiber together, secures them in position, and protects them from corrosion. Through the matrix, the internal loads are transferred to the fiber [Maz01]. Impact tolerance, resistance to damage growth, thermal, and chemical operating limits are also qualities defined by the matrix [Rei98]. Matrix can be produced of ceramics, metals, or polymers such as epoxies and polyesters. The primary functions of fibers are to reinforce the composite, provide stiffness and strength, and to transfer the tensile load through the material. Moreover, the Fiber content, orientation, and arrangements have enormous influence on the produced

component. Essentially, the matrix assures the compressive and transverse properties while the fibers assure the axial properties of the fiber reinforced composites [Unn08]. Depending on the directional orientation of the fibers, three characteristic forms can be produced namely unidirectional in which the highest strength is achieved in fiber direction, bidirectional where fibers lie perpendicular to each other, and multi-directional. For fiber reinforced composite, *the volume ratio of fibers versus matrix* is generally the important property [DHC04]. "The higher the ratio, the stronger the composite [Rei98]". That means that solid and stiff fibers have to be embedded in a matrix of low strength and low stiffness. Typically fibers can be made of aramid, glass, and carbon, or nature fibers.

In recent years, Carbon Fiber-Reinforced Polymer (CFRP) composites have become the best candidates for engineering applications especially in the aviation and aerospace industries [HCM04]. Carbon fiber-reinforced polymers are made of carbon reinforcement fibers and a matrix of epoxy resin. Compared to other fiber-reinforced polymer such as Glass Fiber-Reinforced Polymer (GFRP), CFRP is lighter, more resistant to corrosion and high temperature, and possess higher strength-to-weight ratio [Maz01]. Carbon fiber-reinforced polymers are mostly used as laminated composites fabricated by assembling sheets and resin layers [Gib11]. Layers of different fiber orientations are laid up in plies alternately [Gib11]. These offer many options to the designer to produce the optimal structure with the desired properties. Due to the specific qualities which can be achieved, the application of CFRP is no more restricted to aviation and space fields [Rei98]. Over the last decade, a noticeable increase in the demand of CFRP in automotive, petroleum, biomedical, sport good, and civil infrastructure industries [Cam10].

Despite previously cited advantages, CFRP shows some disadvantages such as relatively high manufacturing cost, intensive labor, limited experience on the long-term properties [TSB03], possibility of occurrence of new unfamiliar failure mechanisms, and lack on theoretical methods [TOI+08]. Therefore, here is still research performed on this topic and especially regarding the numerous defects and damage mechanisms which occur when the structure is in-service.

2.5.1 Damage Mechanisms in CFRP

In structural health monitoring, the definition of the term "damage" is limited to

"changes to the material and/or geometric properties of structural and mechanical systems, including changes to the boundary conditions and system connectivity, which adversely affect the current or future performance of these systems" [FW07].

In case of CFRP numerous microscopic and macroscopic defects and damage mechanisms can be identified. Due to the anisotropic nature of CFRP, damages can occur successively or simultaneously [PD01]. These damage mechanisms can be generated during any process phase including manufacturing, construction, and service life [SP89].

Depending on the applied load, tensile, compressive, or sheer, four main types of damage can occur namely: matrix crack, interfacial debonding, fiber breakage, and delamination [JCV98].

When tensile stress is applied perpendicular to the direction of the fibers, micro cracks appear in the matrix. These micro cracks propagate along the direction perpendicular to the stress and can cause fiber breakage and interfacial debonding. Matrix cracks can also appear when the stress is not sufficiently distributed [JCV98].

If tensile stress is applied in the direction of the fibers, fiber breaking will be produced. When the applied stress exceeds the tensile strength, more fibers will break, and interfaces around the fibers can also rupture and thus leading to a total failure of the structure [Gib11].

Debonding is produced when individual fiber decollate from the matrix [Gib11]. These separations depend on applied compressive load and the quality of fiber/matrix interfaces. When low resistant interface is used, matrix cracks travel through the fibers without inducing breakage, but causes debonding of the fiber/matrix interface. Debonding inhibits the transmission of stress from matrix to fibers, which reduced the quality of the structure [ZH02].

Delamination occurs when the separation between layers is generated due to loads. It depends on the nature of the constituents and of the imposed stress. This damage represents the main damage in the laminated composite material [SWWF10]. Delamination can be either produced by impact damage or resulting from inter-laminar stresses that generate discontinuities [BB06]. The delamination grows under different loads, transmits stresses in layers, and can affect residual stiffness and strength. Delamination often begins on the front edges and extends over the whole of the specimen. An illustration of failure modes in CFRP is shown in Fig. 2.11

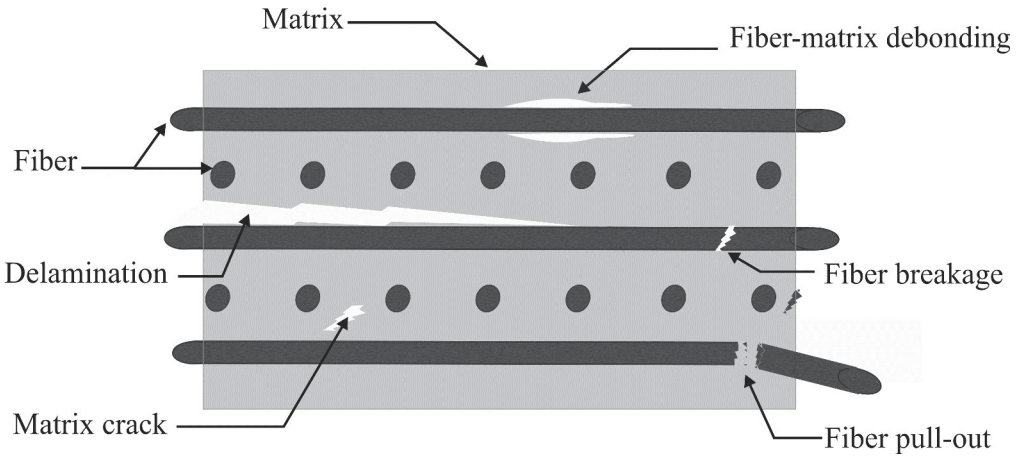

Figure 2.11: Failure modes in fiber reinforced composites

2.5.2 Failure mode Identification

During the progress of this work, this subsection has been partly published/ demonstrated in [BS].

The damage process in fiber reinforced composite materials produce micro- displacements, deformations, and discontinuities in form of matrix cracks, fiber breakage, delamination, and interfacial debonding. These damage mechanisms have been identified as AE sources. But the challenge is how to assign the AE signals to the related failure mechanism?

The extraction of features related to the nature of the damage is considered as a complex and difficult task, due to the alteration of the AE signals during propagation in anisotropic structures such as composite materials. Various AE-based procedures have been developed with the aim of detection, identification, and classification of different failure modes. In this section, a literature review of the most significant investigations, performed on AE-based failure modes identification, is presented.

Many authors reported on the use of the amplitude-based analysis [BR90, BB94, CSV96, CKTR92, KL97b]. Recorded AE signals are analyzed in time domain; amplitude or energy are considered as a unique descriptor and each failure mode is associated with the related amplitude. Their outcomes were different and sometimes contradicted due to the fact that the amplitude depends on fiber orientation, specimen geometry, and sensor location [NI02]. In consequence, AE amplitude is not a significant descriptor for damage classification in CFRP [NI02].

To overcome this limitation, many authors proposed the frequency-based analysis using classical methods such FFT and power spectrum analysis as appropriate alternative. DeGroot et al. [dGWJ95] studied damage behavior of unidirectional carbon/ epoxy material under tensile load tests. In order to separate between failure modes, different types of specimen were used and the frequency spectrum between 50 and 600 kHz was investigated. The authors reported that tensile loaded pure resin samples, that produce only matrix cracking emit signals with frequencies between 90 -180 kHz, fiber pull-out produces signals with frequencies between 180 to 240 kHz, Double-Cantilever Beam (DCB) test causing mainly debonding release signals in the frequency range 240-310 kHz, and tensile tests on uncured prepreg giving rise to fiber breakage emit signals with frequencies above 300 kHz.

Giordano et al. [GCE+98] presented a study to identify AE signature and to isolate the frequency peaks of one specific failure mode namely fiber breakage. Specimens of single carbon fiber with polyester matrix subjected to tensile loaded tests along the fiber direction were investigated. A polarized light microscope was used together with a wideband AE transducer to detect the occurrence of fiber fracture. Fast Fourier analysis was applied to the recorded AE signals. The power spectrum showed frequency peaks up to 590 kHz. Giordano obtained similar results when specimens was subjected to different tensile tests and proposed the use of the same procedure to identify matrix cracking and fiber/matrix debonding.

Ramirez et al. [RJPR+04] used the FFT to examine AE signals occurring during tensile test performed on unidirectional glass/polypropylene composites. Peak frequencies were correlated to the different micro failure mechanisms. Fiber breaks were located in the high-frequency region beyond 400 kHz; fiber-matrix debonding and delamination are located at intermediate frequencies between 200 and 300 kHz, and matrix cracking was identified at 100 kHz. This result supports the conclusions proposed by deGroot [dGWJ95].

Bohse [Boh00] introduced a spectral power density based method for classification of AE source mechanisms in composites. Single-fiber made of glass/epoxy, carbon/epoxy, and glass/polycarbonate were used. The authors determined frequency intervals of matrix cracking, fiber breakage, and debonding in accordance with the criterion that at least 70% of the signal power has to be within the defined frequency intervals. Frequencies due to matrix cracking were allocated in the range of 100 to 350 kHz and frequencies caused by fiber breakage were situated in the range of 350 to 700 kHz. Signals in between were expected to be fiber/matrix debonding.

Bussiba et al. [BKI+08] investigated the acoustic response of graphite/epoxy and carbon/carbon composites under quasi-static loading tests. In addition to the AE Method, light and electron microscopy were applied. Three main damage mechanisms were identified. The FFT was performed in order to characterize the failure modes in term of frequency components. Peaks in the spectrum at 140 kHz were associated with matrix cracking, peaks at 300 kHz were correlated to debonding, and peaks at 405 kHz were related to fiber breakage. Bussiba [BKI+08] demonstrated the ability of the AE method to determine the events sequence. Fiber breakage was firstly observed followed by debonding and matrix cracking.

Eaton [EMF+11] reported the use of frequency content to discriminate between Acoustic Emission signals generated from various damage mechanisms. Tensile and buckling tests were performed on carbon fiber/epoxy plates with different geometries. The obtained result agrees with the above-mentioned studies. Matrix cracking was accompanied by frequencies below 150 kHz whereas fiber failure was accompanied by frequencies above 400 kHz. Eaton devoted special attention to specimen geometry, sensor response and sensor position which can influence the results.

Sause et al. [SH10] used simulated AE waveforms to study the relationship between dominant failure mechanisms in CFRP and the generated AE signals. Frequency-based damage identification was performed and AE signals were analyzed in terms of peak frequency, weighted peak frequency, and partial power. It was observed that matrix cracking, debonding, and fiber breakage had partial power of 0-250 kHz, 250-450 kHz, and 450-800 kHz respectively.

Gutkin et al. [GGV+11] applied the FFT to analyze the frequency content for AE signals emitted during various mechanical tests on CFRP. Results show that based on the peak frequency distribution certain damage mechanisms could be identified and classified. Gutkin determined specific frequency bands related to five failure sources. Frequencies due to fiber pull-out were located in the 500 to 600 kHz, fiber

failure was found to reside in the 400 to 500 kHz. Frequency components between 300 and 200 kHz were produced by fiber / matrix debonding where delamination was given in the interval between 50 and 150 kHz, and matrix cracking released frequencies between 50 and 100 kHz.

In summary, the above-mentioned studies demonstrate that each failure mode is characterized by a specific frequency peak. Frequency-based analysis shows fewer contradictions and betters accordance in comparison to amplitude-based analysis. Because of the non-stationary behavior of AE signals, some researchers have used time-frequency analysis like DWT, CWT, and HHT to obtain more valuable information.

The work of [QBHK97] can be considered a pioneer in the use of DWT for analysis of AE signals. Transient events emitted during static loading of unidirectional and cross-ply CFRP were reported. Acoustic Emission signals were decomposed into 11 levels using Daubechies mother wavelet. Specific frequency range, energy change rate, and percentage of total energy of each level were calculated. They deduced that 98% of AE energy was concentrated in levels 7, 8, and 9 corresponding to frequency ranges 50-150 kHz, 150-250 kHz, and 250-310 kHz, respectively. Each level was assigned to a damage source. Fiber fractures are situated in level 9 with energy percentage about 75%, fiber/matrix debonding is located in level 8 with an energy percentage of 15%, and level7 was associated to matrix cracking with an energy percentage of 8%. In [KHB01] the same approach to study AE emitted due to fatigue load of unidirectional CFRP is used. The identified significant levels were the same as those determined by [QBHK97] and [OAH09], but contrary to Qi, Kamala et al. [KHB01] correlate event with high frequency and high energy to matrix cracking.

Kinjo et al. [KSTO97] proposed a condition monitoring approach for GFRP specimen based on CWT. Firstly, AE signals were identified according to their corresponding fracture mode. Wavelet transform result was considered as an image that was subjected to three classification methods. Discrimination capability as well as classification rate of Matched Filtering, Matched Filtering of Laplacian Image, and Fourier Phase Correlation were tested. The best recognition accuracy was achieved by FPC.

Mizutani et al. [MNTO00] used CWT in addition to the AE waveform analysis to classify fracture mechanisms of cross-ply carbon-fiber composites. Based on Wavelet contour maps four AE-signal types were identified and correlated to their failure modes. In [NI02], it was demonstrated that parameters extracted from time-domain AE signals are often affected by the distance and location of the sensor contrary to frequency peaks that are not influenced by the location of the sensors.

Sung et al. [SKH02] focused his work on AE signals generated due to low-velocity impact damage in graphite/Epoxy laminates. Damage mode (matrix cracking and delamination) and size (evolution of free-edge delamination) were investigated using DWT. Recorded AE signals were decomposed into three frequency levels by means

of Daubechies db4 mother wavelet. Matrix cracking was dominant with frequency above 300 kHz while debonding was characterized by frequencies lower than 250 kHz.

Chao et al. [CPZ11] also reported on the time-frequency analysis of AE signals. CFRP composites under quasi-static tension test were studied. Comparison between STFT, CWT, and HHT was given. Correlation between failure modes and related frequency ranges was established. Results pointed out the superiority of HHT in processing of non-stationary signals. However, the main drawback is high computational time.

Li et al. [LHOL11] proposed the use of AE waveform and wavelet analysis for classification of damage types of CFRP bridge cables under fatigue load. In addition to damage mechanism identification, the sequential accruement was investigated. Signals related to interface friction and fiber fracture were detected firstly followed by signals corresponding to interface debonding, matrix cracking, and fiber fracture which is the main failure mode of CFRP cables.

Han et al. [HZ13] analyzed AE signals, emitted from carbon fiber twill weave under quasi-static test, with several advanced time-frequency techniques. First, empirical mode decomposition was performed to decompose the signals into 6 IMF corresponding to 6 frequency ranges. Peak frequency of each range was calculated using FFT and assigned to the different failure mechanisms. Secondly, HHT was performed allowing a better interpretation of the instantaneous frequencies. The last method applied is the energy entropy analysis based on IMF component. Based on result obtained from the energy distribution, frequencies between 105-145 kHz, 150-240 kHz, and 275-404 kHz were associated to matrix cracking, debonding, and fiber breakage respectively.

Bak et al. [BKA14] applied CWT to identify the time-frequency behavior of the damage mechanisms generated during tensile tests of GFRP. The analysis showed similar results to [Boh00]. Acoustic Emission signals due to matrix failure are situated in frequency range 80-130 kHz, fiber-matrix debonding generated AE signals with frequencies in the range of 130-220 kHz, signals from fiber-tear have frequency range of 220-300 kHz, and frequency range of AE signals caused by fiber breakage are found in range above 300 kHz. Scanning electron microscopy examination was also performed to confirm the presence of the identified damage and to characterize the severity of failure.

Hamdi et al. [HDS+13] studied AE signals recorded from unidirectional GFRP under quasi-static three points bending tests. Pattern recognition approach based on HHT was performed. Frequencies related to four damage mechanisms were identified namely: delamination (30-80 kHz), Matrix cracking (around 150 kHz), debonding (180-280 kHz), and fiber breakage (340-400 kHz). Mean local frequency of the first Intrinsic Mode Functions (IMF) was selected as main descriptor. A comparison of the HHT based clustering with a multivariate statistical analysis using k-means showed the reliability of the introduced HHT-based classification.

Arumugan [AKS+13] submitted a single layer GFRP specimen to tensile testing to identify matrix cracking and fiber breakage while delamination was studied using two-layer specimen with pre- induced defect. In this study, Arumugan used a large number of signal processing techniques and an unsupervised pattern recognition approach based on Fuzzy C-mean (FCM) in combination with PCA. Acoustic Emission count rate and cumulative counts with the commonly time-domain parameters were selected as features to perform automatic clustering. The optimal number of cluster was equal to three which agree with the detected failure modes. As next step, PCA was then carried out and a 2D illustration of the FCM clustering was given. Further, the clustered waveforms were analyzed using CWT and DWT in order to extract relevant frequency components distinguishing different damage mechanisms. Results showed that fiber breakage generates AE signals within frequency range 250-350 kHz and AE events caused due to delamination are situated between 90-180 kHz. Conclusively, the sequence of damage occurring was investigated using ST-FFT.

In Tab. 2.1, a summary of the identified damage mechanism based on studies that have focused on analyzing the frequency content of AE signals generated from various types of FRP is shown. Based on these results, it can be concluded that AE signals emitted due to matrix cracking are characterized by frequency content lower than 150 kHz while Fiber breakage generate AE signals with frequency content higher than 250 kHz. Frequency in between can be caused due to debonding.

With the rapid development of data processing techniques, recent studies have focused on pattern recognition to classify damage mechanisms in composites. These methods are based on the segmentation of several descriptors in clusters. The classification is determined by examining similarities and differences between these descriptors. Successful applications of pattern clustering using multivariate statistical analysis were reported in many studies.

Anastasopoulos and Philippidis [AP95] used the Max-Min distance approach for clustering and Forgy's algorithm, which is a modified version of the k-means method, for classification of AE signals acquired from quasi-static tensile tests performed on glass-epoxy and carbon-carbon composites.

Pappas and Kostopoulos [PK01] identified five damage mechanisms by applying the method of k-means on five time-based parameters extracted from AE signals generated during quasi-static and dynamic-cyclic loading of carbon-carbon composites.

Kessler et al. [KSA+02] presented an approach combining lamb waves method, PCA, and three supervised pattern recognition techniques. In addition to the presence of damage, type and severity were investigated. Acoustic Emission signals were analyzed in both time- and frequency- domain in order to obtain a maximum number of features. In total, sixteen features were extracted; these included inter alia time of flight, maximum value of Power Spectral Density (PSD), actual phase, and mean deviation. More informative and discriminative features were then selected using PCA and ANOVA. Projection plot of the transformed vectors permitted the distinction of three classes corresponding to the common damage mechanisms. The automated

Table 2.1: Summary of failure mode identification using frequency content

Author	**Matrix crack**	**Debonding**	**Fiber breakage**	**Delamination**
DeGroot [dGWJ95]	90-180 kHz	240-310 kHz	> 300 kHz	
Qi [QBHK97]	50-150 kHz	150-250 kHz	250-310 kHz	
Ni [NI02]	< 100 kHz	200-300 kHz	400-450 kHz	
Bussiba [BKI+08]	< 150 kHz	200-300 kHz	> 400 kHz	
Marec [MTG08]	50-150 kHz	170-350 kHz.		
Sause [SH10]	< 250 kHz	250-450 kHz	450-800 kHz	
Gutkin [GGV+11]	< 50 kHz	200-300 kHz	> 400 kHz	50-150 kHz
Han [HZ13]	105-145 kHz	150-240 kHz	275-404 kHz	
Hamdi [HDS+13]	150 kHz	180-280 kHz	340-400 kHz	30-80 kHz
Arumugan [AKS+13]			250-350 kHz	90-180kHz

classification was performed by simple implementation as well as combined implementation of k-nearest neighbor, neural network, and decision tree. Best accuracy was obtained from the optimized Artificial Neural Networks algorithm (100% for damage presence, 100% for damage type, and 77% for damage severity).

Huguet et al. [HGG+02] conducted research on real-time detection of damage in complex GFRP pipes structures, by analyzing the evolution of AE activity. Kohonen's map was used as a statistical tool and nonlinear projection of Self-organizing Map (SOM) technique was applied for the visualization. Numerical separation of the associated signals is performed using six parameters calculated from the waveforms.

Deolivera et al. [dOM08] proposed a two-level clustering approach based on SOM of Kohonen and k-means. Overall eighteen descriptors were selected from time- and frequency domain. Six clusters were identified and assigned to the related failure.

Marec et al. [MTG08] examined AE signals collected during creep tensile tests performed on glass fiber/polyester cross-ply composites. Parametric analysis as well as time-frequency based analysis were applied and compared. Unsupervised pattern recognition approach based on fuzzy C-means in combination with PCA was used

to classify the conventional features extracted from signals in time domain. In order to extract more informative descriptors continuous wavelet transform and discrete wavelet transform were used. Results showed that Matrix cracking has to be found in the frequency range 50–150 kHz while signals occurring due to debonding have the frequency range 50–150 kHz. Using features obtained from the time-frequency analysis several failure modes could be recognized and the clustering result could be improved.

Loutas et al. [LK09] presented a parameter/energy analysis of AE signals measured during a load-unload-reload tests performed on three types of woven carbon/carbon composites. The extracted features in term of amplitude, rise angle, and reverberation frequency were subjected to clustering process using cluster validity criteria. Additionally, cumulative AE energy and cumulative AE hits number were investigated to correlate the identified classes to their failure damages. It was observed that the AE evolution differs from damage to other, which allows in association with the clustering result a better classification.

Gutkin et al. [GGV+11] tested the performance of three pattern recognition approaches: k-means, Kohonen maps combined with k-means, and competitive neural network on carbon-epoxy composite laminates subjected to tensile tests and bending. Clustering results showed that the use of the Kohonen maps combined with k-means proved to be the most effective method to describe the damage.

Wang et al. [WZY11] reported the efficiency of cluster analysis associated with neuronal network for damage identification and classification. Features like amplitude, duration and peak frequency were selected and classified in three clusters using hierarchical and k-means cluster analysis respectively. Two layer feed-forward artificial neural network was then developed to identify three typical failure modes namely matrix fracture, interface debonding, and fiber breakage.

Oskouei et al. [OHAF12] evaluated the use of fuzzy C-mean data clustering in combination with a PCA to analyze the damage mechanisms of glass fiber specimens with different interfacial layups types subjected to DCB tests. Energy, amplitude, rise time, counts, peak frequency, and duration were considered as descriptors and were clustered into three classes. Frequency distribution was calculated to correlate clusters to the related damage mechanisms based on the knowledge that each damage is characterized by a specific frequency range.

Sause et al. [SGUH12] introduced a pattern recognition approach based on an exhaustive screening and k-mean clustering to distinguish between different AE waveforms. Signals recorded during four-point bending test on multi-layer CFRP specimens were analyzed using FFT. To differentiate between fiber breakage, interface failure, and matrix cracking, seven frequency-based features (average frequency, reverberation frequency, initiation frequency, peak frequency, frequency centroid, weighted peak frequency, and partial power) were selected. Three clusters could be identified. Result pointed out the importance and the influence of the feature combination. Compared to other pattern recognition approach, computation efficiency

has to be improved.

Sause [SMHH12] demonstrated the ability of CWT to distinct between AE signals caused from different failure mechanisms in CFRP. In addition to features extracted from the CWT, the accumulated amplitude was selected as time-domain parameter. This feature combination allowed an optimal clustering of the AE signals into three classes corresponding to matrix cracking, interface, and fiber breakage.

Kempf et al. [KSA14] reported on the use of AE analysis and unsupervised pattern recognition techniques for damage characterization and classification in glass and carbon fiber reinforced exposed to static and dynamic tensile load. Frequency-based damage identification was performed and AE signals were analyzed in terms of peak frequency, weighted peak frequency, and partial power. The k-means algorithm was realized to classify the pattern in three clusters belonging to the different failure mechanisms. In order to visualize the clustering results in 2D and to improve the classification, PCA was performed. The method showed promising AE signal classification independent of material and loading direction.

In Tab. 2.2, a summary of clustering approaches and the selected features for damage identification and classification is shown.

2.5.3 Summary and Discussion

In this section, a brief introduction into composite materials, their properties as well as the main reasons leading to the increasing use of CFRP is given. Despite many advantages, CFRP exhibits a complex failure mode analysis because of the different damage mechanisms, which can occur simultaneously. Owing to the lack on failure theory in CFRP, health monitoring systems are strongly required to obtain information about the internal state of the structure. From the literature review, it can be seen that AET is an effective method for detection, identification, and classification of failure modes in CFRP. Generally, three AE analysis methods are used to study AE signals. The majority of the proposed investigations were based on similar approaches. Using AE amplitude, author's findings are different and sometimes contradicted due to the fact that the amplitude depends on fiber orientation, specimen geometry, and sensor location. Consequently, AE amplitude seems not to be a reliable descriptor for damage classification. Using either time-frequency analysis or multivariate statistical approach in combination with clustering or pattern recognition techniques, qualitative as well as quantitative information about damage can be deduced. In terms of SHM-related conclusion, the above-mentioned studies demonstrate that each failure mode is characterized by a specific frequency peak. Frequency-based analysis shows fewer contradictions and betters accordance in comparison to amplitude-based analysis. The main drawback of the multivariate procedures lies on the fact that multivariate approaches are mostly based on parameters extracted from signal in time-domain. Many tests have to be carried

out in order to extract sufficient number of parameters allowing better classification performance.

Table 2.2: Summary of failure mode identification using clustering and classification approaches

Author	**Features**	**Method**
Pappas [PK01]	Amplitude, rise time, energy, counts, and duration	k-mean
Kessler [KSA$^+$02]	16 features: mean deviation, maximum value of PSD, and actual phase	PCA, ANOVA, ANN, k-nearest neighbor, and decision tree
Deolivera [dOM08]	Amplitude, rise time, energy, spectrum's center of gravity	SOM of Kohonen and k-means
Loutas [LK09]	Amplitude, rise angle, and reverberation frequency	Cluster validity criteria
Oskouei [OHAF12]	Energy, peak frequency, rise time, and duration	Fuzzy C-mean and PCA
Gultkin [GGV$^+$11]	Amplitude, energy, rise-time, and duration peak frequency,	Kohonen maps, competitive ANN, and k-means,
Wang [WZY11]	amplitude, duration, and peak frequency	Cluster analysis and ANN
Sause [SGUH12]	frequency centroid, weighted peak frequency, and partial power	Exhaustive screening and k-mean
Kempf [KSA14]	peak frequency, weighted peak frequency, and partial power	k-mean and PCA

2.6 Acoustic Emission Examination of Electrochemical Cells

In recent years, special focus has been set to batteries, as result of the proliferation of electric mobility. Battery is a vital component in an electric vehicle (including hybrid electric vehicles and plug-in hybrid electric vehicles). Primarily because the performance of a battery has a strong influence on the safety, reliability, and the operating efficiency of the vehicle. Drivers of internal combustion engine driven cars are accustomed to checking a gas gauge to estimate the amount of driving for which their vehicle is currently capable. Measurement of the remaining gasoline available is a fairly simple problem solved by measuring the level of fluid in the tank. In contrast, gauging the amount of charge remaining and therefore cycle life expectancy is still a challenging task. Accordingly, advanced battery management systems are required to monitor the internal battery state and to provide diagnostic information for the benefit of the driver [XMTP11].

Lithium-ion is the optimal choice of battery at the moment until better storage systems are found [DHPS07]. Lithium-ion battery has major advantages over others sources, most importantly higher energy / power density and extended cycle life [AF13]. Lithium-ion battery is a rechargeable battery in which lithium-ions migrate from the anode to the cathode through the electrolyte during discharge. There, current travels from the cathode to the anode through an external load. Inversely, when charging, electrons move from cathode to anode in opposite direction to lithium-ion batteries utilize intercalated lithium compound as the electrode material. Basically, the negative electrode (anode) consists of graphite and the positive electrode (cathode) is a form of Li-based oxide while the electrolyte is an organic solvent. The electrochemical functions are reversed between anode and cathode depending on whether the battery is charging or discharging. The equations of chemical reactions of a lithium battery, with a lithium cobalt oxide cathode are defined as follows:

Anode $\mathrm{LiC_6} \rightleftharpoons \mathrm{Li_{1-x}C_6} + \mathrm{xLi} + \mathrm{xe^-}$ and

Cathode $Li_yCoO_2 + \mathrm{xLi^+} + \mathrm{xe^-} \rightleftharpoons \mathrm{Li_{y+x}CoO_2}\,.$

The potential of battery is determined by the anode and cathode materials, the nature of the interfaces between the electrodes, electrolyte, cell design, impurities, type of application, profile of use, and design [SBB04, TA01]. Consequently, aging behavior is individual and varies from battery manufacturer to battery manufacturer [WM04].

2.6.1 Aging Mechanisms of Lithium-based Batteries

Estimation methods for State of Health (SoH) and State of Charge (SoC) of lithium-ion batteries are essentially related to the main aging mechanisms responsible for

capacity decrease and power reduction. An aging mechanism is defined as an irreversible loss of performances caused by implication of material change. It is cognizable by increasing the internal resistance and time elements and decreasing the capacity [SBB04].

The aging process of lithium-ion batteries is complex and complicated. A large number of processes and their interactions cause capacity decrease and power fading [VNW+05]. Moreover, most of these processes occur simultaneously, complicating the investigation of a single aging mechanism. Generally, all components (anode, cathode, electrolytes, additives, and interfaces) of a battery can age. "The degradation of these components during battery operation adversely affects the energy delivery of the lithium-ion battery" [AF13]. Suppress of rest periods and increase of stress factors are main effects that accelerate aging mechanisms.

The aging mechanisms in Li-ion battery have been well discussed in the literature [RHWP02, AWD98, LCY08, BMFF11]. It is generally accepted that aging mechanisms occurring at the interface between electrodes and electrolyte are the most influential. Furthermore, it is helpful to consider aging mechanisms occurring at the anode side and the cathode side separately. On the anode side the degradation factors are passivation layer stability, the layer structure/composition (effect of additives in electrolyte and formation process), and polluting agents [SBB04]. On the cathode side, degradation is mainly related to the material structure evolution and organic solvent oxidation.

Two types of aging processes can be distinguished. In addition to aging due cycling, battery ages even when is in storage due to the progress in time. According to [BBB+05], "aging on storage is due to side reactions resulting from thermodynamic instability of materials in presence." This type of aging may, however, be reduced by taking same measures such as reducing the humidity [Det11], storage in ambient temperature conditions, and maintaining the average SoC [RLB+01].

Aging on cycling is described in [BBB+05] as " The result of degradation of active materials reversibility, especially the positive, coming from phase transformations during lithium insertion". During the first charge, or the formation period, a stable surface film layer known as Solid Electrolyte Interface (SEI) is formed on graphite anode. Task of SEI layer is to protect the anode for corrosion and the electrolyte from further reaction [ZW08]. During further charging cycles the thickness of SEI grows, becomes unstable, and breaks. Subsequently, the protective function cannot be successfully realized. As result, the internal impedance increases and recyclable lithium-ions are lost which affects significantly the performance of lithium-ion battery. Similar to anode, during charging and discharging, cathode material is strongly influenced by the intercalation and deintercalation of lithium. This leads to structural changes, chemical decomposition, and surface film modification. A general overview on the main aging mechanisms within a lithium-based battery, demonstrating the changes at the anode/electrolyte interface and cathode/electrolyte interface, is illustrated in Fig. 2.12. In summary, battery aging depends on manifold

electrochemical process. Accordingly, capacity decrease, power fade, and impedance increase cannot be assigned to specific effects. Generally, the total degradation, represented by SoC and/or SoH, is considered.

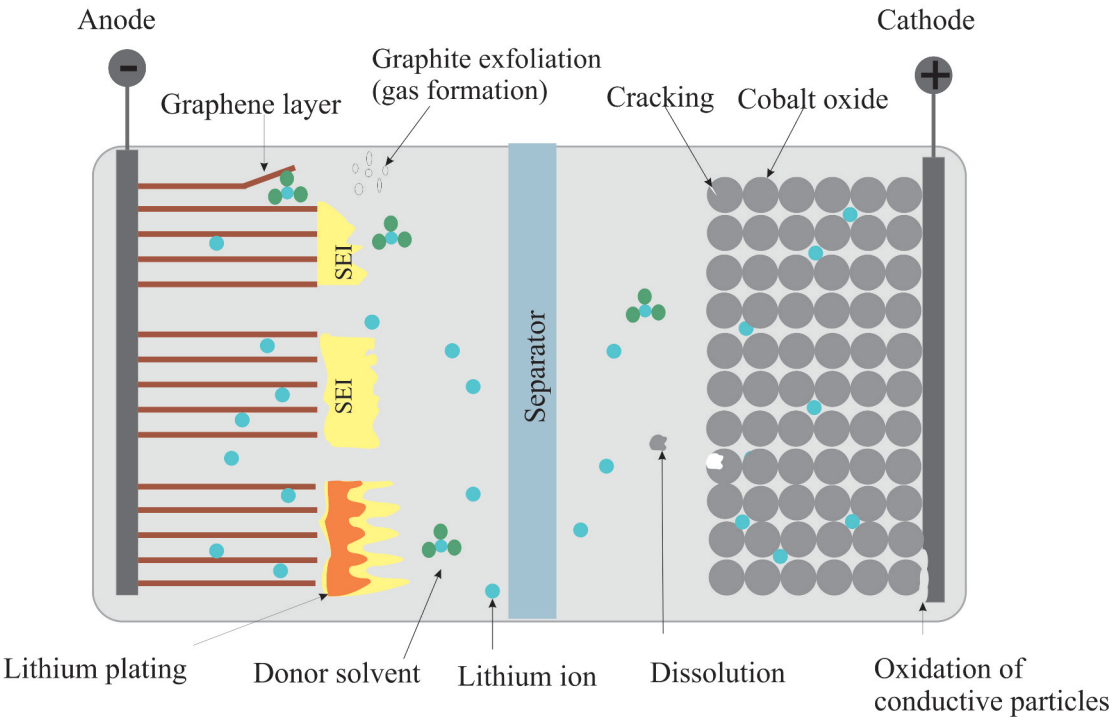

Figure 2.12: Depiction of main aging mechanisms within a lithium-based battery

2.6.2 State of Health / State of Charge Estimation

During the progress of this work, this subsection has been partly published/ demonstrated in [SB].

Health monitoring of batteries is generally performed aiming at providing a statement in real-time about the actual degradation level. In general, information related to degradation is given by estimating the state of charge and the state of health of battery. State of charge (SoC) is the energy amount remaining in the battery and is defined as the percentage of the maximum possible charge that is present inside the battery [CF10]. State of charge determines the remaining number of pulses that can be obtained from a battery during one cycle [PBNR05]. State of Health (SoH) expresses the state of a battery and its potential to provide the designated performance in relation to a new battery. The SoH is a relative indicator for battery aging

and it depends on the effect of previous battery history such as the storage time, storage temperature, and SoC [RBM+11, GQH+14].

In order to estimate the SoC/SoH, many non-destructive methods have been developed based on physical parameters such as charge acceptance, internal resistance, voltage, and self-discharge rate, measured during laboratory aging tests [PBNR05]. Estimation methods can be divided into direct measurements, bookkeeping estimation, and adaptive systems. Estimation methods based on direct measurements include Open Circuit Voltage (OCV), Terminal voltage impedance based methods, and internal resistance based method. Applications showing advantages and drawbacks of the mentioned method are proposed in [CSK11, RBKF12, PWLZ14, XHPT14]. Conventional Coulomb Counting (CC) and modified coulomb are the main methods associated with bookkeeping estimation, Here, battery discharging current is the parameter used for SoC calculation. This technique has some drawbacks namely wrong current measurements add up to make huge errors, charging/discharging losses do occur, and also initial SOC cannot be calculated [KKB+09, PPJ01]. With contemporary advancements made in the field of artificial intelligence, many new adaptive systems have been developed for SOC estimation. These include Back Propagation Neural Networks (BPNN) [ABC+03], Radial Basis Function Neural Networks, fuzzy logic methods [SVWR06], Support Vector Machine [HW05] and Kalman Filter (KF) [XHSZ13]. These adaptive systems are capable of automatically readjusting themselves. This property is of high importance because of nonlinear behavior of the different chemical factors. However, these methods need to be improved before any industrial application.

Recent successful application of AET to fuel cells [LTB+10] made it a promising nondestructive technique for monitoring and evaluation of aging mechanisms in lithium-based batteries. Kirscheva et al. [KGCT13] investigated the viability of Acoustic Emission as a tool to gauge the aging of the LiAl/LiMn02 cell. The main aim was to identify and to investigate the electrochemical and structural processes which appear into the negative lithium-aluminum electrode and the positive LiMn02 electrode. Acoustic Emission being a nondestructive tool was utilized to monitor activity inside the cell. During the discharge process, AE was stronger as result of phase transformation as well as the intercalation of lithium-ions in the Mn02 to LIMn02. Besides AE, X-ray diffraction XRD), and scanning electron microscope (SEM) were employed. The final results conclusively showed that the capacity fading (state of health) correlates accurately to the fading of AE activity and thus can be used as a battery SoH-indicator.

Matsuo et al. [MUC11] used AET together with a clustering approach to generate and obtain AE signals produced as a result of battery degradation. A Highly Oriented Pyrolytic Graphite (HOPG) together with lithium metal were used as working and counter electrodes respectively as well as a glass fiber sheet as a separator. Derived AE signals from gas evolution and graphite damages were considered. To be able to characterize AE signals from a degrading battery, clustered signals were contrasted to artificial AE signals generated by simulations of deteriorating batteries.

Hiroshi et al. [Hir12] suggested a method to characterize the active materials of Li-ion, as well as nickel-metal hydride batteries. Active materials like SI, SN, etc. used in lithium batteries have a high capacity which is good for use in electric and hybrid vehicles, but they are unfortunately susceptible to cracks. Intercalations/decalations occur at both electrodes in lithium batteries, therefore, active materials that crack easy as a result loss capacity in a short time. Since it is an established fact that lattice volume size can be used to estimate state of charge, studying the cracks during intercalation/deintercalation (which leads to capacity loss) using in-situ stress and crack analysis of AE are employed to estimate the SoH (capacity fade).

Kircheva et al. [KGCT13] developed a technique to validate the use of Acoustic Emission Techniques as tool for battery diagnosis system for LiFePO4/graphite and LiAl/LiMnO2 cells in conjunction with Proton Exchange Membrane Fuel Cells (PEMFC) systems. The AE was shown to be a good indicator of deterioration of active materials that culminates in capacity fade. In addition several origins of AE were spotted including the expansion of lattice volume of the active materials during the intercalation period, change in structure of the passivation on the surface of the anode as well as the electrochemical unreliability of the substances and their likely deterioration. The SoH can thus be inferred and used in battery management systems.

Etiemble et al. [EIR11] used AE to classify the electrode wear process depending on electrode structure and cycling state. Together with electrochemical measurements, AE is implemented to in-situ monitoring of the pulverization of electrodes for Ni-MH and Li-ion batteries. Considering silicon electrodes for lithium-ion batteries, it was shown that the AE data indicated that the electrode wear is associated to the development (charging) and vanishing (discharging) of the crystalline phase. The acoustic activity reaches its maximum during the first charge (lithiation) and discharge (delithiation) and decreases rapidly with cycling.

2.6.3 Summary and Discussion

Advanced battery management systems are required to guarantee reliable and safe battery operation. Therefore, monitoring systems have to be implemented in order to provide an integrity assessment of the actual state. Several techniques such as OCV, CC, KF, and internal resistance studying aging mechanisms, as well as capacity degradation, were developed. Owing to the complexity of internal electrochemical mechanisms, SoC and SoH estimations are still a complicated task. However, SoC can be determined by available techniques with sufficient accuracy whereas the evaluation of SoH and the determination of the battery capacity are not yet satisfactorily solved. Newly, the Acoustic Emission Technique is proposed as an alternative method for SoH estimation [KGCT13, EIR11, Hir12]. Research on this topic demonstrated the ability of AE to detect and identify different aging mechanisms (phase transformation. intercalation, ...). Nevertheless, a precise statement about the actual SoH could not be achieved.

3 Development Concept of an AE-based SHM System

The technological improvements in sensing, acquiring, and processing approaches has significantly contributed to the development of advanced SHM systems. However, the majority of AE-based SHM approaches cited in the previous chapter is not appropriate for a real-time application. They are limited to online sensing and acquisition while processing and interpretation of the data are usually realized at a later point in time. In addition, many presented algorithms are not suitable for real-time implementation. As a consequence, diagnosis cannot be instantly performed, and an immediate intervention cannot be achieved. This chapter presents the development of a more accurate and cost efficient SHM system able to analyze AE data in real-time through implementation of filtering modules in FPGA. First, the general process and the main components of SHM system are explained. Second, a description of the developed measurement chain used for sensing and acquisition of AE signals is provided. Here special attention is given to the FPGA and its advantages over other technologies regarding the real-time implementation of digital signal processing algorithms. Furthermore, the design and FPGA implementation of STFT module are presented, and the ability of the real-time application of the developed system is demonstrated. In the last section, necessary arrangements for settings and the evaluation of the used instrumentation with respect to dispersion sensitivity and sensor location are presented.

During the progress of this work, parts of this chapter have been published/ demonstrated in [BDS11, DS11]

3.1 SHM Process

The development of an SHM system involves four interrelated important components [SUS13]. These components include

(i) Structure: defined by type of material, design, nature of damage, physical phenomena, and accessibility.

(ii) NDT method: determines the scheme for SHM (passive/active or local/global).

(iii) Sensing technology (Hardware part): involves sensor system, data acquisition system, and other instrumentation used to record and store the data.

(iv) Signal processing tools (software part): contains basic algorithms, advanced filtering techniques, pattern recognition and classification approaches. The properties of these components define the applicability and the performance of the SHM system.

In Fig. 3.1, an illustration of the main components of SHM system is shown.

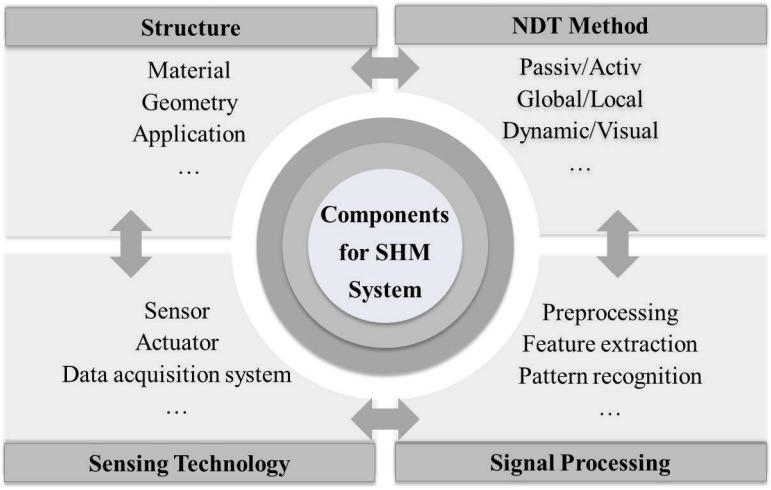

Figure 3.1: Components of structural health monitoring system

The principle of SHM systems is based on the measurement and analysis of the structural response of a structure with the aim of identifying, localizing, and quantifying the damage. The SHM process, adapted for various applications, consists of four sequential levels supported by a multi-layer data processing architecture and is described in [FW07] as following:

1. Damage detection: this level represents the primary objective of an SHM system. In this stage, information regarding the existence of damage and how to distinguish between signal changes due to structural damage and changes related to environmental noises are given at an early stage with a minimum false rate.

2. Damage localization: this level provides indication of the probable damage position and can determine where the damage occurs.

3. Damage assessment: this level is a main research focus that receives high attention in the literature. This processing stage deals with damage characterization, identification, and classification. It provides information about type and size/severity of the damage.

4. Life prediction: this level concerns the progressive deterioration of the structure, the residual structural life estimation, and prediction of possible breakdown.

Levels 1 to 3 build the diagnostic part of the SHM process which is fundamentally considered as a statistical pattern recognition paradigm [FDN01]. This paradigm is strongly related to considerations concerning safety, costs, and environment. Common SHM systems are often able to perform level 1 and level 2, but are not capable of identifying and estimating accurately the damage severity. The procedure for damage diagnosis involves operation evaluation (implementation of damage identification capability), data acquisition (sensing, storage, and transmittal hardware), feature extraction (selection of damage sensitive parameters, and reduction of data quantity), and classification. The main objective of this thesis is to address the damage diagnosis in the context of AE technique by focusing on the measurement and the signal processing chain.

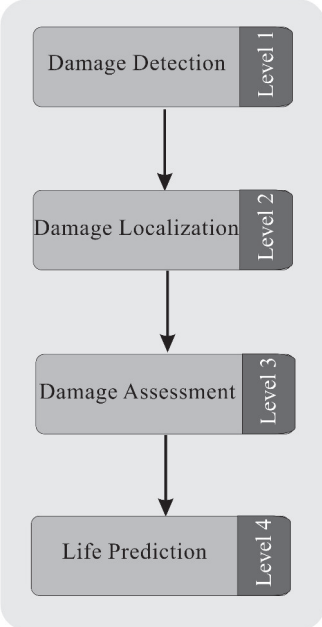

Figure 3.2: Main levels of SHM process according to [SUS13]

The concept of the developed SHM system is illustrated in Fig. 3.3. The adopted design allows the implementation of the SHM system in many application fields independently from applied materials and type of damages. The multi-layer signal processing chain defines the core of the damage identification system because of the challenges regarding the effective interpretation of the complex AE data. Furthermore, AE signals have to be recorded using a high sampling rate which produces a large volume of data not always easy to manage, analyze, and interpret.

The multilevel processing approach consists of four modules:

Preprocessing: it is a necessary step to improve the AE signal quality. Preprocessing approaches used in this work include normalization, centering (zero offset correction), whitening, and filtering (denoising).

Feature extraction: this module extracts the potentially damage-sensitive features from the preprocessed AE signal. A feature is defined as a single-valued quantitative characterization of a signal. A damage related feature should remain unaffected by varying operational condition. In this thesis, frequency- and time-frequency-based features were extracted using several advanced filtering techniques such as STFT and CWT in order to detect signal changes and to establish a relationship between these features and possible damage.

Feature selection: this module concerns the dimensionality reduction of the extracted features and the selection of the most representative and less redundant features by using statistical approaches such as PCA and KDE. Further, specific patterns can be determined and assigned to the related damages. This step is essential to improving the classification accuracy and to increasing the computational efficiency.

Classification: this module deals with the classification of the defined patterns into different classes corresponding to the different failure modes. Compared with the other modules, the classification module is complex and needs a certain mathematical background. The classification can be performed using supervised or unsupervised approaches. In this thesis, a multiclass SVM is applied allowing the automated classification.

The introduced signal processing approach represents the general process of damage detection, identification, and classification. A detailed description of the signal processing chains utilized in each experiment will be introduced later.

The developed SHM system aims at noticeably enhancing the identification and classification of damage mechanisms and also proving the efficiency of the applied multilevel processing approach. The presented methodology will allow an automated structural health monitoring and therefore would be an important step forward in the development of safe and reliable structures.

It should be noted that, there is no predetermined processing approach, able to solve all problems for all structures. The signal processing methods have to be adapted to the measured AE data which depends on experiment, test duration, and operational condition. This will be demonstrated in the next chapters by three application examples.

3.2 Measurement Chain

A number of experiments have been carried out to study the AE behavior in different materials/structures. The measurement chain and experimental equipment were kept as constant as possible throughout all tests conducted in this thesis.

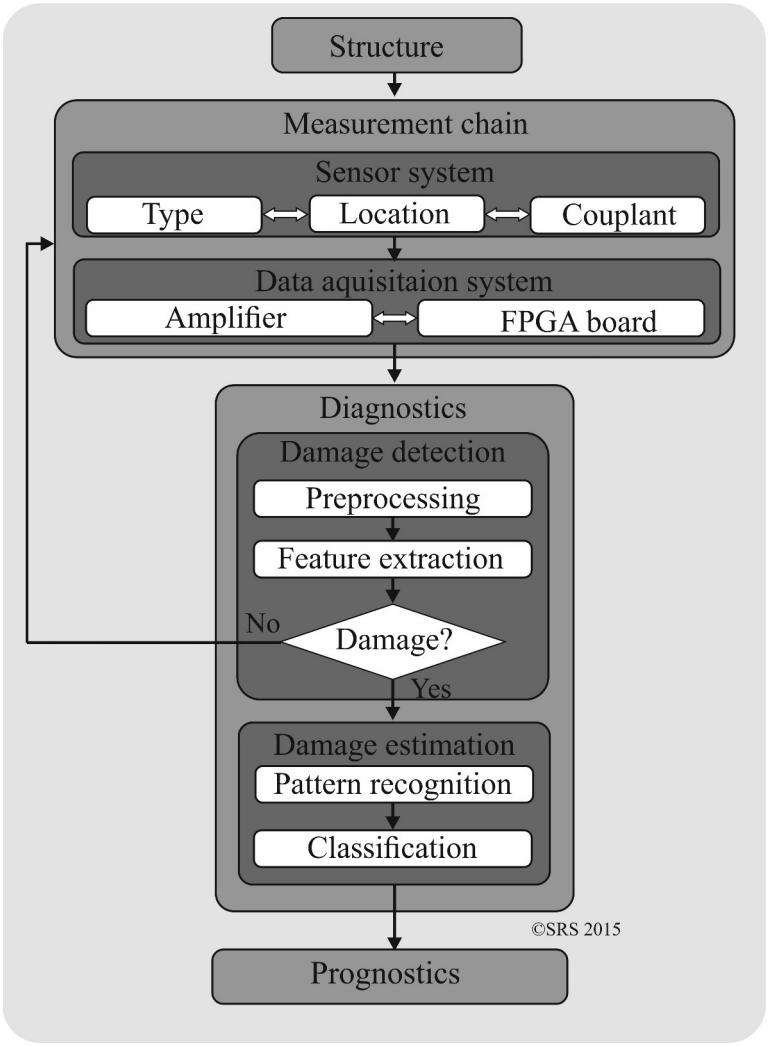

Figure 3.3: Development process of the structural health monitoring system

3.2.1 Sensing System

An AE-based SHM system requires a performant and sensitive sensing system able to measure material changes of relative small dimensions and very short duration. Principally, a sensing system includes transducer, couplant medium, and amplifier.

Transducer

The quality of the acquired AE waves strongly depends on the sensor technology. Therefore, AE transducers have to meet certain specifications. The sensors should be highly sensitive to the presence of damage and low sensitive to environmental noises, small, and easy to couple. In addition, AE transducers should have a nearly flat response over a wide frequency range, easy electrical wiring, and an optimal

reliability cost ratio. Unfortunately, despite all efforts realized in this area, there is no transducer that fulfills all these requirements. However, sensors based on piezoelectric materials are among the most suitable transducers used to sense micro surface displacements [Shu02].

Piezoelectric element transforms mechanical vibrations into electrical voltages and vice versa. Piezoelectric materials based on lead zirconate-lead titanate (PZT) are commonly used due to their strong electromechanical coupling, low cost, and robustness. Moreover, they are manufactured in diverse forms and dimensions which assist in spreading their application area.

In terms of frequency response, AE transducers can be divided into broadband sensors and resonant sensors. Resonant sensors are characterized by a high sensitivity around the resonance frequency and a good signal to noise ratio. Though, frequencies near from the resonance frequency and frequencies far from the resonance frequency are transmitted very differently. On the other hand, broadband sensors have an ideally flat frequency response allowing a similar treatment for all frequencies. Contrary to resonant sensors, broadband sensors are more sensitive to background noise [OGOP06].

The selection of a convenient transducer is very important, in term of sensitivity, for the transfer of the AE waves. Hence, in this work, low-cost piezoceramic components with wrap-around electrodes manufactured by PI ceramics were chosen. The sensor is disc-shaped and has a diameter of 10mm and a thickness of 0.55mm, resulting in a serial resonance frequency of 3.6 MHz.

To minimize the attenuation of the emitted AE signals, the sensor has to be glued as close as possible to the damage zone and should always have a full face contact on the structure [ZPS12].

Couplant

To obtain an effective transmission of AE waves, a good coupling of the sensor to the test structure is necessary because AE waves are not effectively transmitted through air that represents a severe acoustic impedance mismatch. Even an extremely thin air gap between sensor and structure prevents efficient AE energy transmission. Couplant effectiveness is determined by acoustic impedance, acoustic absorption, and application thickness [TZA08]. Couplants can be viscous, nontoxic liquids, gels, or pastes. A number of common substances such as grease, water, silicon, and glue can be used as couplant medium [TZA08]. The latter one is also able to hold the sensor securely in place so that no further clamps or tapes are needed. To minimize the attenuation, a thin couplant layer is required. In this work, a single component adhesive made of cyanoacrylate is used. The medium is free of grease and cures at room temperature [BBHF07]. The used glue makes the coupling between the sensor and the surface of the plate permanent and very stiff.

The electrical insulation provided by the couplant is not sufficient. Therefore, to ensure complete insulation, a very thin polyvinyl chloride (PVC) layer with an appropriate acoustic impedance and attenuation was glued between transducer and surface of the structure. A schematic representation of the PZT ceramic and insulating layer attached to an arbitrary structure is depicted in Fig. 3.4.

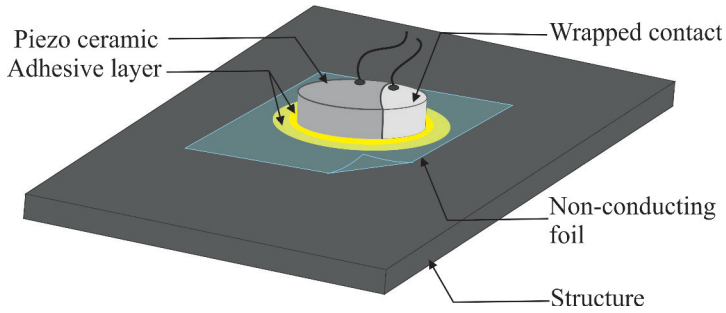

Figure 3.4: Schematic representation of the PZT ceramic and insulating layer attached to an arbitrary structure

Preamplifier

The piezoelectric voltage is often very feeble; hence preamplifiers are used to magnify the recorded AE signals and to reduce background noise. Preamplifier should be placed close to the sensor (up to one meter) to avoid pickup of electromagnetic interference. Typically, preamplifier providing a gain of 40 dB and a flat frequency response are used.

The developed preamplifier is characterized by high input impedance, low output impedance, and high dynamic range. Additionally, it comprises an embedded balanced potential divider to ensure the functionality of the A/D-converter by avoiding exceedance of the maximum input voltage. The balanced potential divider is designed such that the ratio can be varied by DIP switches from 1:1 to 4:1 conversion. Accordingly, the output of the amplifier can be adjusted to special applications to match the maximum input ratings of the resilient A/D-Converter [Det11].

3.2.2 FPGA-Board

The rapid development of digital technologies has highly improved the digitization, acquisition, and storage of AE data. Today, a wide range of systems are available allowing fast and multiple acquisitions. For reasons of costs and implementation flexibility, a special system based on FPGA was developed capable of testing, implementing, and evaluating complex digital signal processing algorithms.

Field Programmable Gate Array is configurable and re-programmable semiconductor device consisting of logic elements, I/O blocks, interconnection wires, and

switches [BV00]. Logic blocks are look-up tables (LUTs) which contain storage cells used for implementation of small logic functions. Compared to Digital Signal Processing (DSP) engine, FPGAs provide the advantages of lower cost, shorter design cycle, flexibility. They can be graphically programmed. In terms of density and speed, new FPGAs can support double-precision floating point arithmetic allowing the implementation of complex algorithms [HU05]. This advantage increases the effectiveness of highly configurable hardware and can spread their application area. To program hardware specifications, Hardware Description Language (HDL) is required. In this work, Very High Speed Integrated Circuit Hardware Description Language (VHDL) is used to implement several filtering algorithms in a Xilinx Spartan 3A FPGA. Beside the FPGA, the utilized board is equipped with AD-converters with a resolution of 16 bits and maximum sampling frequency of 25 MHz. The AD-converters are directly connected to the preamplifier allowing fast discretization of the recorded AE signals.

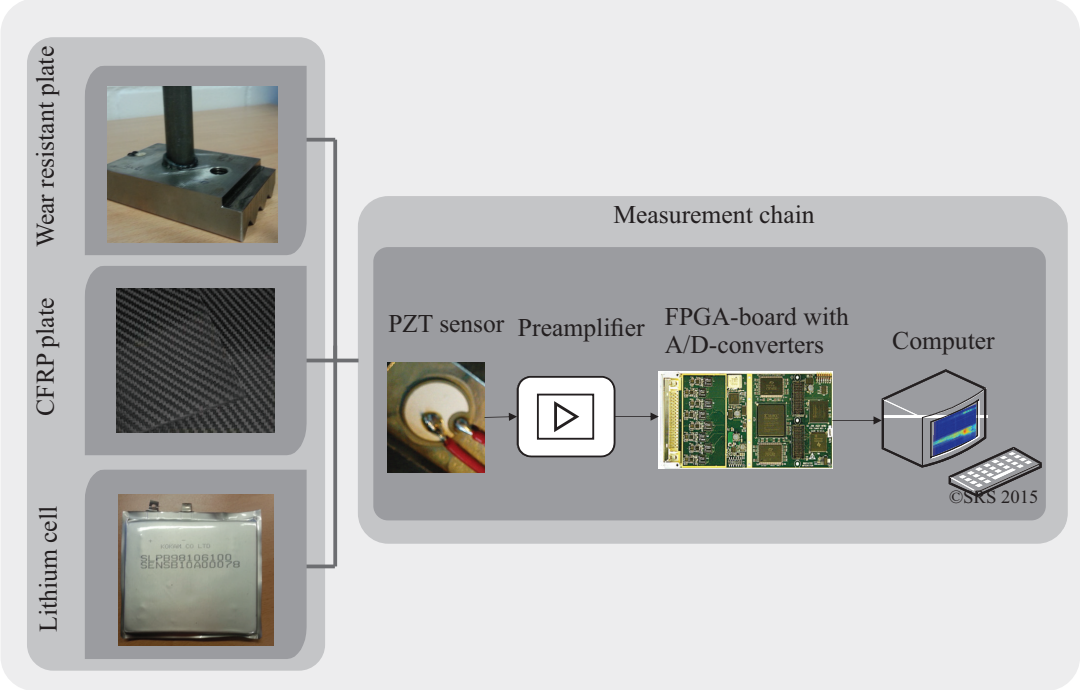

Figure 3.5: Schematic diagram of the developed measurement chain easily adaptable to different structures

3.3 FPGA-based Implementation of STFT module

During the last years, the use of FPGA has seen a remarkable increase in the development of SHM systems. Liu et al. [LY08] have conducted an FPGA-based wireless station associated with a piezoelectric element to identify damage in aluminum plate. In [MMV+09] the application of FPGA for on-line monitoring and detection of defects in laser welding is demonstrated. Azarbayjani et al. [AJEOT11] presented an innovative field application of SHM using FPGA and wireless communication technologies to monitor a reinforced concrete bridge. Wandowski et al. [WMO+13] reported on the realization of an FPGA-based embedded signal processing subsystem through implementation of filtering algorithms in order to localize damage in aluminum alloy plate. Fast Fourier Transform is one of the most important processing approaches that are implemented in FPGA for monitoring purposes. It represents a challenge in terms of execution time, required device area, trade-off between, and architecture of pipelined-streaming.

3.3.1 Design process

The software platforms Matlab, Simulink, and the Xilinx System Generator (XSG) are used for the design and implementation of an STFT module. System Generator is a "system level modeling tool that facilitates FPGA hardware design" [Xil12]. It extends Simulink in many ways to provide an environment that is well suited to hardware design. The tool provides high-level abstractions that are automatically compiled into an FPGA.

The Hardware in the loop co-simulation of XSG provides the ability to "incorporate a design running in an FPGA directly into a Simulink simulation" [Xil12]. Hardware-Co-simulation compilation targets automatically generate a bitstream and associate it to a block. This block is used in a Simulink model such an ordinary XSG block. The bitstream contains the hardware associated with the STFT module and also contains additionally interfacing logic that allows XSG to communicate with the module by connecting the FPGA and the PC using a JTAG-USB cable. During simulation, this block interacts with the FPGA, automated tasks such as device configuration, data transfers, and clocking. This allows a faster simulation time and easier hardware verification. In Fig. 3.6, the development process for the design and implementation of algorithm into FPGA is shown.

The STFT is designed using FFT module and an FIFO block that realizes the windowing of the signal. In Fig. 3.7 a detailed view of the different XSG blocks and the different control signals used in the STFT module is shown. The core of the module is the FFT block. It computes 4096-points Discrete Fourier Transform (DFT) using the radix-4 Cooley-Tukey algorithm. The proposed architecture is very efficient for FFT computation.

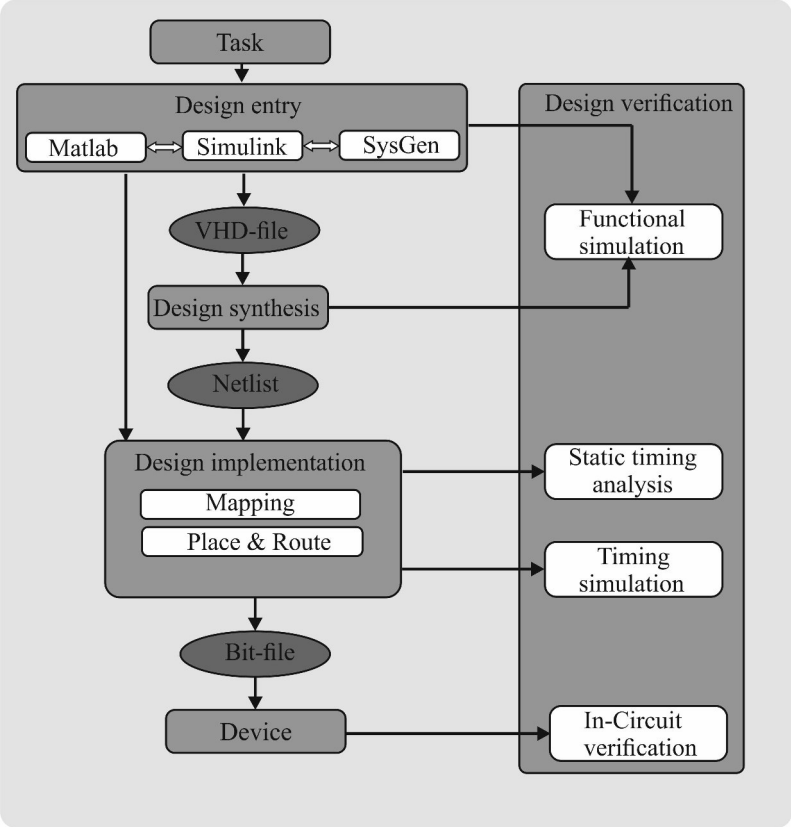

Figure 3.6: Development process for the design and implementation of algorithm into FPGA [Xil12]

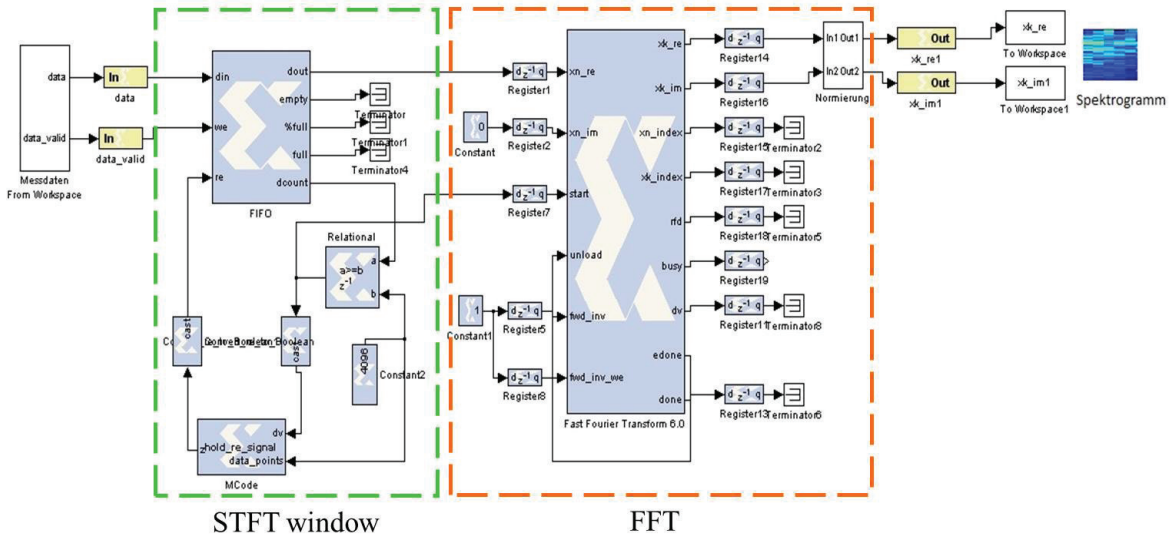

Figure 3.7: Detailed overview of the System Generator STFT module [BDS11]

3.3.2 Implementation Results

Continuous AE signals, as well as mixed AE signals, were used to test the ability of the designed STFT module. The severity of the change can be indicated by typical transient frequencies which appear in the STFT spectrum.

Here, two simulation methods have been used. First, simulation of the designed module, in Simulink, is performed in order to obtain a reference result. Secondly, the STFT module implementation in the FPGA is conducted using HW co-simulation. The results of the simulation and the implementation are shown in Fig. 3.8. It can be seen that results obtained from the HW co-simulation are identical to those performed in Simulink. The similarity of the results proves the ability of the developed module as well as the application of the FPGA board for the realization of online damage detection.

It can be concluded that approaches towards integration of FPGA technologies in SHM systems permit the continuous and real-time monitoring as well as the simultaneous processing of many sensors data. This overcomes a fundamental challenge met by actual systems.

3.4 Preliminary tests of the Measurement Chain

The measurement chain is developed with the goal to be implemented and used in several applications. Therefore, specific tests and test setups have been carried out to investigate important effects that have a major impact on the measured AE signal. In this part, the influences of the couplant medium, the sensor arrangement and the sensor location on the AE signals are discussed in details. The main objective of the preliminary tests is to understand the limitations and the use of the measurement chain in order to select the proper equipments that allow an exact reproducibility of the different experiments.

3.4.1 Effect of the Couplant Medium on AE Signals

The choice of couplant medium depends on many factors. In this thesis, the factors acoustic transmission and long-term stability are of high importance given the type and duration of the conducted experiments.

Principally, the amplitude is the parameter the most affected by the couplant medium. Accordingly, vibration tests focusing on the signal amplitude were performed.

Single-component cyanoacrylate adhesive, double-side adhesive tape, and silicon grease were selected for testing the influence of the couplant medium on AE sensor sensitivity. The measurements were performed on 350mm x 350mm CFRP plate.

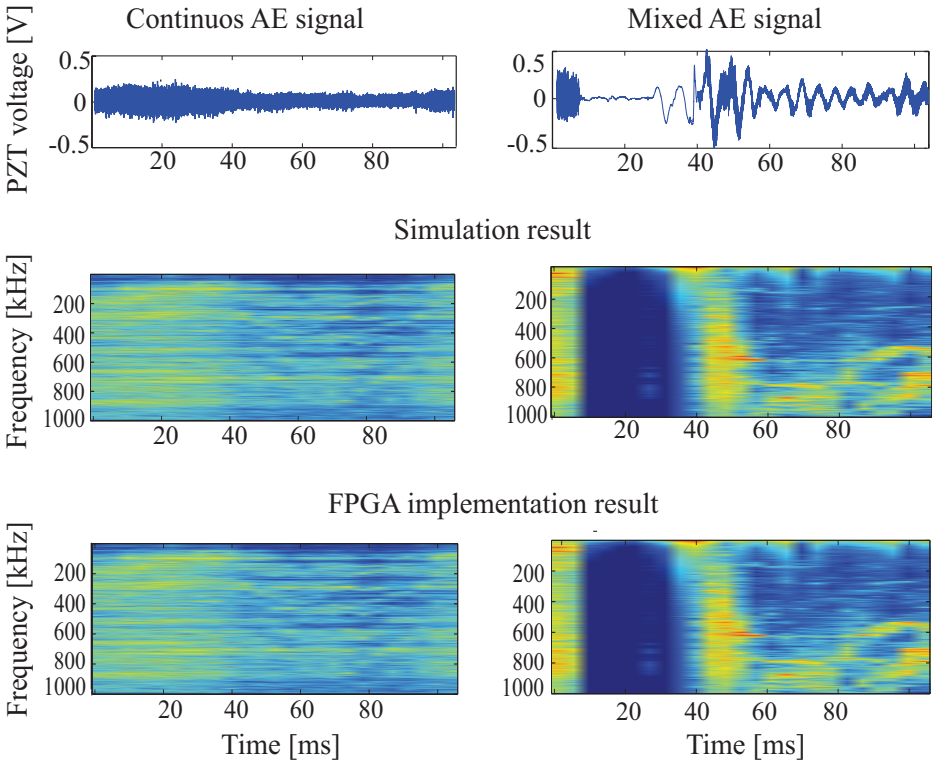

Figure 3.8: Results of the simulation and FPGA implementation of the STFT module [BDS11]

Three PZT sensors were mounted on the surface, equidistant from the plate center using the different coupling mediums. The CFRP plate was excited at the center using a Bruel & Kjaer 4809 electrodynamic vibration shaker. The excitation sinusoidal signal with an amplitude of 500 mV and a frequency of 20 Hz was generated using a function generator and amplified using a Bruel & Kjaer 2706 power amplifier. The response signals measured by the three PZT sensors are shown in Fig. 3.9.

From the amplitude of the signal responses, it can be observed that the couplant medium has a significant effect on the sensitivity (amplitude) of the sensor. Single-component cyanoacrylate adhesive provides the highest acoustic transmission. The thereby transmitted signal has an amplitude of 425.5 mV that represents 85.1% of the excitation signal. Double-sided adhesive tape has an acceptable acoustic transmission. The amplitude of the response signal amounts 210.9mV which is equal to 42.8% of the applied signal voltage. Conversely, the response signal silicone grease shows a poor acoustic transmission which does not exceed 9.01%. This was expected because during vibrations the PZT sensor was not permanently fixed to the plate. In conclusion, results show that the couplant medium can suppress the amplitude of the measured AE signals and therefore strongly affect the sensitivity

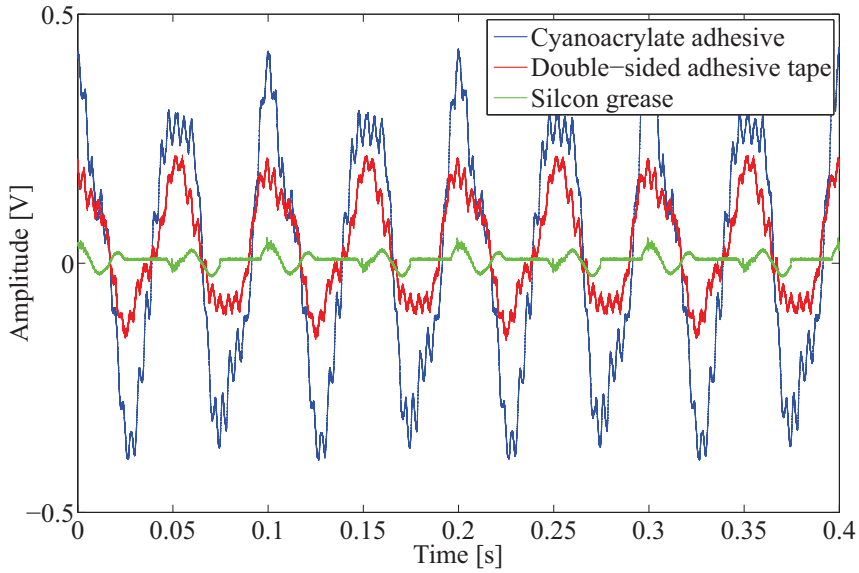

Figure 3.9: Response signals measured by three PZT sensors bounded using Single-component cyanoacrylate adhesive, double-side adhesive tape, and silicon grease

of the measured chain.

3.4.2 Evaluation of the directional sensitivity

As introduced in sec. 2.1.2, wave propagation properties are dependent on the plate thickness. Therefore, in case of thick plate, it is essential to test the sensor arrangement in terms of attenuation and directional dependency of AE signals in order to ensure that the sensor is mounted appropriately.

In this thesis, impact hammer tests were performed on a metal plate to investigate the propagating direction effects on the amplitude and frequency of the AE signals.

Transient stress waves were generated in a thick wear-resistant plate with dimensions of 104mm x 58mm x 13mm by applying a manual low energy hammer impact. Three PZT sensors were bounded on the structure, one on the upper surface, one on the right side face, and one on the front side face. The structure was impacted at the same position during all tests. The impact location was as possible at an identical distance to the three sensors. A sketch of the wear-resistant plate and the sensors arrangement is depicted in Fig. 3.10.

The Acoustic Emission responses of sensor 1 and sensor 2 are shown in Fig. 3.11. It can be seen that there is a huge difference between the amplitude values. The peak amplitude of the signal measured by sensor 1 is equal to 4.83 V, while the peak amplitude of the signal measured by sensor 2 is equal to 0.97 V. In contrary, the

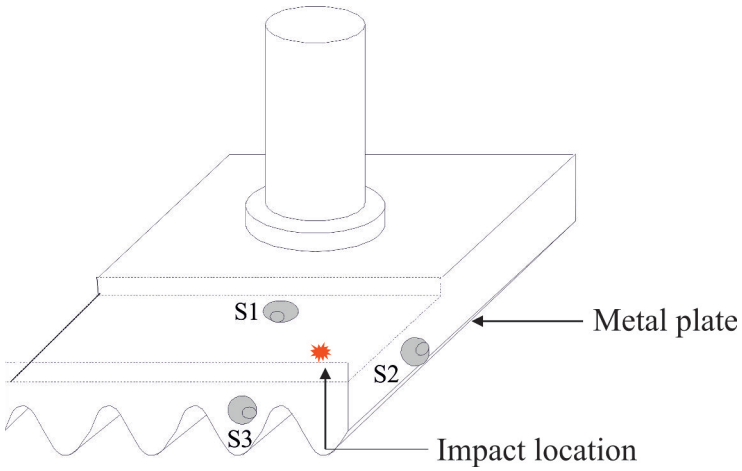

Figure 3.10: Sketch of the impact hammer test

frequency spectra indicate that the sensor responses are characterized by the same frequency components with narrow difference of the magnitude values.

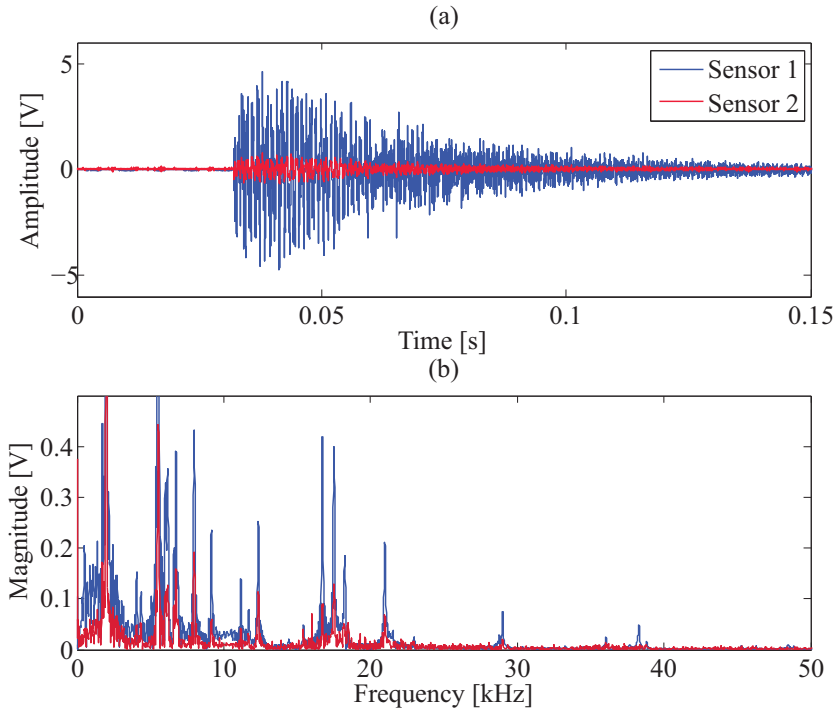

Figure 3.11: (a) Acoustic Emission responses of sensor 1 (upper surface) and sensor 2 (front side surface) and (b) the corresponding frequency spectra

In Fig. 3.12, the Acoustic Emission responses of sensor 1 and sensor 3 are observed. Also here, it can be seen that the amplitude values of the sensor responses differ significantly whereas the related frequency components are similar. However, the

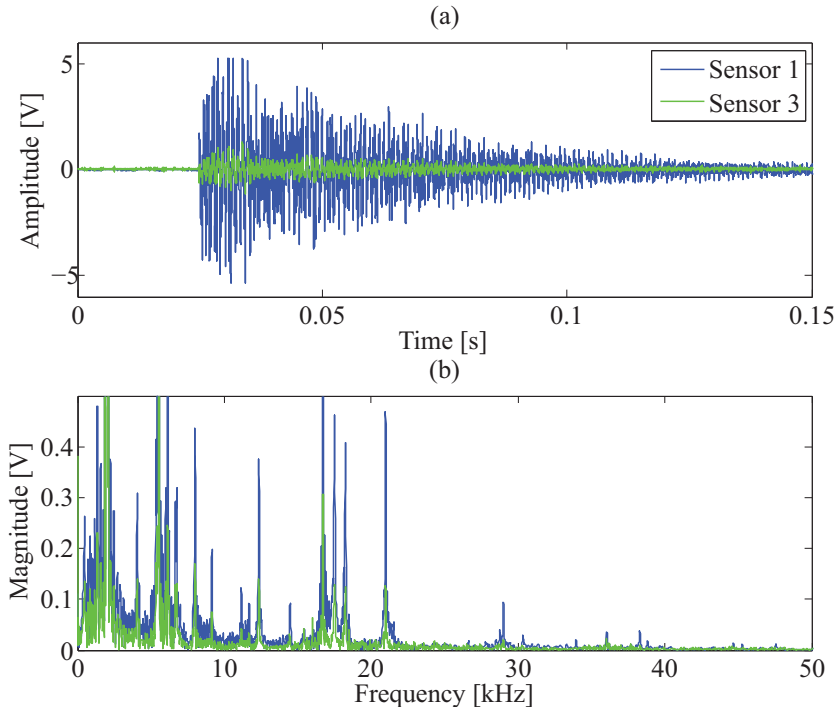

Figure 3.12: (a) Acoustic Emission responses of sensor 1 (upper surface) and sensor 3 (right side surface) and (b) the corresponding frequency spectra

magnitude value of the frequency peaks corresponding to the signal measured by sensor 3 is a bit smaller. A plot of the signal responses of sensor 2 and sensor 3 is depicted in Fig. 3.13 (a). As expected, the amplitude values of the measured signals are a quite bit different and the corresponding frequency spectra show a similar behavior.

From the impact hammer tests, it can be concluded that the sensor arrangement directly influences the signal amplitude. In contrast, the related frequency content does not depend on the sensor location and are qualitatively similar. In addition, the conducted tests are efficient in terms of repeatability on the frequency response, which was tested and confirmed.

3.4.3 Evaluation of the Sensor Location

The effect of the sensor location on the AE signals is commonly performed using pencil lead breaks tests (also called Hsu-Nielsen-Source). The test consists of generating artificial Acoustic Emission by breaking a pencil lead at selected location on a plate. Pencil lead breaks test is standardized under ASTM976-05 [AST05] and is considered as a simple test method that can repeatedly simulate broadband AE without affecting or damaging the plate.

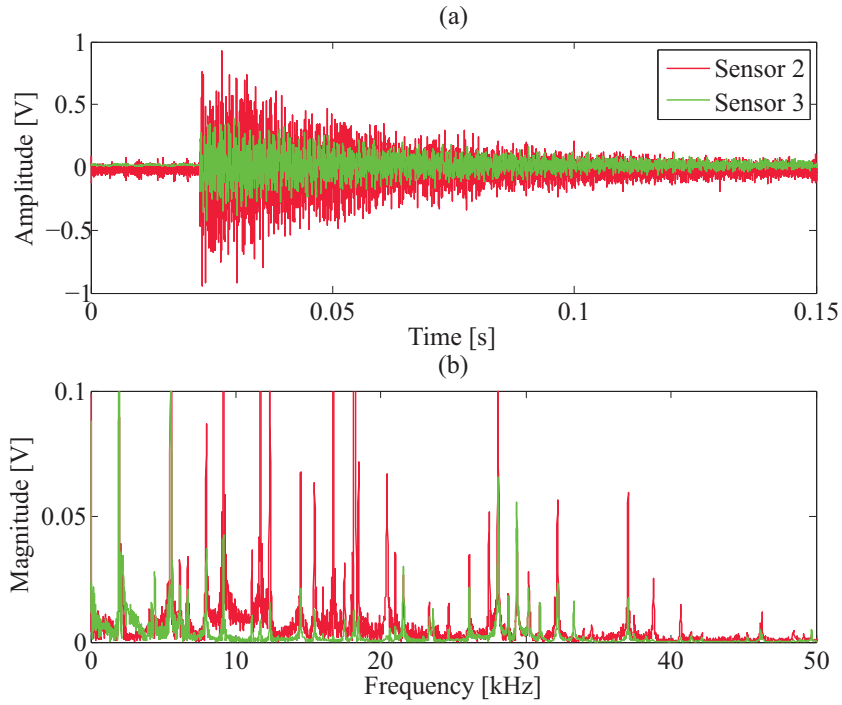

Figure 3.13: (a) Acoustic Emission responses of sensor 2 (upper surface) and sensor 3 (right side surface) and (b) the corresponding frequency spectra

To perform pencil lead breaks tests, pencil-lead with a diameter of 0.5mm and a length of 3 mm was used. In order to improve the repeatability of the test, the same lead length was broken for all tests and a circular ring was utilized to keep the angle of the lead and the material constant. Nevertheless, variations in the sensor response characteristics are not excluded.

The tests were applied to a CFRP plate with dimensions of 350mm x 350mm. Two PZT sensors were positioned at the same distance to the plate center. As indicated in Fig. 3.14, two lead break positions were selected to assess the response of the sensor regarding the AE source location.

The signal responses of sensor 1 and sensor 2 to lead break at equidistant position are presented in Fig. 3.15. It can be seen that the generated waves arrive at the sensors at the same time and with similar amplitude. It can also be observed that both signals have a peak amplitude of about 500 mV. The time-frequency analysis of the simulated AE signals, shown in Fig. 3.16, demonstrates that the signals possess the same frequency components.

As next, pencil lead break test was performed at a position close to sensor 2. As shown in Fig. 3.17 the simulated AE waves arrive at sensor 2 at an earlier time. It can be seen that the amplitude value of the sensor responses differ significantly and decreases with increasing propagation distance. In contrast, the time-frequency analysis of signal responses of sensor 1 and sensor 2, presented in Fig. 3.18, shows

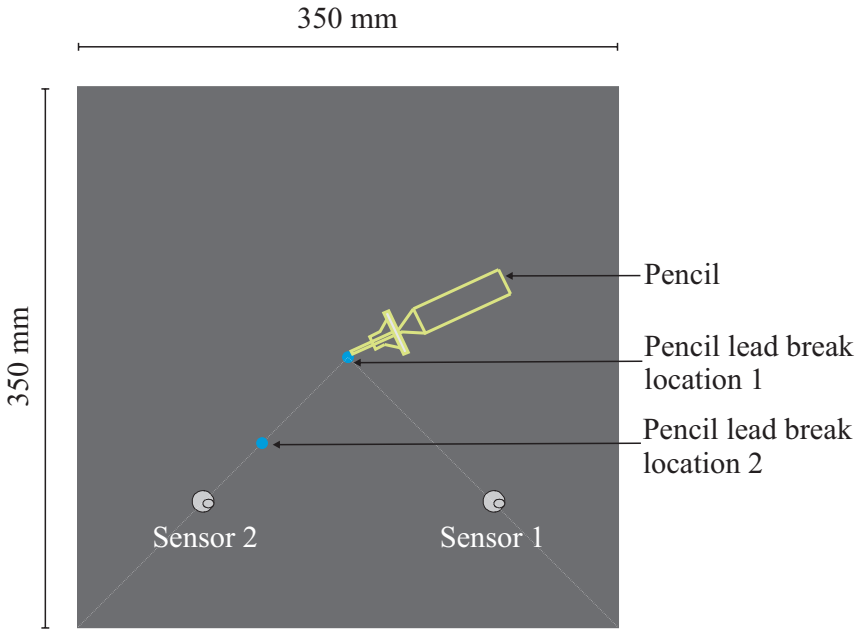

Figure 3.14: Schematic illustration of the pencil lead breaks tests

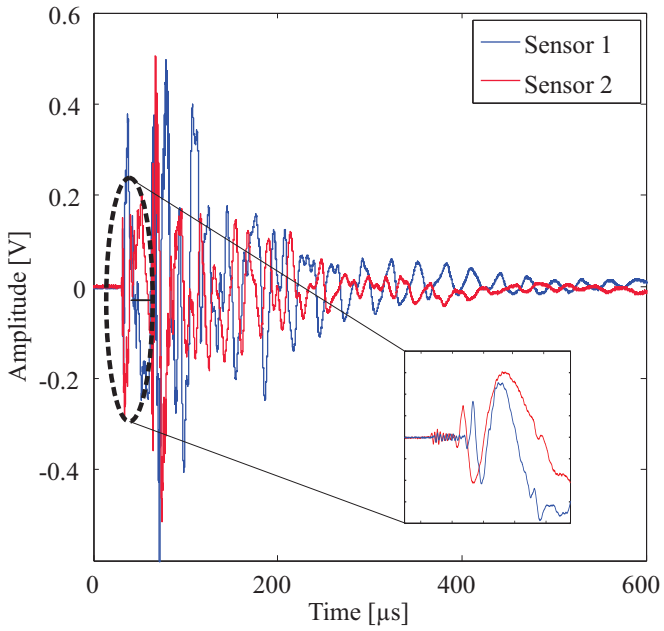

Figure 3.15: Signal responses of sensor 1 and sensor 2 to pencil lead break performed at an equidistant position

that the sensor location does not have any influence on the frequency components which remain similar.

It can be concluded that the sensor sensitivity can be affected by different factors.

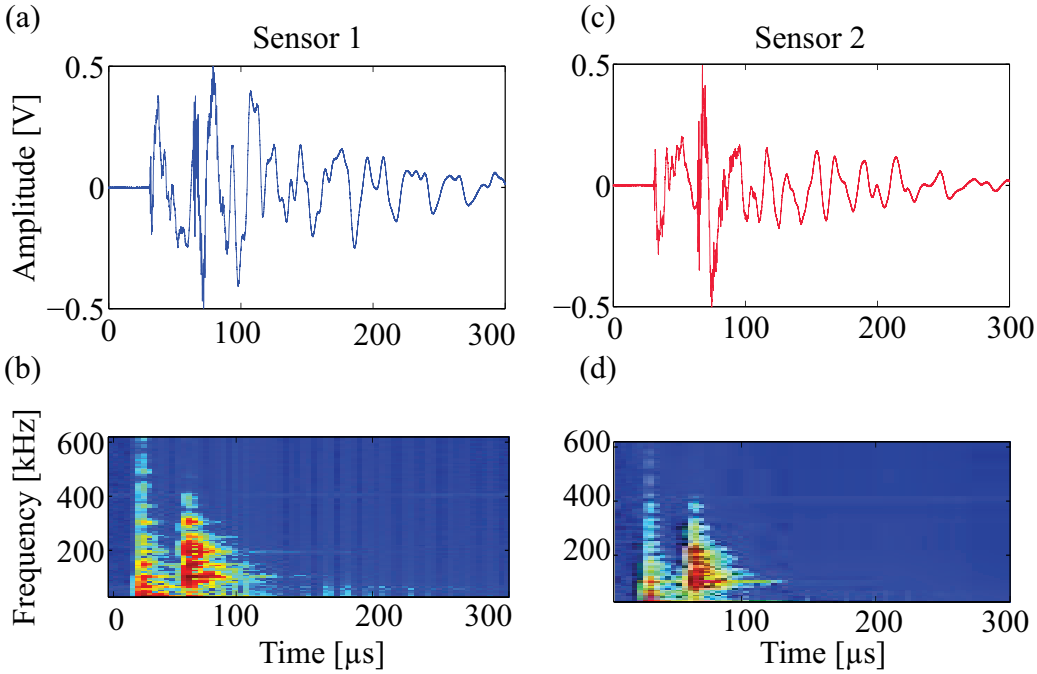

Figure 3.16: Time-frequency analysis of signal responses of sensor 1 and sensor 2 to pencil lead break performed at an equidistant position

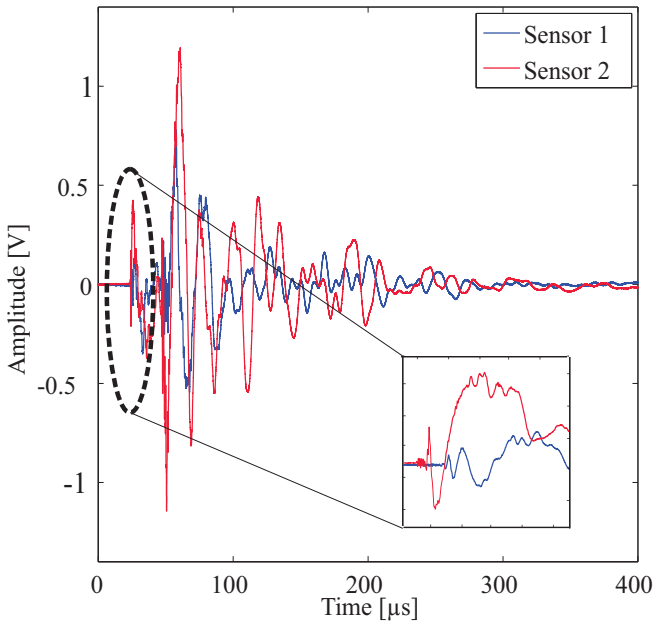

Figure 3.17: Signal responses of sensor 1 and sensor 2 to pencil lead break performed at a position close to sensor 2

The performed preliminary tests demonstrate that the amplitude is strongly dependent on couplant medium, sensor arrangement, and sensor position. By contrast,

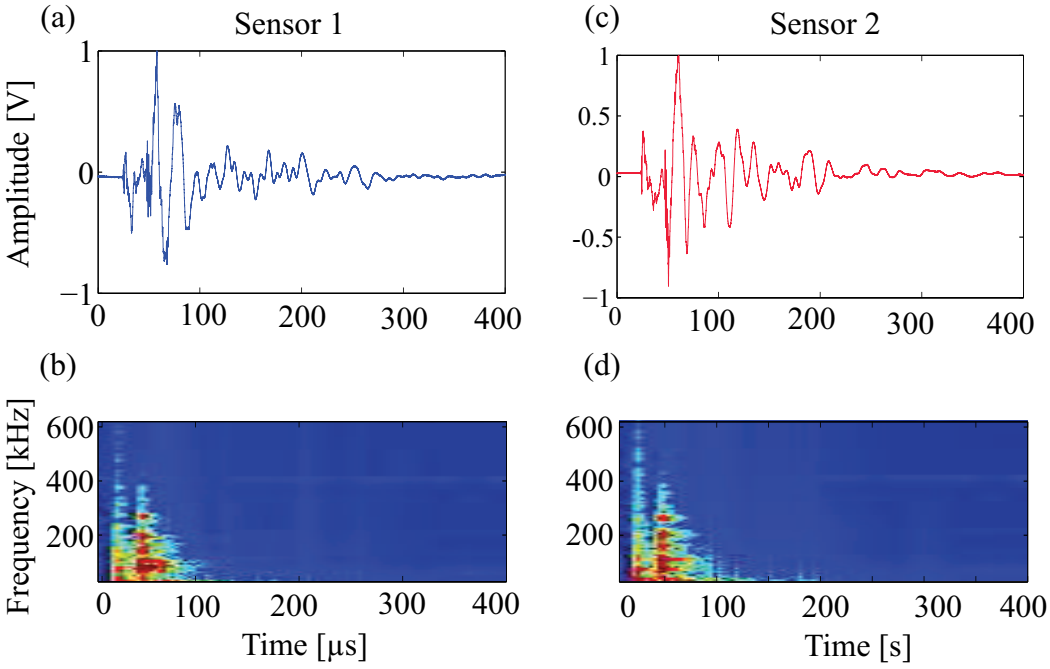

Figure 3.18: Time-frequency analysis of signal responses of sensor 1 and sensor 2 to pencil lead break performed at a position close to sensor 2

the frequency shows a better resistance to the above-mentioned factors and can be considered as the AE feature; the less influenced. Consequently, in this thesis, the investigation of damage mechanisms is mainly based on features extracted from frequency domain and time-frequency domain.

3.5 Summary and Conclusions

This chapter introduced the development concept of the SHM system with focus on the measurement chain used for all experimental tests carried out during this work. The FPGA-based equipment and the process of recording AE signals were explained, and the effectiveness of the developed hardware with regard to the real-time implementation of advanced filtering techniques was demonstrated. In addition, preliminary tests and test setups have been carried out to investigate important effects that have a major impact on the measured AE signal. Furthermore, the influences of couplant medium, sensor arrangement and sensor location on the AE signals are discussed in details and demonstrated through generation and analysis of artificial AE sources. The main objective of the preliminary tests is to understand the limitations and the use of the measurement chain in order to select the proper equipments that allow an exact reproducibility of the different experiments. All tests showed that the amplitude is the parameter the more influenced contrary to the frequency which remains unchanged. Therefore, the analysis of AE signals and

hence the damage detection will be mainly based on time-frequency analysis.

4 Acoustic Emission Monitoring of a Tribological System

This chapter presents the application of the proposed SHM system for online detection and automated classification of wear phenomena. The first section gives a general overview of wear process and the related failure rate. The second section is devoted to the experimental procedure including test rig and the developed signal processing approach. The third section concentrates on the experimental evaluation and validation of the SHM methodology introduced in Chapter 3. Furthermore, experimental results demonstrating the effectiveness of using AE-based SHM system to establish a direct correlation between state-of-wear and the generated AE are presented.

During the progress of this work, main parts of this chapter have been published in [BDS11, BS12b, BS13, BS15].

4.1 Introduction

Tribology is defined as "the science and technology of interacting surfaces in relative motion" [Ast06]. In addition to the complete field of wear and friction, tribology encompasses lubrication and boundary-layer interactions. Tribological phenomena such as wear and friction can be detected by visual inspections and surface observations. However, wear detection and monitoring are complex and difficult especially for materials under sliding conditions. Due to the permanent contact, the material surface remains during tests non-accessible for optical inspection. Therefore, tests have to be interrupted, and the specimen has to be removed from the test rig which causes significant loss of labor, cost, and time. Moreover, the above-mentioned methods can be realized at considerable expense for certain materials and in many cases they do not meet the industrial applications necessary requirements. Consequently, an online, automated, and continuous monitoring is necessary for the detection and identification of wear phenomena. During monitoring, the wear process is not periodically stopped and the test conditions (temperature, humidity, lubrication etc.) are not changed.

The severity of wear is application-oriented and depends on the related tolerable level of deterioration as well as to the load history of the system. Hence, this is

an individual characteristic that has to be quantized and quantified beforehand, so that the related knowledge can be also used to better understand the basic wear mechanisms (abrasive, adhesive and, surface fatigue) involved in system performance and failure.

System failure due to wear comprises different failure phases. The three major phases to be distinguished are

(a) The run-in phase (self-accommodation): this phase is characterized by an excessive wear generation, "which in most cases is not posing a danger to the future operation of the system" [GT08].

(b) The permanent-wear phase: this phase is characterized by an ideally constant failure rate.

(c) The wear-out phase (degradation): within this phase, the system failure is mainly caused by surface fatigue [GT08].

The failure rate of each phase can be described by the bathtub curve. The bathtub curve is a statistical description of the relative wear/failure rates against time that visualizes the failure rate during the wear process. The failure rate and the related curve shape change significantly dependently on the considered system and the operation condition.

During the wear process, materials emit energy in the form of high frequent mechanical vibrations. These emissions, defined as Acoustic Emission, propagate throughout the surface of the material as Rayleigh waves within the frequency range from 100 kHz to 1 MHz [EM08]. Thereupon, real-time measurement of the amount of wear and identifying the wear mechanism is possible using AET. For this purpose, the developed SHM system is applied to distinguish and interpret the different damage states occurred during sliding contact and thus, to establish a direct correlation between state-of-wear and emitted AE with regard to the three failure phases. In detail, the effects of the damage progression process have to be described quantitatively and qualitatively.

4.2 Experimental set-up and signal processing

To investigate the relationship between AE generation and state-of-wear of sliding contact system, a number of tests have been performed using laboratory test rig extended by the developed SHM system. The test rig is designed so that it tracks the real wear situation of an industrial scrap bailing press that is mainly applied in the automotive industry, especially in car body plants.

4.2.1 Test rig

The analyzed tribological system consists of two "wear resistant" plates with a martensitic microstructure. The plates are of different sizes (body: 150mm x

2100mm and counter-body: 60mm x 106mm) sliding against each other. The body is firmly clamped on the test rig. The counter-body is clamped to a sliding carriage which is connected to a differential hydraulic cylinder. The horizontal movement is generated and realized by an electro-mechanical valve. To accelerate the wear process, the system is stressed by an adjustable normal load performed by controlled pneumatic cylinder and a lever arm (double T beam). In addition, the test rig is equipped with several sensors and actors allowing the real-time controlling as well as the record of different measurements such as hydraulic pressure, normal force, position, and temperature. Long duration tests with fixed operating conditions (force, pressure, temperature) and variable parameters (lubrication type, lubrication interval, and plate hardness) were performed. A test consists of many sequential steadily repeated cycles. During one cycle, the counter-body strokes 38 times the distance of 50mm and pauses for 70s. In Fig. 4.1 the "wear resistant" plates and the related test rig construction is shown.

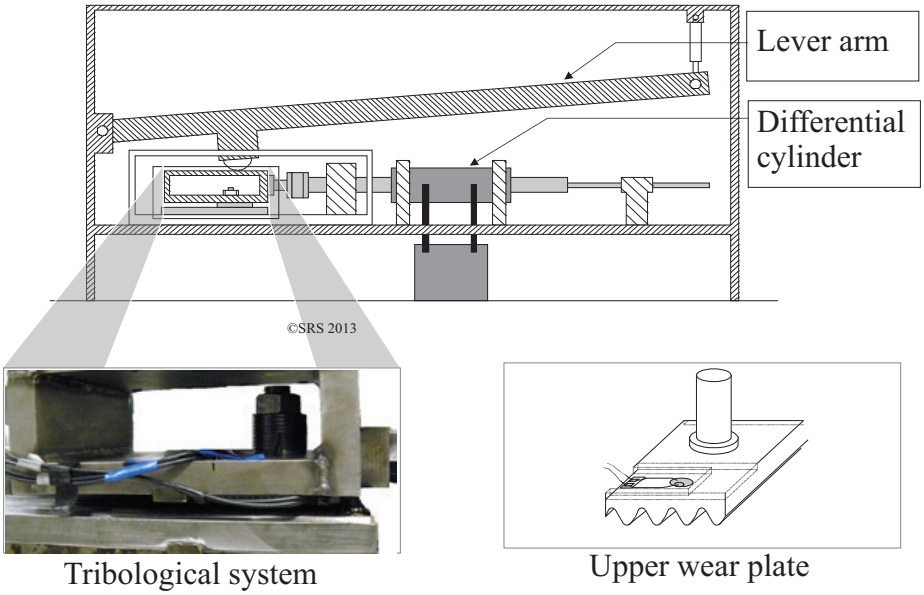

Figure 4.1: Sketch of the test-rig, Chair SRS, University of Duisburg-Essen, Germany [BS15]

To realize the AE measurements, the sensor was glued on the upper surface of the counter-body, as close as possible to the wear zone. The coupling between the sensor and the surface of the plate was permanent and very stiff. An appropriate sampling rate of 4 MHz is chosen to assure a high resolution of the discretized piezoelec-

tric voltage of special interest. For identifying AE properties, specific filtering and analysis functions including STFT and CWT are developed.

The complete experimental set-up and data acquisition scheme used for the experiments are presented in Fig. 4.2.

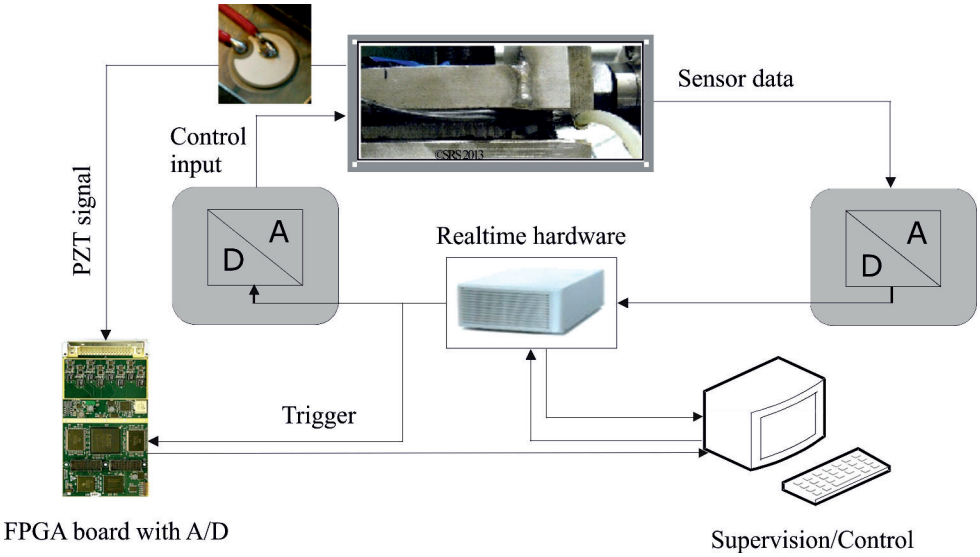

Figure 4.2: Sketch of the tribological system extended by the developed SHM system and the control unit, Chair SRS, University of Duisburg-Essen, Germany [BS13, BS15, BS12a]

4.2.2 Signal processing chain

One of the key challenges regarding the signal processing approach is the development of a successful approach capable to manage, analyze, and interpret the big volume of AE data recorded during the wear process without losing wear-relevant information.

The recorded AE signals are non-stationary and appear as transient signals with undefined waveform. Signal processing in time-domain is not efficient to extract frequency information of interest. However, a frequency-based analysis is limited to stationary and periodic signals and cannot retrieve the time related information. According to [LHL+12], the meaningful AE characteristics, occurring due to instantaneously physical character, vary in time and frequency. Hence, time-frequency analysis such as STFT and CWT are capable of revealing the AE specifications undetectable in the original signal and provide the possibility to evaluate the time-variant character of the frequency components.

In this thesis, a new approach for wear-state detection, identification, and classification is developed. The developed method involves a number of processing steps and

can be implemented in real-time. The proposed procedure is a multilevel processing approach comprising five processing steps. In order to extract relevant characteristics distinguishing different wear states from the related AE signals, a combination of STFT and CWT was performed. The analysis is mainly focused on the investigation of the frequency-based AE energy.

First, the recorded AE signals are converted into an appropriate format and STFT is cyclic applied to the preprocessed AE data. An additional band pass filter with the range of 40 kHz to 1 MHz is applied to extract frequency of interest. The STFT result of each cycle is then investigated for its frequency content to identify relevant transient events, amplitudes, patterns, etc. Secondly, based on the fact that high AE energy are referred to significant changes in the physical properties of the structure, frequency-based AE energy is generated by calculating the root mean square of the STFT power spectrum so that each cycle is represented by an energy value defined as

$$E(\omega) = |X(\omega)|^2, \tag{4.1}$$

where $X(\omega)$ defines the Fourier transform of the AE signals measured during one cycle.

Furthermore, to extract more relevant information corresponding to specific wear-states, the cumulative energy over the number of cycles was carried out. The cumulative energy is given by the equation

$$Cum(E) = \int E(\omega) d\omega. \tag{4.2}$$

The last step of the processing approach consists of the decomposition of the STFT power spectrum into four frequency levels. The AE energy contained in each frequency band is then analyzed by using CWT allowing the detection of specific patterns distinguishing the different wear states. This multilevel approach permits an effective computational performance regarding the analysis of large data set, making possible the extraction and selection of wear-related features without losing relevant information. An illustration of the proposed methodology is given in Fig. 4.3

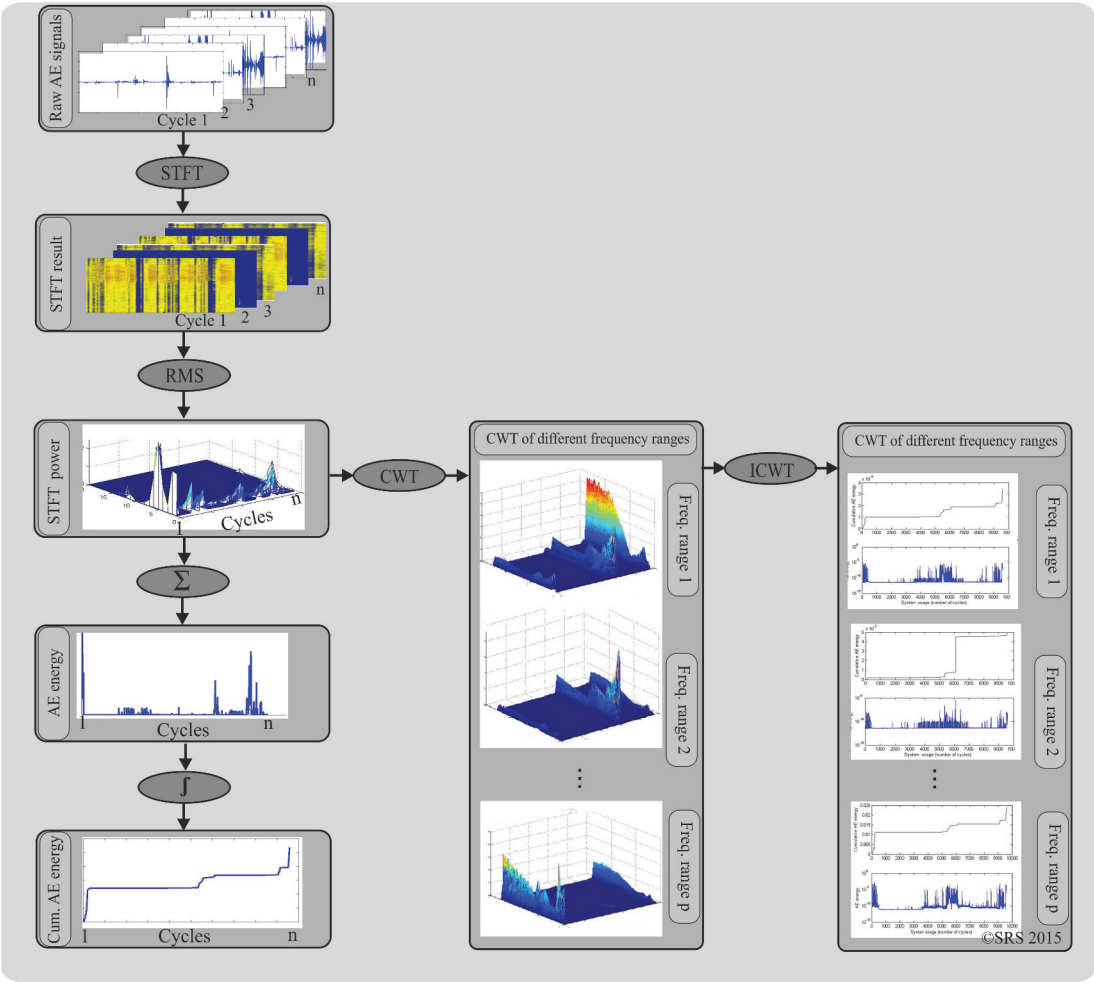

Figure 4.3: Overview of the developed signal processing chain

4.3 Experimental Results

Scanning Microscope Electron analysis

During the shaping process, a thin coating with very brittle microstructure occurs on the surface of the wear plates. Some tensile cracks can be observed in the coating before applying load. During the first hours of the application of the load this coating is eroded, particles scratch the surface leading to abrasive wear. After that, fatigue cracks appear and may grow into the ground material. Additionally some small cracks appear near the surface. In Fig. 4.4 Scanning Microscope Electron analysis (SEM) of a plate sample after 40 days endurance test is shown. The identified main wear effects are related to abrasive wear and surface fatigue. Surface fatigue initiates and propagates cracks after a certain number of cyclic events and leads to system failure.

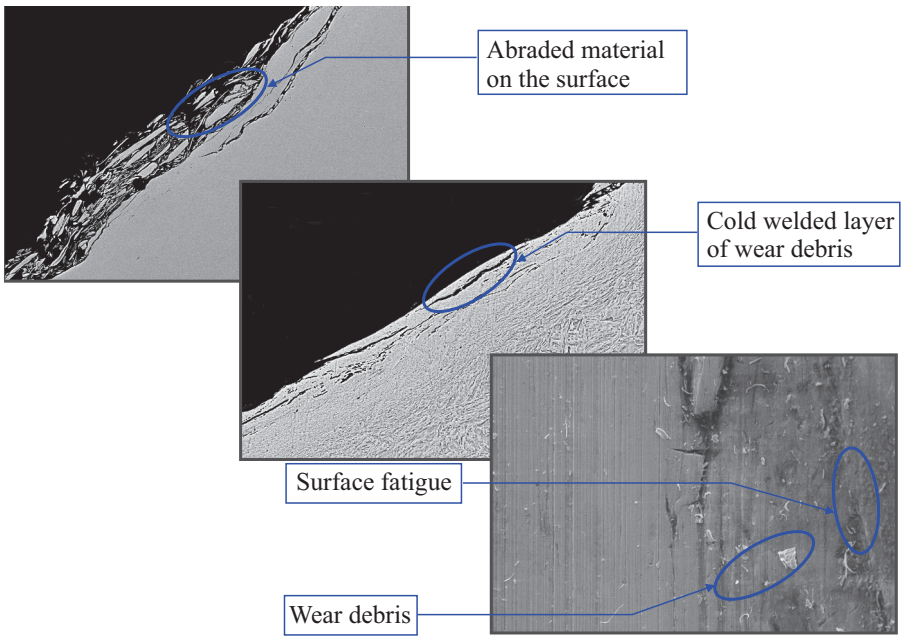

Figure 4.4: SEM analysis of plate surface after 40 days endurance test, results from tests realized at Chair SRS, University of Duisburg-Essen, Germany [BS15]

Short-Time-Fourier-Transform of AE signals

To investigate a correlation between these physical effects and the occurring Acoustic Emissions, transient events and characteristic frequencies for these stochastically appearing effects were analyzed. The severity of the wear process change should be indicated by characteristics of transient events, amplitudes, and specific frequencies appearing in time and/or frequency domain.

In Fig. 4.5, as illustration examples, segments of the raw AE signal and the corresponding STFT result generated during three different process cycles are shown. Burst and continuous AE signals are detected. The type of AE signal depends on the nature of the energy release. Burst type AE signals correspond to a discrete micromechanical event well separated in time, characterized by short duration and high amplitude [GO08]. Acoustic Emission bursts are principally caused by phase transformations and crack initiation and propagation in a brittle material [JMV+05]. Continuous AE signals are closely spaced in time, characterized by low amplitude and caused by plastic deformation, diffusion-controlled phase transformations [JMV+05]. The detected AE signals show dissimilarities in amplitude, frequency, severity, and waveform. This proves that AE changes when the wear mechanism changes. In figure 3 is shown that the STFT results of the signals in run-in- and wear-out phase are nearly identical in comparison to the STFT results of the signal measured during the permanent wear phase.

To extract relevant characteristics distinguishing different wear stages from related

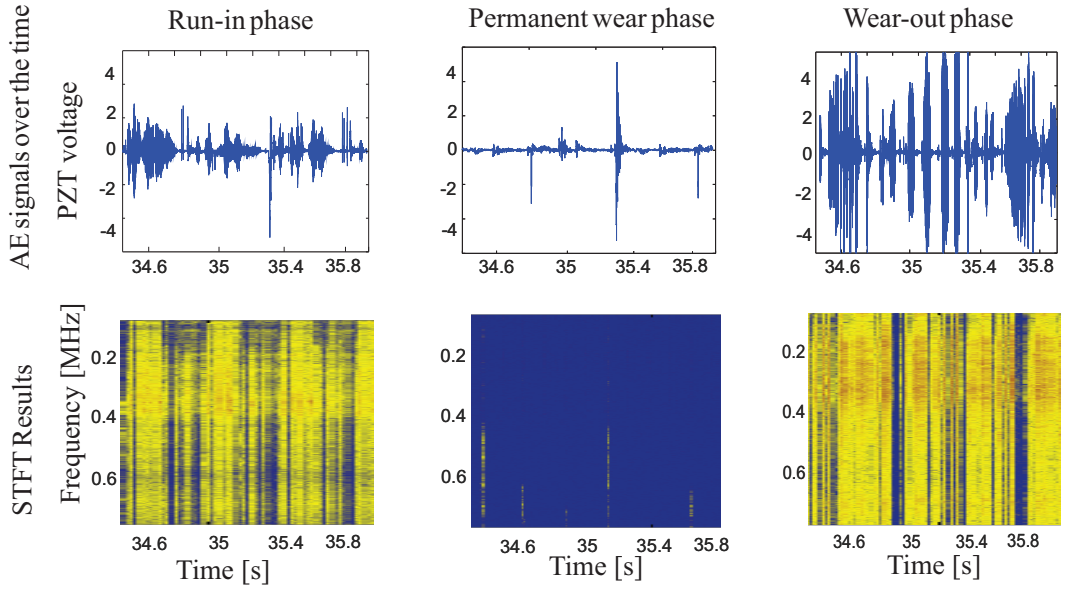

Figure 4.5: STFT analysis of AE signals generated during run-in, permanent wear, and wear-out phase [BS13]

AE signals, the analysis is focused on the AE energy generated during the wear process. To calculate the AE energy, the STFT X(ω) of the AE signal of each cycle was generated and the Root Mean Square (RMS) of the power spectrum was calculated so that each cycle was assigned by the energy value

Referred to [ZMP06, JMV+05, FB94], the AE behavior over the system usage allows the distinction of three main characteristic states. The three major phases to be distinguished are (a) the run-in phase, (b) the stable phase (permanent wear phase) and, (c) the wear-out phase. Within the run-in phase, AE energy increases rapidly and systems have a high probability to fail. The permanent wear phase is indicated by a decrease of AE energy, which still constant until the wear-out phase begins. During the wear-out phase, AE energy increases continuously until system fails.

To illustrate the mentioned phenomena, the emitted AE energy is shown as function of the number of cycles in Fig. 4.6. Significant regions of the process and irregularities of the energy events related to wear effects are detected. During the first 40 cycles, the AE energy appears with high amplitude. Next the amplitude decreases strongly and reaches a stable value. After approximately 3200 cycles, a sudden grow of AE energy, detectable by discontinuous impulses, appears. The AE energy increases until the end of the experiment. It is also noticed that the amplitude of the individual AE energy measured during the run-in phase and the wear-out phase are similar. The distinction of the different wear mechanisms based on the signals amplitude seems not be possible.

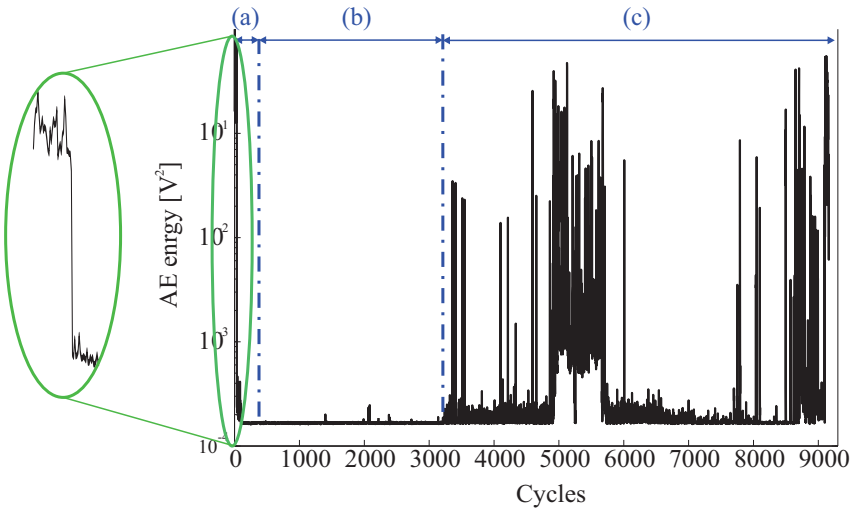

Figure 4.6: AE energy as a function of cycles [BS15]

To extract more relevant information corresponding to specific wear-states, the cumulative energy over number of cycles was carried out. The cumulative energy is equal to the integral of the AE energy distribution. In Fig. 4.7 the integrated AE energy as function of cycles is shown. It can be observed that continuously with the ongoing integrated AE, the system's damage progress develops showing the different wear stages. The run-in phase is represented by the first gradient. The stable-wear phase begins when the gradient attains approximate the normalized value of 0.15 and remains constant until the next gradient indicating the beginning of the wear-out phase. Based on the experimental results, it becomes clear, that investigating the AE energy distribution and cumulative energy qualitative information about the wear state as well as the level of deterioration of the system can be established. From Fig. 4.6 it cannot be concluded that the run-in phase and the wear-out phase can be identified based on the information connected to the individual transient events. Assuming that it will be helpful to differentiate in the minimum the three wear state phases from those individual events, this allows us to conclude that this lack should be solved.

The indicated behaviors of the AE energy distribution and the related cumulative AE energy are not restricted to a specific test. The majority of the conducted tests show that the AE energy describes three failure phases. The severity and the occurrence time of the generated Acoustic Emission significantly depend on the operation conditions and specifically on the lubrication medium. In Fig. 4.8, the AE energy and the related cumulative AE energy over system usage of two different tests are shown. The tests were carried out under identical operational parameters

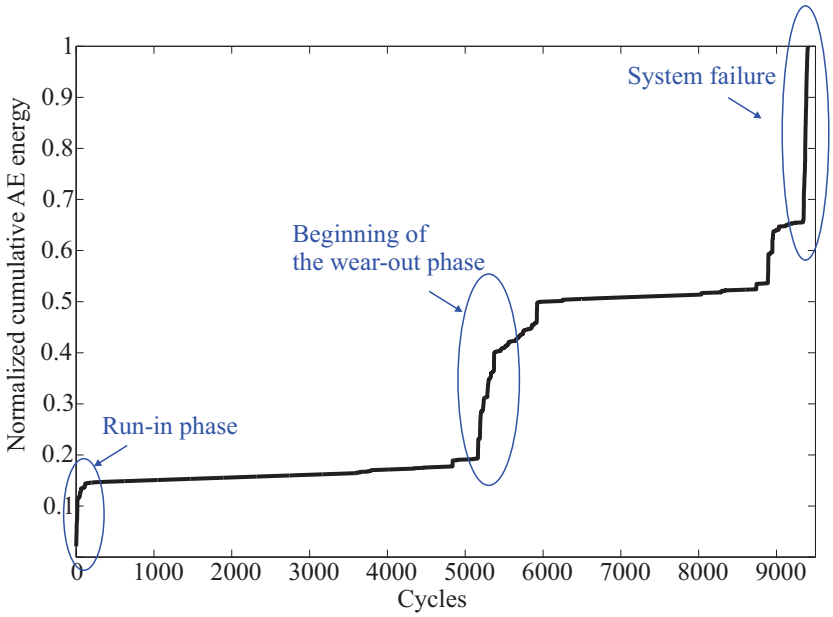

Figure 4.7: Damage progression based on accumulated AE energy as a function of usage cycles [BS15]

(pressure, applied force, and plate hardness) with two different lubrication mediums (oil and emulsion). It can be shown that during the test realized with oil, the wear-out phase is reached after more than 10000 cycles where in case of emulsion the wear-out phase is attained much earlier (after 900 cycles). Consequently, it can be concluded that the lubrication medium plays a crucial role on the lifetime of the system. Hence, using an appropriate lubrication medium can extend the structure lifetime and increase the reliability of operation.

Wavelet Transform of AE energy

In this work, the AE energy is examined the frequency components using CWT with respect to learn about options to distinguish wear phases with the aim to use it for automation, control, and supervision/monitoring purposes.

The CWT results of the AE energy are exhibited in Fig. 4.9. It can be seen that during both phases, the run-in phase and the wear-out phase, frequency components within the range of [40 kHz, 1000 kHz] with nearly similar energy content occur. Using a decomposition of the AE signal into frequency ranges of equal length, hidden information connected to the occurred damage can be detected.

In Fig. 4.10, the obtained CWT of the decomposed signals is shown. It can be observed that during each phase AE signals occur with specific frequency components. This knowledge allows a correlation between the wear state and the corresponding frequency range. In the sequel detailed frequency-band-wise explanations are given.

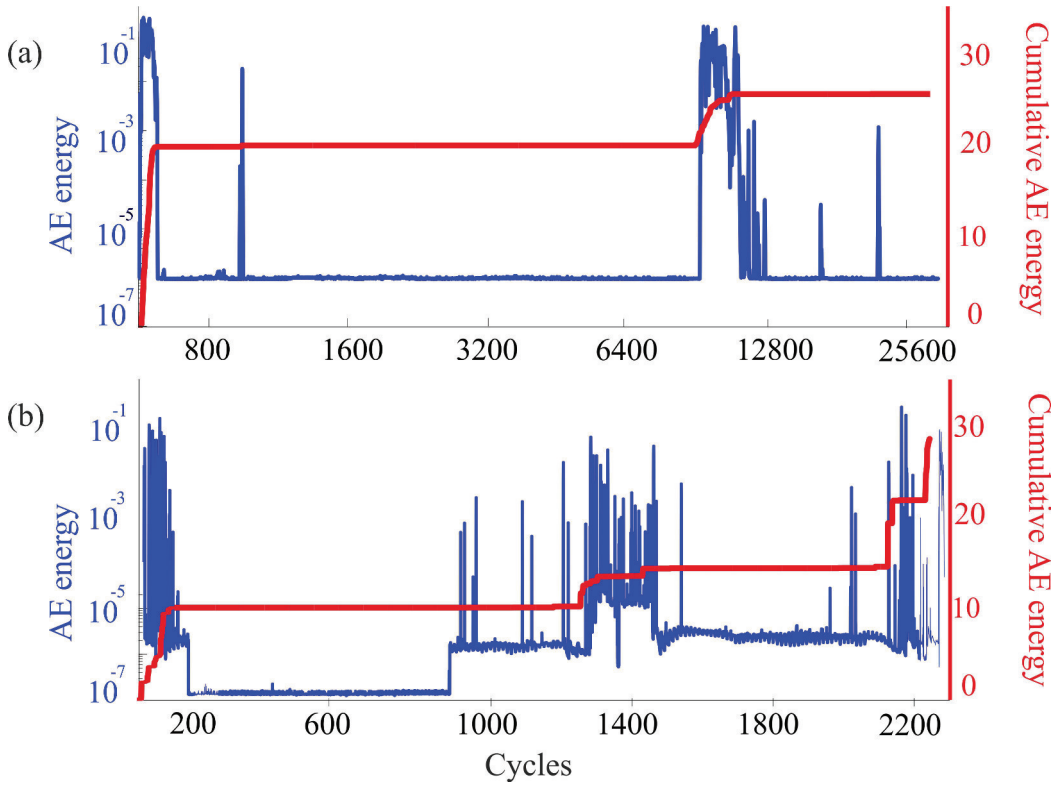

Figure 4.8: AE energy distribution over system usage of (a) test carried out with oil and (b) test carried out with emulsion

In the first frequency band, only the run-in phase shows AE, which means that AE signal with frequencies between [100 kHz, 300 kHz] are mainly related to wear mechanism affected during the run-in phase. Frequency components in the range of [300 kHz, 500 kHz] occur in each phase and dominate over the complete process because of their high energy content. The beginning of the wear-out phase is characterized by AE signals with frequencies between [700 kHz, 900 kHz]. Right before system failure, frequency components located in the range of [500 kHz, 700 kHz] can be shown. These results can be used, based on the introduced filtering technique, to build a wear-related behavior model.

This frequency repartition is also observed in the individual cumulative AE energy. The signals reconstructed from the CWT coefficients and their correspondent cumulative AE energy are shown in Fig. 4.11. Here the beginning of the wear-out phase is obviously characterized by a steep and great gradient related to the signal with frequency components between 700 kHz and 900 kHz.

The distribution of frequency components during the three process phases can be summarized as illustrated in Fig. 4.12. Comparing this result with the SEM results, it can be deduced that frequency components up to 500 kHz can be associated to tensile cracks detected in the thin coating developed during the shaping process.

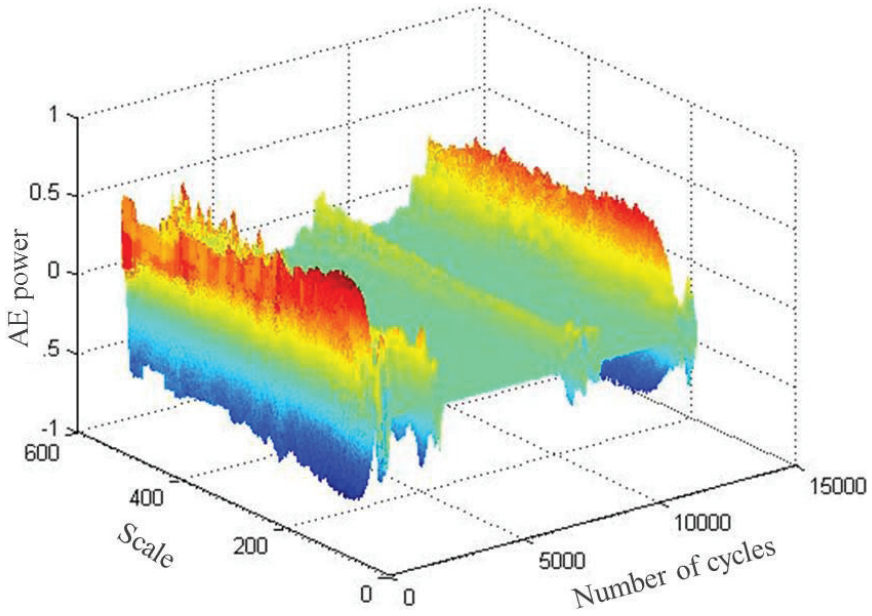

Figure 4.9: Continuous wavelet transform of AE energy distribution [BS15]

Frequency components in the range of [300 kHz, 900 kHz] can be related to abrasive wear and fatigue cracks which grow into and below the ground material. It can be concluded that the combination of the parameter-based AE method and the frequency-based AE method is appropriate to describe the incremental damage and therefore also to distinguish the three different phases.

4.4 Discussion and Conclusions

In this thesis, a tribological system effected by sliding wear is studied. Acoustic Emission-based SHM system including an advanced multilevel signal processing approach was applied, and a measurement chain based on FPGA was developed and tested. To reveal the occurring time and the energy content of the transient event, several analysis functions have been developed. By applying the STFT to the AE raw signals, frequency-based AE energy was calculated. The energy distribution and the accumulated AE energy allow the identification of three wear phases. It can be shown that the first and the last wear phases were accompanied by AE events of high energy contents. In order to distinguish the different wear mechanism occurring during the sliding process, the AE energy was decomposed into four frequency levels, and the CWT was applied to each frequency band. From the related experiment it can be concluded that each wear phase is associated to specific frequency

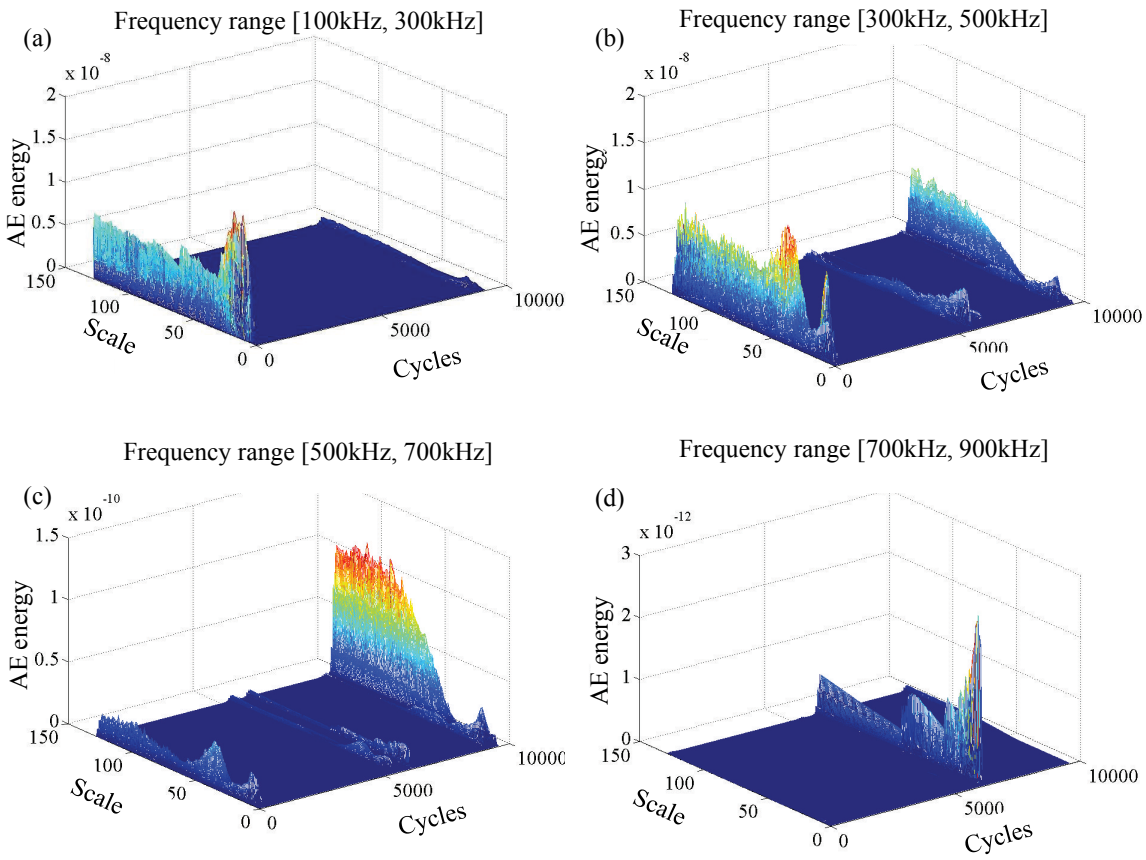

Figure 4.10: Result of CWT in different frequency ranges: (a) frequency range [100 kHz 300 kHz], (b) frequency range [300 kHz 500 kHz], (c) frequency range [500 kHz 700 kHz], and (d) frequency range [700 kHz 900 kHz] [BS15]

components so that a clear connection between material changes like abrasive wear, small cracks close to the surface, and surface fatigue can be determined. It can be observed that the examination of the wear process using the cumulative AE energy and CWT analysis allows the detection and quantification of the state-of-damage and the damage progression. As the next step, the obtained results will be used for continuous process monitoring and maintenance.

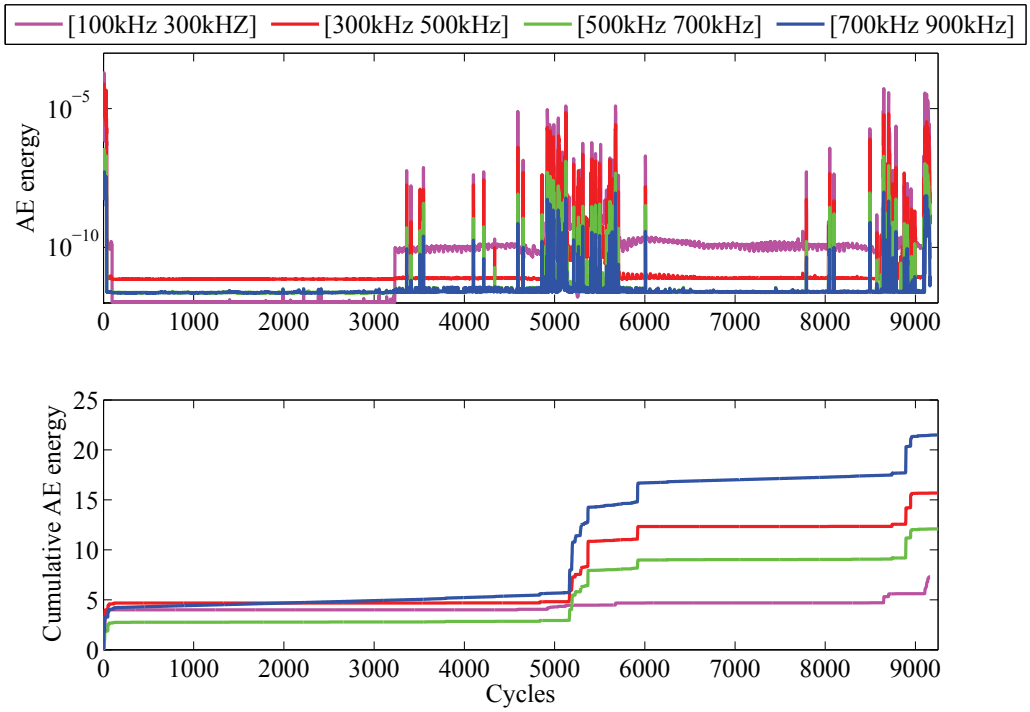

Figure 4.11: Reconstructed signals and their corresponding cumulative AE energy [BS15]

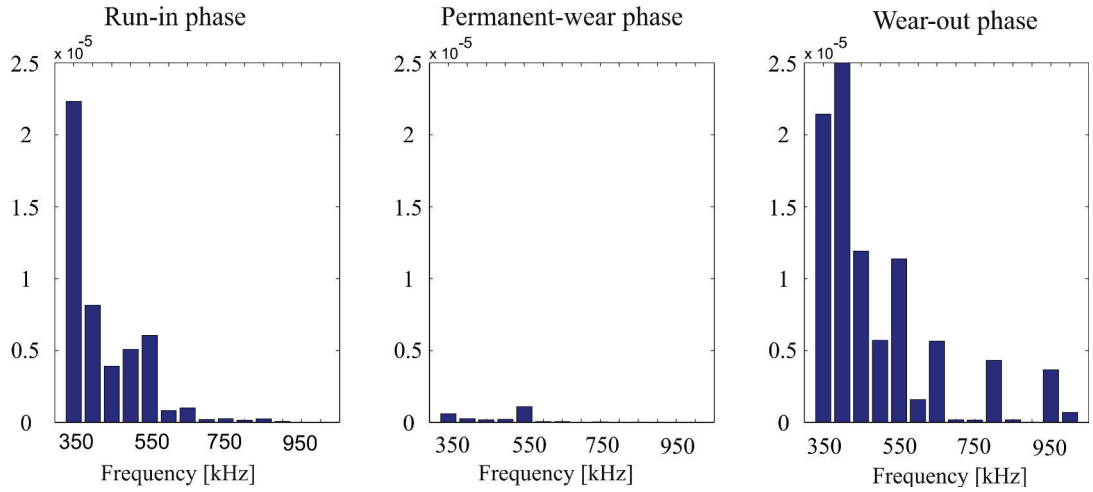

Figure 4.12: Histogram of specific frequency contents in the three wear phases [BS15]

5 Acoustic Emission Monitoring of Composite Structures

This chapter presents the application of the proposed SHM system for online detection and automated classification of failure modes produced in composite structures subjected to indentation tests. The first section introduces the experimental procedure including test rig and the signal processing approach which is considered as the core of the SHM system. The developed method is a new classification approach based on multivariate statistical analysis of wavelet coefficient matrices. The aim is to improve the classification method by extracting characteristic similarities from AE data and correlating them to related failure modes occurring during indentation load in CFRP laminate. The proposed method comprises four processing steps. In contrast to the cited literature, for pattern determination and classification no time-domain based parameters are taken into consideration, only wavelet coefficients are defined as descriptors. Furthermore, experimental results demonstrating the effectiveness of using AE-based SHM system to detect, identify, and classify different damage mechanisms are presented.

During the progress of this work, main parts of this chapter have been published in [BS].

5.1 Experimental Setup

To investigate the relationship between AE generation and damage mechanism, a number of tests have been performed using laboratory test rig extended by the developed SHM system. The test rig is designed so that the maximum of possible failure modes can be produced.

The specimens used in this study are manufactured by laying three inner unidirectional carbon fiber/epoxy prepreg [0°/90°/0°] and two outer woven carbon/epoxy prepreg. The specimens have a dimension of 350mm x 350mm x 2mm. Static indentation tests are performed under laboratory conditions by manually applying a compressive load by an indentor. The severity of the induced damage depends on the geometry of the indentor. In this study, a metal indentor manufactured so that the surface shape forms a cone with rounded top is used. The contact area between specimen and indentor is very small compared to the surface of the CFRP plate.

In order to avoid buckling, CFRP plates are fixed by means of a clamping system. The experimental set-up of the testing is illustrated in Fig. 5.1.

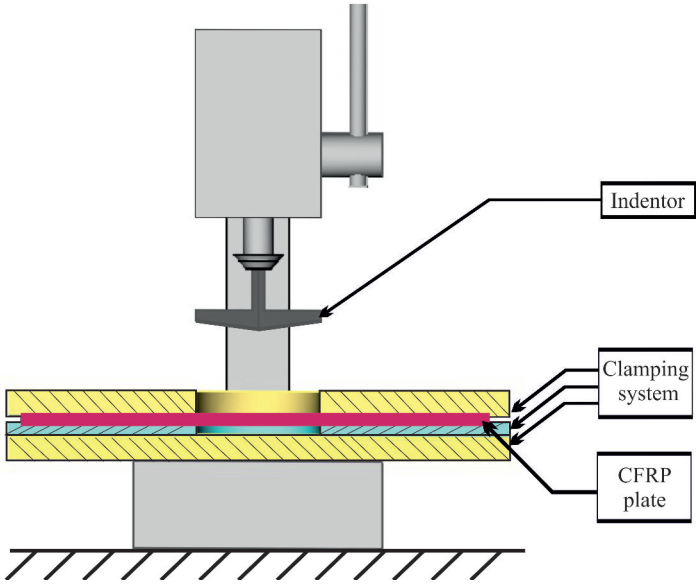

Figure 5.1: Experimental set-up [BS]

To realize the AE measurements, the sensor was glued at the CFRP plate surface as close as possible to the AE source. The coupling between the sensor and the surface of the plate was permanent and very stiff. An appropriate sampling rate of 4 MHz is chosen to assure a high resolution of the discretized piezoelectric voltage of special interest. The complete experimental set-up and data acquisition scheme used for the experiments are depicted in Fig. 5.2.

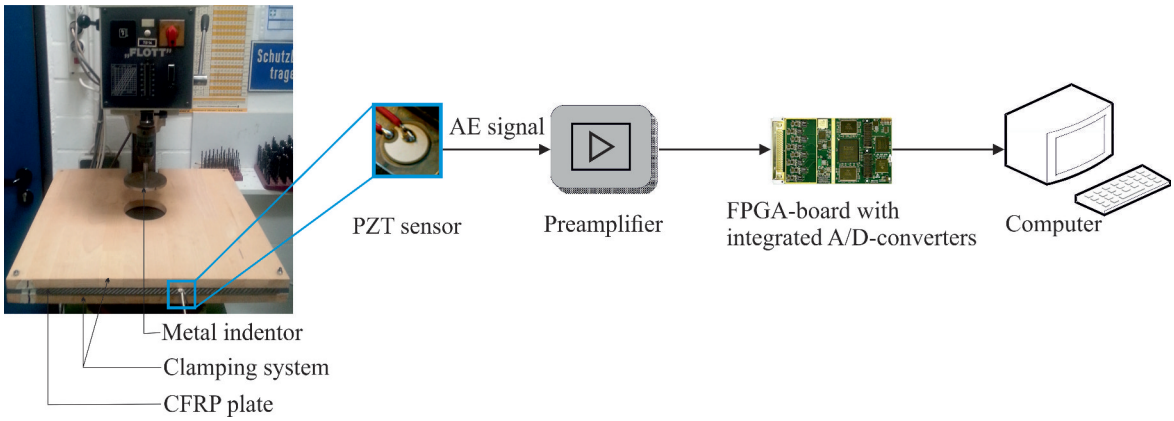

Figure 5.2: Test rig extended by the FPGA-based measurement chain for Acoustic Emission [BS]

5.2 Signal Processing Chain

In this study, a new pattern recognition approach for damage detection involving a number of processing steps able to be implemented in real-time is developed. The damage detection method is based on statistical features derived from time-frequency domain. Unlike common classification approaches reported by [MTG08, HDS+13, OAH09, GGV+11], here only CWT coefficients are considered as relevant features.

The recorded AE data are firstly preprocessed using the centering and whitening methods. Centering and whitening are preprocessing techniques that eliminate the mean covariance information and are generally performed for Blind Source Separation (BSS) and Independent Component Analysis [LZ98]. Centering of a time series X is carried out by subtracting the mean $E(X)$ transforming it to a zero-mean vector. Geometrically, centering is equivalent to shifting the coordinate center to the origin. Whitening is a linear transformation which makes observations uncorrelated and with unit variance. Geometrically, whitening is a scaling transformation. After centering and whitening data have zero location, unit scale, and zero correlation coefficients [WSP+06]. Centering and whitening are used for highlighting features, not readily detectable in the raw data, by the mean and covariance. An example of centering and whitening of AE signal is depicted in Fig. 5.3.

The second step involves the feature extraction. Owing to its capability for generating simultaneously time and frequency information, the Continuous Wavelet Transform is used as feature extraction tool.

The third processing step comprises the feature selection process. Redundant and irrelevant features are excluded through reducing the dimension of the wavelet coefficient matrices by performing the Principal Component Analysis (PCA). The two first principal components corresponding to each AE signal are projected in a two-dimensional space. Based on this projection, similarities or differences between the patterns cam be identified. In order to obtain a better classification accuracy, the PCs are then forwarded for further analysis using Kernel Density Estimation (KDE). The obtained distribution of each feature set allows the determination of a specific pattern for each fault-specific AE signal considered.

In order to correlate the obtained pattern with failure modes, frequency content and waveform provided from CWT are also in-depth examined and compared with fundamental results reported by various authors [GGV+11, MTG08, HDS+13, dOM08, dGWJ95].

Finally, the damage signatures obtained from the KDE are automatically classified using a multiclass Support Vector Machine (SVM). The introduced procedure improves the damage classification and can be used for automated evaluation applications of safety related relevance.

The flow chart detailing the processing steps of the proposed methodology is shown in Fig. 5.4

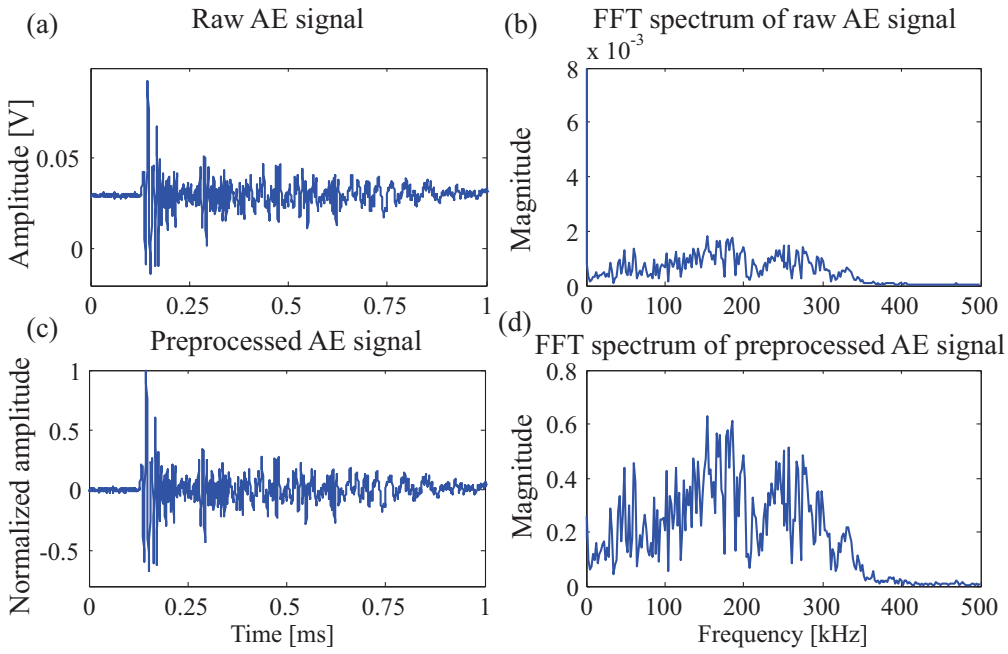

Figure 5.3: Acoustic Emission signals and corresponding FFT spectrum: (a) raw AE signal, (b) FFT spectrum of raw AE signal, (c) centered AE signal, and (d) FFT spectrum of centered and whitened AE signal

5.3 Experimental Results

In this section, experimental results demonstrating the capabilities of the multilevel processing approach to detect, identify, and classify different failure modes in CFRP laminate are presented.

5.3.1 Scanning Electron Microscope Analysis

To identify the different types of damage mechanisms occurred during the indentation tests, the specimens were carefully examined by using a Scanning Electron Microscope (SEM). The SEM examinations were carried out at the Chair of Materials Science and Engineering (Prof. A. Fischer), University of Duisburg-Essen. The SEM micrographs of the main CFRP failure modes are shown in Fig. 5.5. The damage mechanisms are observed in a region of very small dimension in which the specimen is considered failed. The identified failure modes are matrix cracking, fiber breakage, and fiber/matrix debonding. It can be seen that fiber/matrix debonding

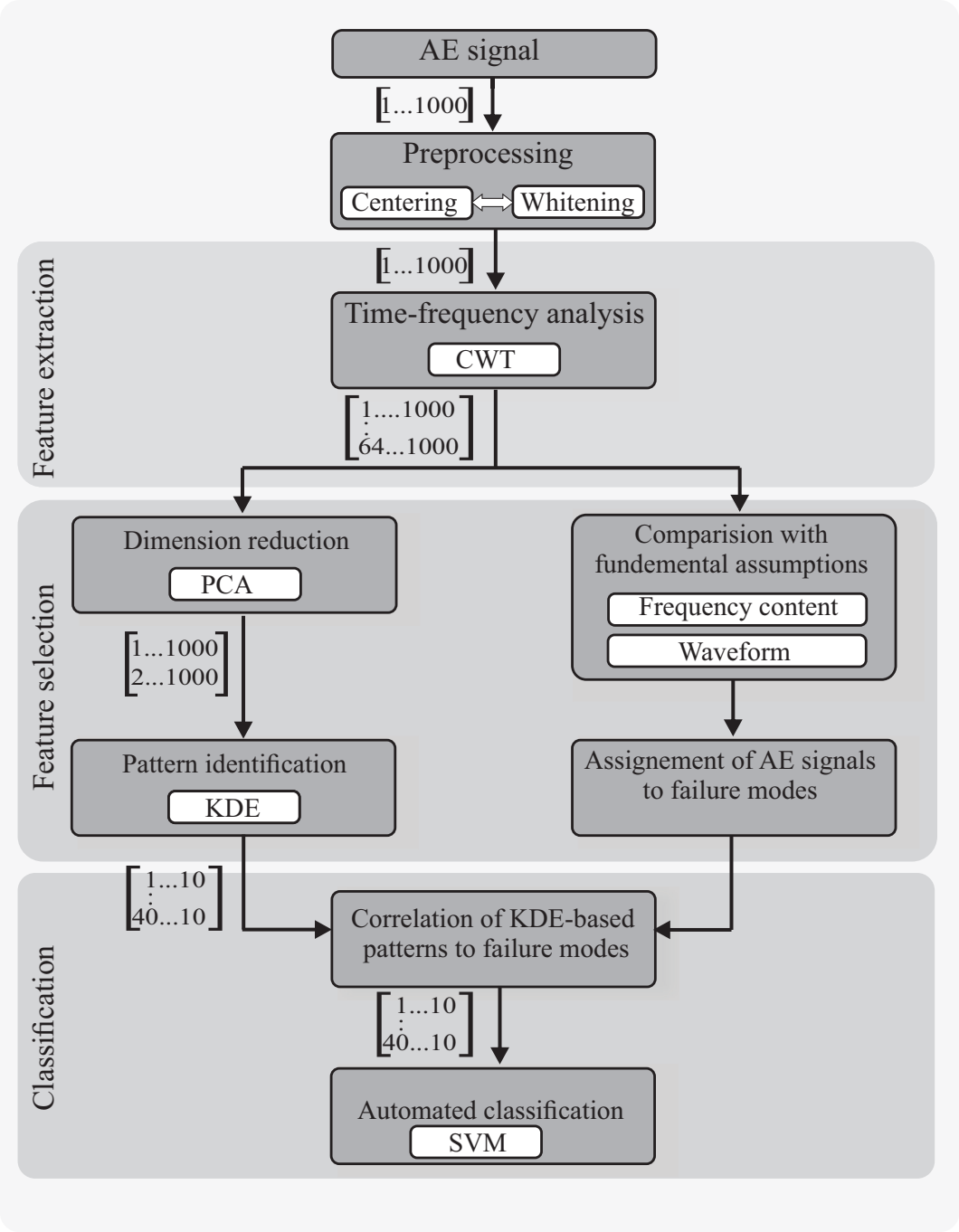

Figure 5.4: Multilevel processing approach for analysis of AE signals [BS]

is accompanied by numerous matrix cracking along the fiber direction. The result of the SEM investigation is used as solid statement to confirm the AE-based damage identification.

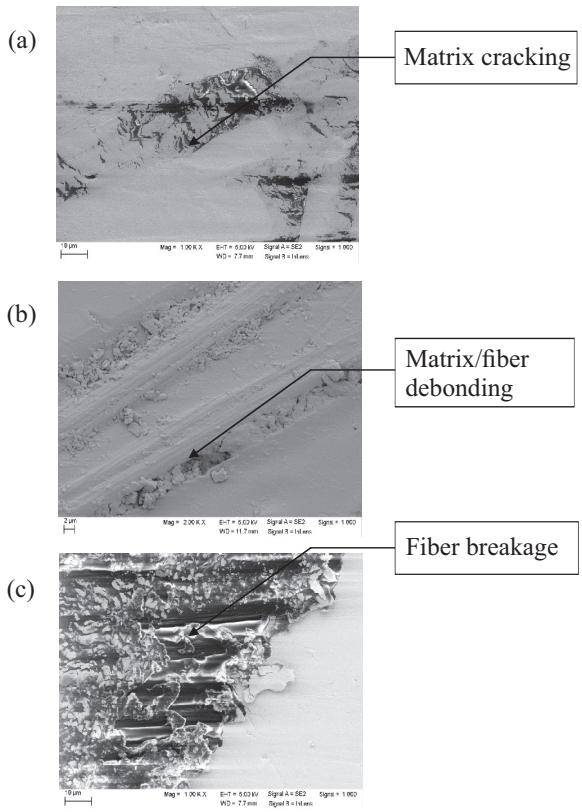

Figure 5.5: SEM images of failure modes occurred during indentation tests realized at Chair SRS, University of Duisburg-Essen, Germany [BS]

5.3.2 Energy-based Analysis

Classical energy-based analysis was chosen as a first evaluation technique to obtain an insight about the damage and the related clusters. The cumulative AE energy of 13 AE events was calculated aiming to find typical clusters representing the different failure modes. The evolution of the cumulative AE energy of the considered events is illustrated as function of time in Fig. 5.6. Five different clusters were identified. It can be observed that AE events showing similar behavior were classified into two clusters namely cluster 2 (grey) and cluster 4 (red). The misclassification can be due to reflection or border effect which strongly influences the AE energy. However, the result presented shows that the evolution of the cumulative AE energy differs according to failure mechanisms whereas the sensitivity of this method depends on many factors. This was interpreted as limiting for the objective of this study. Therefore, the identification and classification of failure modes was mainly based on multivariate statistical analysis of wavelet coefficients.

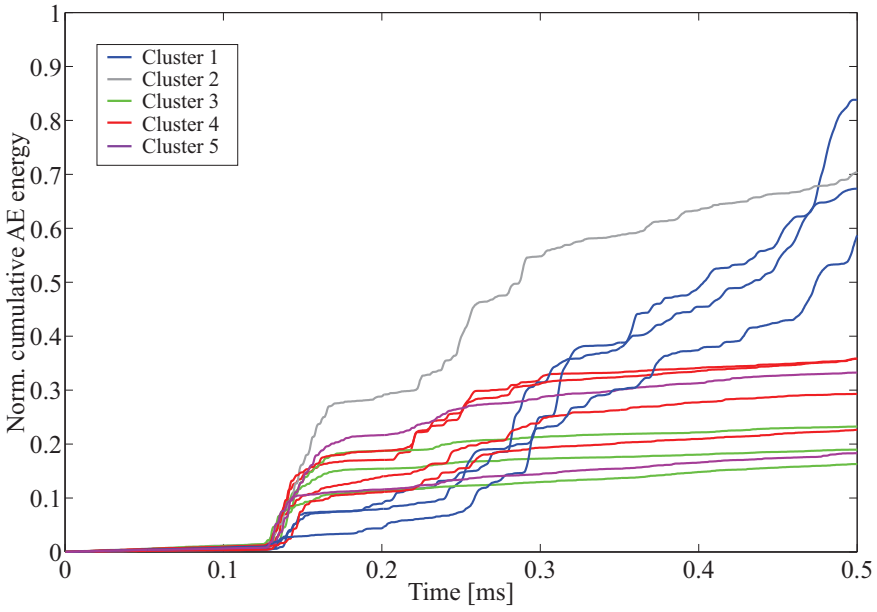

Figure 5.6: Clustering of 13 AE events based on normalized cumulative AE energy

5.3.3 Multivariate Statistical Analysis

Multi-level processing approach based on wavelet coefficients is performed in order to identify and classify failure modes according to their AE data. As mentioned in sec. 5.2, CWT is performed after preprocessing the AE raw signals. Each selected AE event comprises 1000 samples is analyzed using a 64 scaled CWT. The obtained coefficients are extracted as features so that an AE data set representing a single event comprises 64000 features. To reduce the dimension of feature sets, PCA is applied to every AE data set separately. Score matrices derived from PCA show that more than 83% of the data variances are retained in the two first components PC1 and PC2. The percentage of the variability explained by the first principal component and the second principal component of four selected events is shown Tab. 5.1.

Table 5.1: Data variance in the two first components of four selected AE events

	PC1 [%]	PC2 [%]
AE event 1	76.6	13
AE event 2	58	25
AE event 3	63.7	11
AE event 4	82	6.5

In total, four new data sets are generated by PCA. Each data set represents only one AE event and implies 2000 features. The PCA results are used for pattern

identification. Two-dimensional projection of the first and second principal components is shown in Fig. 5.7. The visualization of the PCA results obtained from CWT coefficients of raw AE data and of preprocessed AE data indicates the existence of four different clusters. In despite of a non-optimal feature distribution, clustering resulting from coefficients of centered and whitening AE signals shows a minimal overlapping and allows a better distinction of the different clusters. The visualization of the PCA results obtained from CWT coefficients indicates that each AE event is characterized by a certain features distribution. Accordingly, specific patterns can be attributed to the different examined AE events. Separation between patterns is inferred based on features distribution's direction and form. To overcome the overlapping problem and to improve the distinction between the different related patterns with respect to the feature dispersion, KDE is adopted to remove redundant and irrelevant features and to restrict the zone with high feature density.

The result of kernel density estimation applied to the four identified patterns is shown in Fig. 5.8. Based on regions of high concentration, here colored in brown/red, different patterns can be distinguished. The main emphasis for applying KDE is to determine a specific pattern for each AE event in order to improve the classification. By using these patterns as input data for the supervised learning approach, the computational complexity should be reduced by selecting the most representative features. The results show that considering each wavelet scale as AE descriptor better classification can be obtained. It can also be deduced that the introduced multilevel processing approach can enhance the classification accuracy.

The obtained result is not restricted to the four examined AE events. The same outcomes are observed for more than 36 AE events generated in CFRP laminates subjected to indentation tests. The AE events, CWT-, PCA-, and KDE- results of all AE events are shown in Appendix 7.3.

5.3.4 Waveform- and Wavelet-based Analysis

The waveform analysis, also called modal analysis, consists of studying the flexural and the extensional modes of the AE signal with respect to amplitude, frequency, and duration ratio. In the last years, modal analysis has proved to be capable to distinguish between different damage failures. Increasing success when leading with AE source location has been shown in [dOM08, OHAF12]. In this paper, a thorough analysis in terms of waveform and frequency content of AE signals is performed in order to establish a correlation between the obtained patterns and different failure modes.

Time and time-frequency representation of AE signal C1 related to the pattern 1 is illustrated in Fig. 5.9. During indentation tests, this type of signal (C1) occurs by maximum load applied and is followed by an important number of events of different types. The number of events associated to this type is relatively low. The signal C1 is characterized by the existence of two modes namely extensional mode and flexural

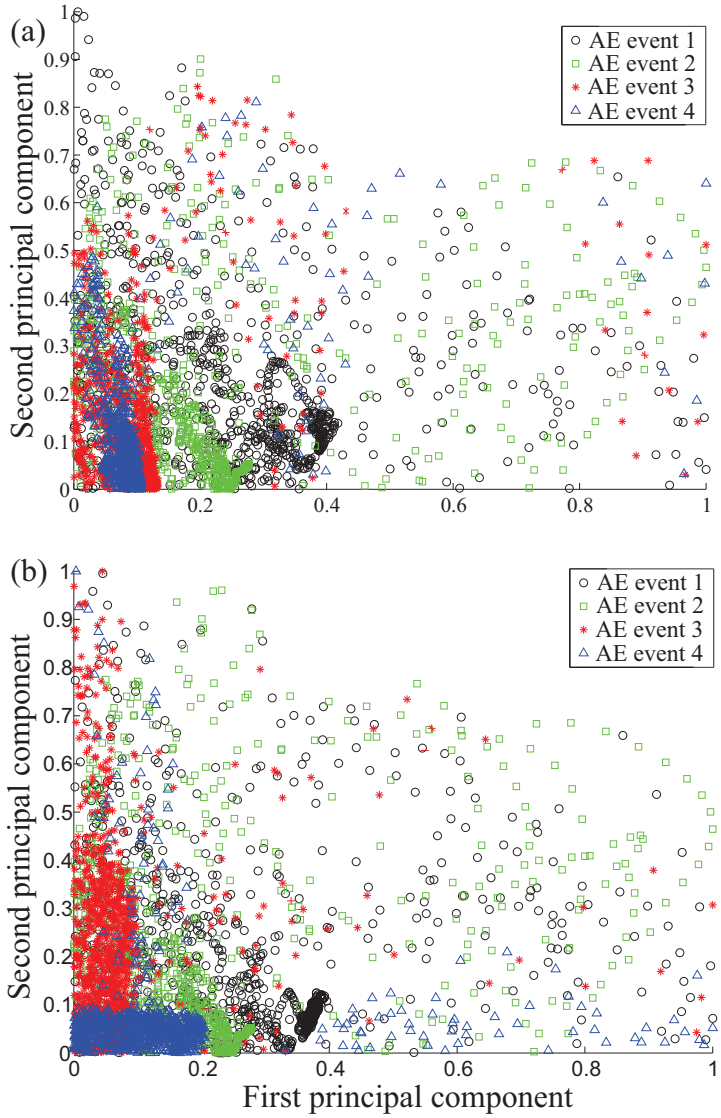

Figure 5.7: PCA visualization of coefficients selected from (a) raw AE data and (b) centered and whitened AE data [BS]

mode. The flexural mode is dominant and dispersive. Results of CWT shows that the high energy area is located in the frequency range less than 120 kHz. This waveform was also observed by [dOM08]; the authors attributed this type of AE signal to 'out-of-plan displacement' which is due to delamination. In [GGV+11] and [HDS+13], the same frequency range was also assigned to delamination in contrary to [MTG08] that correlated this signal type to matrix cracking.

In Fig. 5.10, time and time-frequency representation of AE signal C3 corresponding to pattern 3 is shown. This type of signal occurs at early stage. High number of AE events is generated during all stages of loading. The signal C3 is characterized by a dominant extensional mode and high flexural mode. The high en-

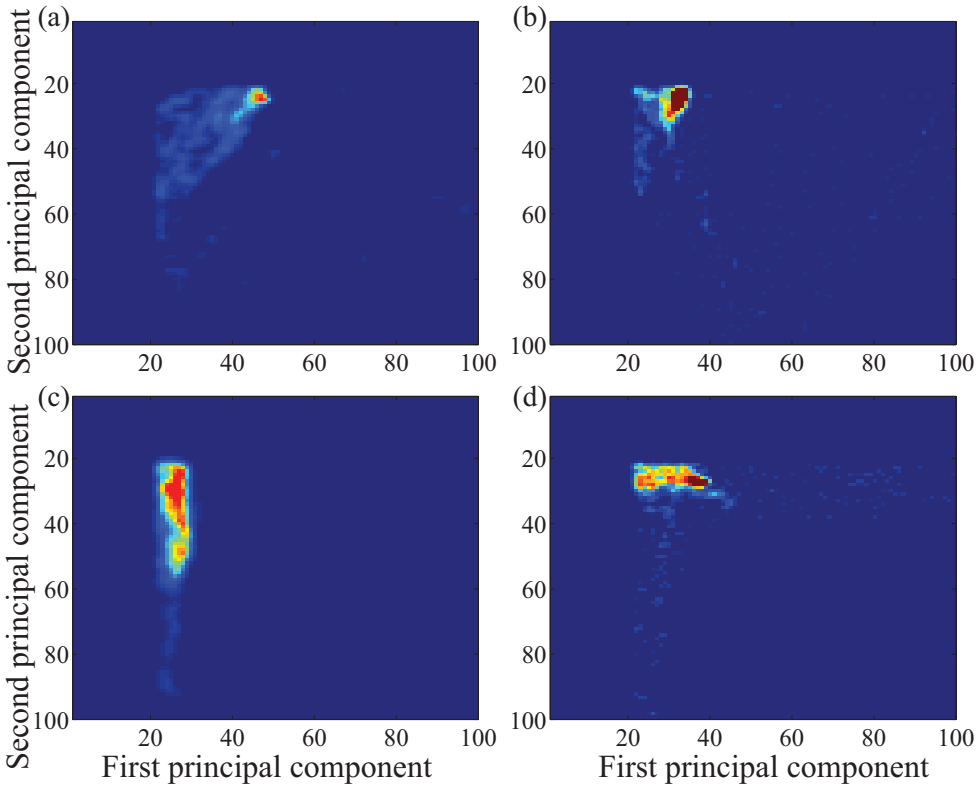

Figure 5.8: Kernel density estimation of (a) pattern 1, (b) pattern 2, (c) pattern 3, and (d) pattern 4 [BS]

ergy area shows that the flexural mode is the most energetic component with frequency contents within the range of 100-150 kHz. Based on the waveform and frequency content, signal C3 is correlated to matrix cracking. This statement was also reported by [dOM08, OHAF12]; they observed the same waveform when 'transverse matrix cracking' occurred. Regarding the frequency content, many authors [GGV+11, MTG08, MNTO00, JG00, CPZ11], associated this frequency range to matrix cracking.

The time and time-frequency representation of AE signal C4 related to pattern 4 is shown in Fig. 5.11. This type of signal is characterized by an extensional mode free from dispersion. It is the most dominant signal and is generated commonly during all loading stages. Here, wavelet results show that the high energy area is locally distributed and found in the frequency range of 350-500 kHz. According to the majority of studies, this signal is related to fiber breakage which is always characterized by higher frequency.

In Fig. 5.12, time and time-frequency representation of AE signal C2 corresponding to pattern 2 is given. Here the extensional mode and the flexural mode have almost similar dominance. In comparison to signal type C1, this type of signal is frequently generated during indentation tests and is characterized by dispersive en-

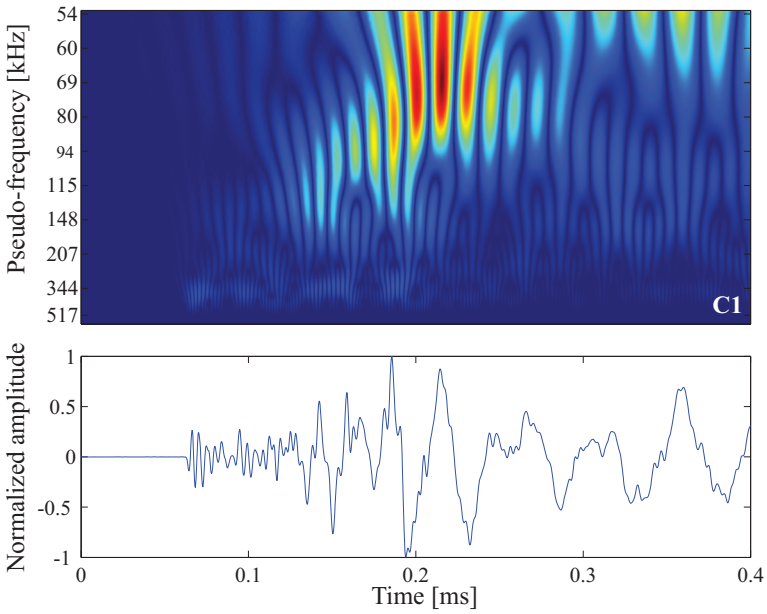

Figure 5.9: Time and time-frequency representation of AE signal (C1) corresponding to pattern 1 [BS]

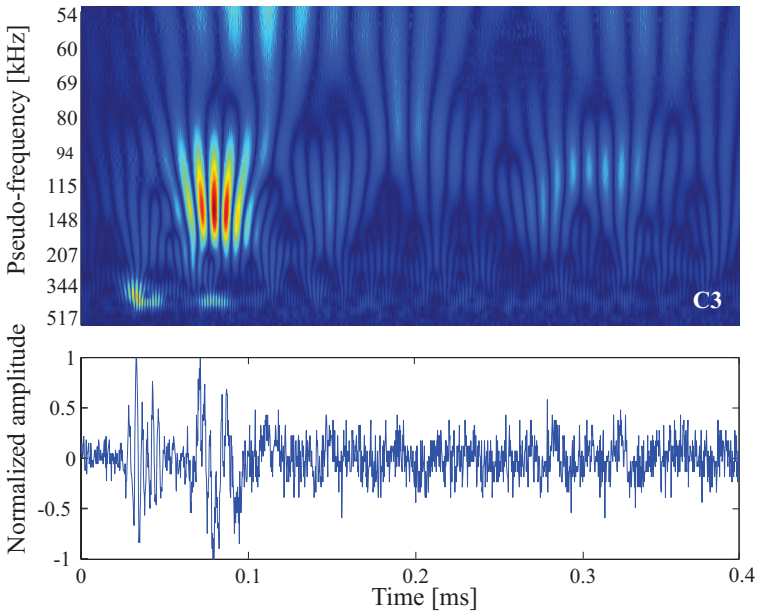

Figure 5.10: Time and time-frequency representation of AE signal C3 corresponding to pattern 3 [BS]

ergy. In addition to high frequencies, frequencies in the range of 150-250 kHz are shown. Compared to the literature [OHAF12, dGWJ95, HDS+13] this AE signal

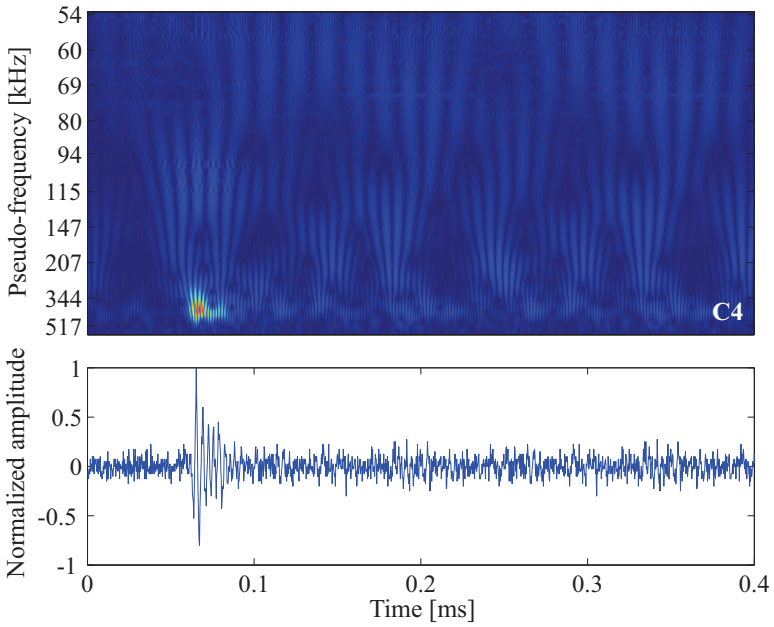

Figure 5.11: Time and time-frequency representation of AE signal C4 corresponding to the pattern 4

is attributed to fiber/matrix debonding. Moreover, time-frequency representation of signal C2 shows the generation of more than one failure mode at the same time or simultaneously and demonstrates that a failure mode, in this case fiber/matrix debonding can include other damage mechanisms such as matrix cracking and fiber breakage. It can be seen that based on the observed waveform and frequency contents extracted from CWT, quantitative and qualitative specifications belonging to each signal are highlighted, and distinctions between the different damage mechanisms achieved.

5.3.5 Support Vector Machine-based Classification

The automated classification and recognition of the identified damage signatures was performed using a multiclass Support Vector Machine (SVM). One class was attributed to each failure mode. The data sets considered for the classification are the 120 x 120 matrices generated by the kernel density estimation. In total, 36 samples were selected (9 for each class). The classifier is trained with samples randomly chosen. For each data set, 3 samples are used for training and the rest (6 samples) is used for testing. Every training or testing vector consists of 100 features that are extracted from each coefficient matrix. Samples of the patterns selected for training the SVM are shown in Fig. 5.13. Each damage (class) is represented by one pattern containing 14400 features.

In order to estimate the margin trade-off parameter and to select accurate kernel

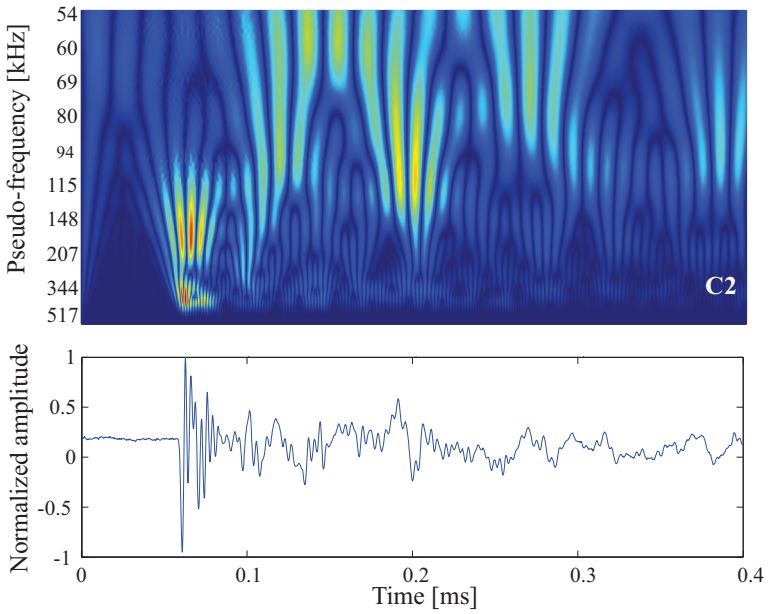

Figure 5.12: Time and time-frequency representation of AE signal corresponding to the pattern 2 [BS]

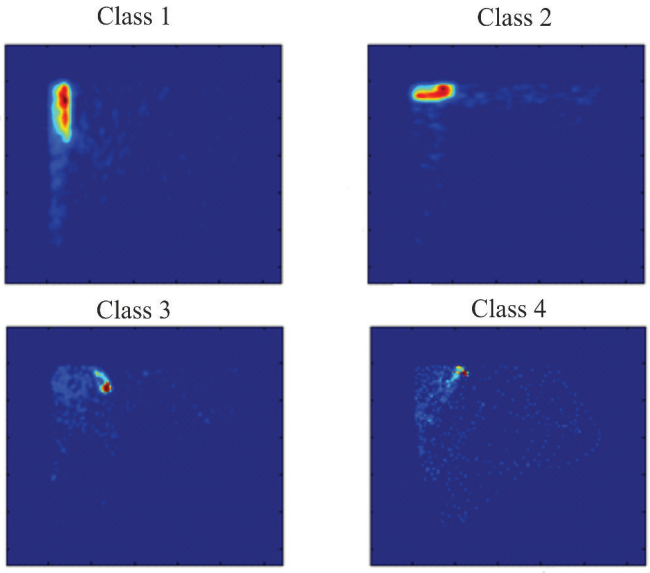

Figure 5.13: Samples of training data sets [BS]

parameters, a cross-validation procedure was used. The cross-validation allows the optimization of the classification performance and the avoiding of over-fitting and under-fitting problems [WKS+09]. For this purpose, the training data set is divided into equal individual data sets. A part of these data sets is considered unknown and not taken into account for the training of the classifier. This method allows

then the determination of the test-accuracy. Once this has been carried out for all individual data sets, the cross-validation can be calculated as the mean value of the test classification. Using this training-process, the optimal parameters C and γ can be determined for all hyperplanes and are then used for the classification.

The accuracy of the cross-validation, which represents the percentage of the correctly classified data, is shown in Fig. 5.14. The optimal parameters C and γ used for the classification are given in Tab. 5.2.

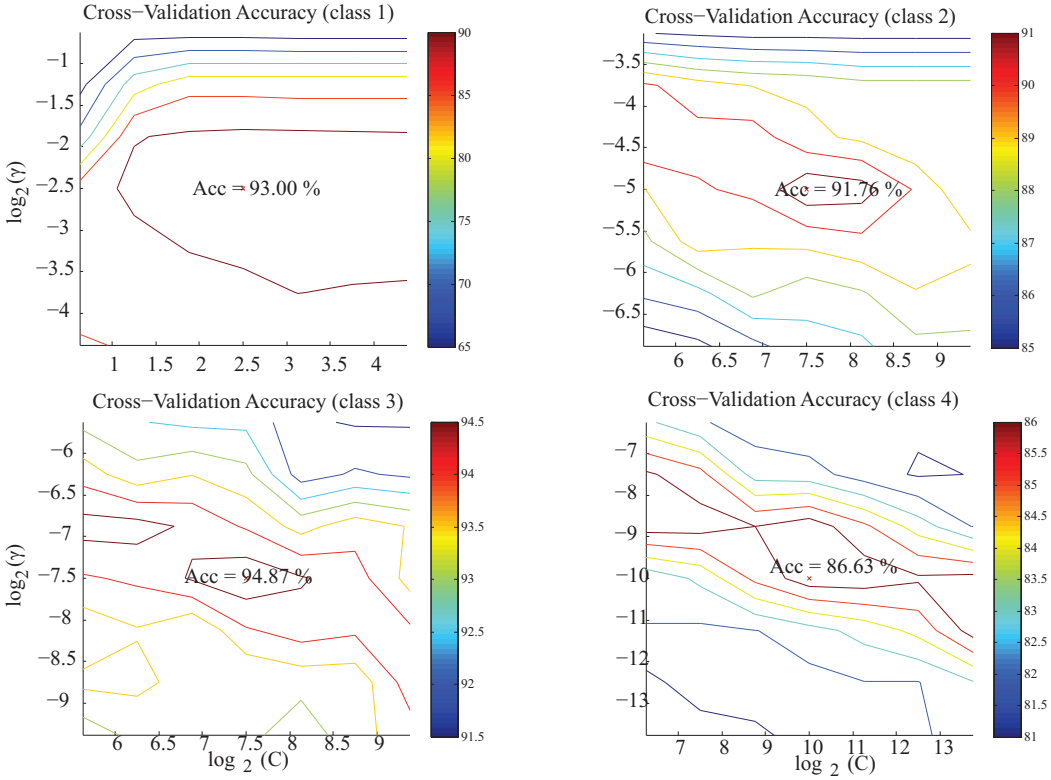

Figure 5.14: Results of the cross-validation

Table 5.2: The optimal parameters C and γ for each data set

	C	γ
Data set 1	2.5	-2.5
Data set 2	7.5	-5
Data set 3	7.5	-7.5
Data set 4	10	-10

The trained classifier was used to classify the results of the KDE into four classes. To test the classifier, 6 data sets for each class were selected. Samples of the patterns selected for testing the trained module are shown in Fig. 5.15.

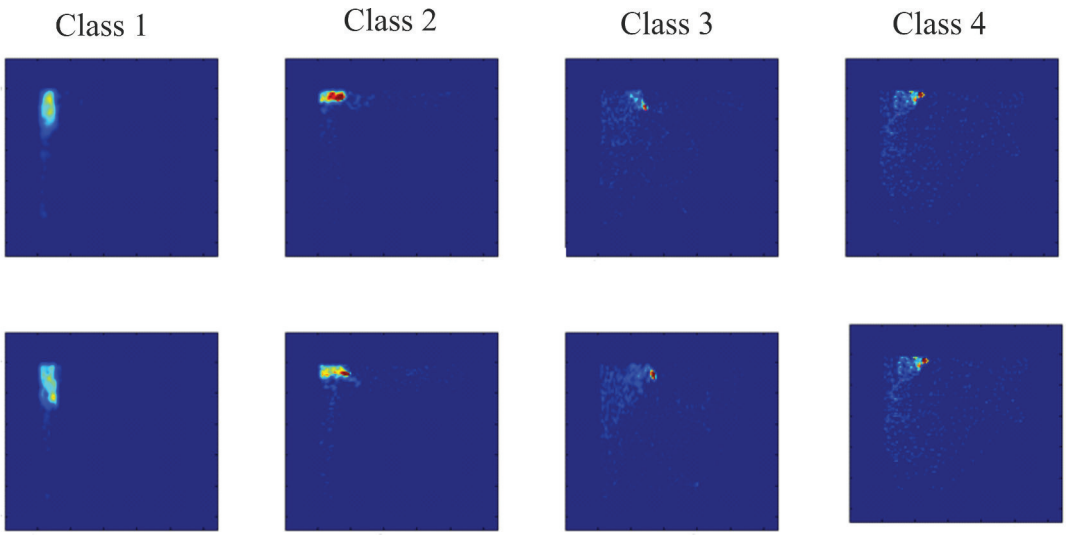

Figure 5.15: Testing data sets

The input data sets for each class are samples from the same class so that only true positive assessment TP and false negative assessment FN are possible. The results of the model is given in percent and represents the detection rate which is defined in this case as

$$Detection\,rate = \frac{TP}{TP + FN}. \tag{5.1}$$

The performance of SVM classification of selected KDE-based patterns and the associated damage mechanisms is summarized in Tab. 5.3. The obtained detection rates of all classes are quite satisfactory. The best classification rate (94.69%) was achieved by AE event C2 which is related to fiber/matrix debonding. AE event C1 corresponding to delamination and AE event C4 related to Fiber breakage have a detection rate of 86.81% and 85.24% respectively. Patterns corresponding to matrix cracking have a slightly reduced recognition rate (79.72%). This is probably due to the selected testing pattern. However, the result shows that using KDE-based features, SVM can be effectively used to recognize and classify AE events generated from different damage mechanisms.

Table 5.3: Support Vector Machine classification results of KDE-based patterns and the associated damage mechanisms

	Class 1	Class 2	Class 3	Class 4
Detection rate [%]	85.24	79.72	94.69	86.81
AE event	C3	C4	C2	C1
Damage	Fiber breakage	Matrix cracking	Debonding.	Delamination

5.4 Discussion and Conclusions

The aim of this chapter was the investigation of the developed AE-based SHM system for online detection and automated classification of failure modes produced in composite structure. A test rig and an advanced multilevel processing approach combining CWT and multivariate statistical analysis were developed. Indentation tests were performed on CFRP plates, and the generated AE signals were recorded by the introduced measurement chain. In contrast to the cited literature [HDS+13, HZ13, LK09, GGV+11, MTG08], for the pattern identification no time parameters were taken into consideration, only wavelet coefficients were used as descriptors.

Continuous Wavelet Transform was firstly performed on preprocessed AE data to extract relevant features. Next, the dimension of the wavelet coefficient matrices were reduced using PCA, so only features contained in the two first components were selected. Further, KDE was used in order to restrict the zone with high feature density by smoothing the two highest principal components (PC1 and PC2) for better pattern identification and classification. Finally, a classification procedure was carried out for the results obtained from the KDE by using a multiclass SVM.

Based on experiments conducted at the Chair SRS, University of Duisburg-Essen, AE signals were deeply examined in terms of waveform and frequency content. The obtained frequency ranges were in accordance with those known from the literature. Specific frequency ranges could be assigned to the failure modes based on fundamental assumptions reported by various authors. Signals related to delamination have the lowest frequencies while signals generated by fiber breakage have the highest frequencies. Acoustic Emission signals with frequency range less than 120 kHz was assigned to delamination. Matrix cracking emits signals with frequencies between 100-150 kHz. Frequencies caused by fiber breakage were situated in the range of 350 to 500 kHz. Signals in between were expected to be related to fiber/matrix debonding.

From the classification results, it can be concluded that the selected features are effective indices of the different damage mechanisms. The SVM was trained to recognize damage represented by one pattern containing 14400 features. The classification performance was successful reaching 94.69% for certain classes.

The advanced multilevel processing approach showed high reliability in terms of detection, identification, and classification of failure modes. The new introduced AE-based SHM system leads to a noticeable better identification and classification of damage mechanism and also proves the efficiency of wavelet coefficients as representative descriptors. The presented methodology will allow an automated health monitoring of CFRP structures and, therefore, contribute increasing safety and reliability of composite-based constructions in engineering applications like aeronautic and aerospace.

6 Acoustic Emission Monitoring of Lithium-Ion Batteries

This chapter presents the application of the proposed AE-based approach to online estimation and therefore automated classification of State of Health (SoH) of lithium-ion battery. The first section introduces the relationship between the SoH and related aging effects. The second section is devoted to the applied aging procedure for accelerated testing. Here, the test rig and the developed signal processing approach are introduced. The third section presents the experimental results which demonstrate the effectiveness of using AE-based battery management systems to establish a direct correlation between SoH and the generated AE. This approach is, according to the knowledge of the authors, not applied before and is considered as a novelty in this field.

During the progress of this work, main parts of this chapter have been developed and written in [SB].

6.1 Introduction

For practical implementation of batteries into next generation technologies, advanced battery management systems are required. Accurate in-situ monitoring of the battery can provide diagnostic information for the benefit of the user, facilitate the maintenance, and allow a better utilization of the capacity of the batteries. Typically, battery monitoring deals with the evaluation of the battery integrity, in terms of energy remaining and degree of deterioration. Advancements made in the field of signal processing and artificial intelligence have contributed to the development of several online estimation techniques such as OCV, CC, KF, and internal resistance. Using these methods, SoC can be derived with sufficient accuracy, unlike SoH, which is still a complex and unsolved task. The estimation of SoH is based on a comparison of actual capacity with capacity when the battery is new. The SoC is conventionally derived by using available external measurements such as voltage and current. These measurements are collected from aging tests with relatively simple load cycles. Based on these experimental data and on statistical or mathematical methods, empirical models can be built for SoH estimation [LJN+05, SVWR06, WCM+03]. However, the empirical models require a significant computational effort and show a non-satisfactory performance when dealing with complex load cycles [PLAA14].

In this thesis, a new SoH estimation method based on Acoustic Emission is investigated. The method utilizes the AE signals measured during aging tests to study

the degradation processes of lithium-polymer battery aiming at evaluating the SoH and thus providing information about the remaining useful lifetime. This filtering methodology, including measurement and signal processing chain, is for the first time applied to battery related aging process.

6.2 Aging Tests

6.2.1 Test rig and measurement chain

In this research, 10Ah Superior Lithium Polymer Battery cells manufactured by KOKAM are used for aging tests. Detailed electrical characteristics of the batteries are shown in Tab. 6.1.

As charging source, a DC power supply is used. The device is able for current up to 60A and 80V. To discharge the battery, an electronic load allowing a discharge current of 10mA to 50A within a range of 2.5V and 80V is utilized. For the automation of the test procedure, the power supply and the electronic load are connected to the battery via a low impedance switch box composed of solid-state relays. The voltage at the terminal clamps of the battery is measured and transformed into an adequate output voltage using a buffer amplifier. Further, the temperature of the battery is continuously observed. All devices are remotely controlled by a real-time process control system.

To realize the AE measurements, PZT sensor is glued in the middle of the battery surface. A suitable coupling material with an appropriate acoustic impedance and attenuation is chosen. The coupling between the sensor and the battery was permanent. An appropriate sampling rate of 4 MHz is selected to assure a high resolution of the discretized piezoelectric voltage of special interest. The measured voltage is fed to the FPGA-board. Subsequently, the measured signal is analyzed by various signal processing methods. The test rig and the data and signal flow of the experimental arrangement used for the aging tests are illustrated in Fig. 6.2. One of the

Table 6.1: Electrical characteristics of KOKAM lithium polymer cell

Cell Specifications	Range
Nominal capacity C_n	10Ah
Max. discharge rate	50Ah
Nominal voltage U_n	3.7V
End of charge voltage U_{EoC}	4.2V +/- 0.03V
End of discharge voltage U_{EoD}	2.7V
Max. conti. charge current $I_{C,max}$	20A
Max. conti. discharge current $I_{D,max}$	30A
Operation temperature T	-10°C...+55°C

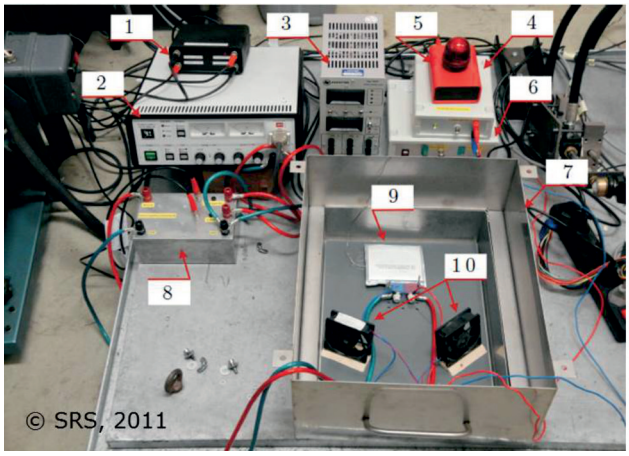

Components
1. Galvanic isolation
2. Power supply
3. Electronic load
4. Voltage sensor
5. Warning light
6. Temperature sensor
7. Safetybox
8. Switch box
9. KOKAM li-battery
10. Ventilators

Figure 6.1: Test rig for aging tests, Chair of Dynamics and Control, U DuE, Germany [SB]

key features of the introduced test rig equipment is the ability for realizing arbitrary charging and discharging profiles.

6.2.2 Aging test procedure

The aim of the aging test is to accelerate the battery deterioration at each cycle by charging and discharging the battery with electrical characteristics/parameters exceeding those proposed by the manufacturer. In this work, the aging procedure is composed of three parts:

1. Basis test, here the battery is charged and discharged following the constant current (CC) / constant voltage (CV) charge protocol [Det11]. Within the CC-phase the battery is charged with a constant current of 1.5C until the end of charge (EoC) voltage reaches 4.2V. After that, the power supply switches to CV-phase where the battery voltage is held at 4.2V until the charging current drops to 0.5A. The discharging is performed using a constant current of 3C until the end of discharge (EoD) voltage reaches 2.7V.
2. Open-circuit voltage (OCV) test is defined in [CSK11] as the battery voltage under equilibrium conditions, i.e. the voltage when no current is owing in or out of the battery. Due to the fact that different charge amount cause different open circuit voltages, a close relationship between the SOC and the OCV can be established [XHPT14]. Thus, methods based on OCV measurements are commonly applied for SoC estimation. The SoC-OCV test consists of discharging 5% of the charge with 30A for 60s after that the battery is for 20 minutes in idle mode. This procedure is repeated until the EoD is reached.
3. Aging cycles represent the main part of the aging test and are used for targeted aging of the battery under defined operating parameters. The aging cycles are

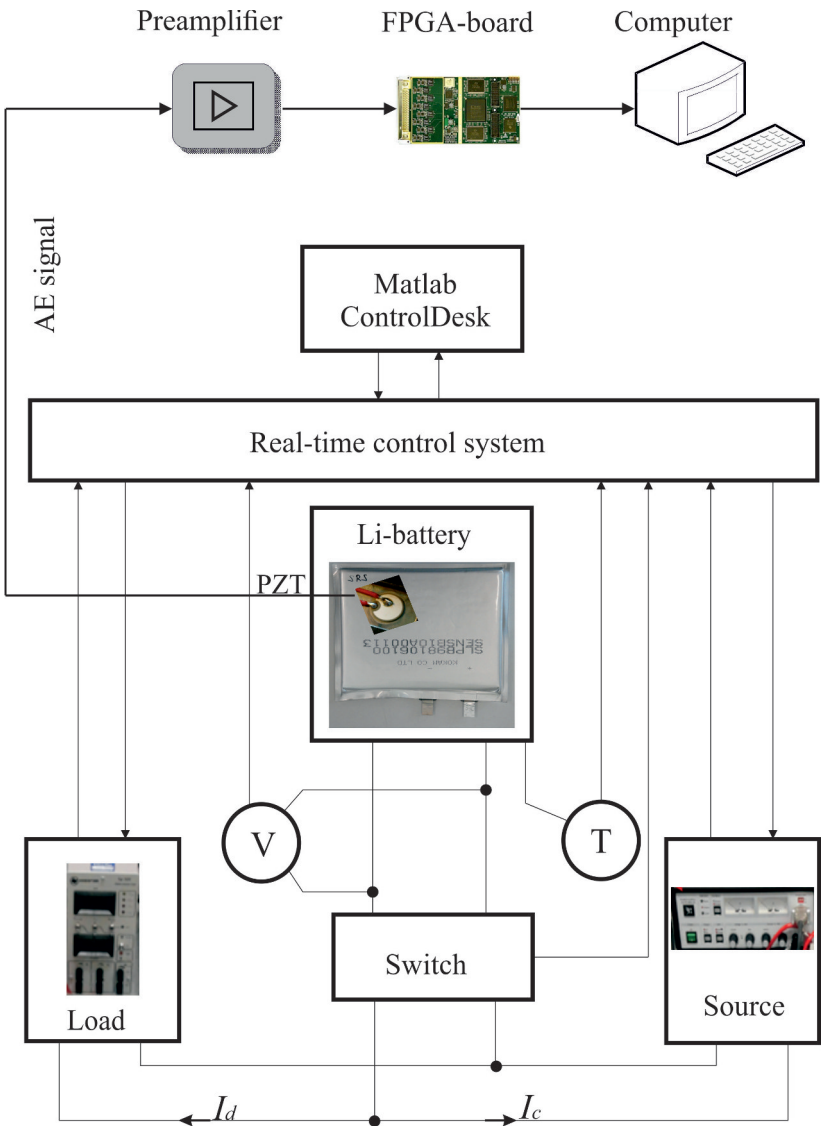

Figure 6.2: Data and signal flow of the experimental arrangement used for the aging tests, Chair of Dynamics and Control, U DuE, Germany [SB]

performed according the CC-CV procedure using different aging factors (such as EoC and EoD) which stimulate different aging process. In order to accelerate the aging process, the battery is overcharged and the aging test is carried out under maximum operating conditions. The influence of the temperature on the battery aging is not considered. Therefore, all measurements are carried out at constant room temperature.

A typical aging test comprises one basis test, one SoC-OCV test, and twelve aging cycles. During this process the emitted AE was measured either continuously throughout the whole process or during a certain period.

6.2.3 Signal processing chain

The introduced method is based on the approach used in sec. 5.2. It involves a number of processing steps that can be implemented in real-time. The proposed procedure is a multilevel processing approach comprising five processing steps. Relevant AE-based features characterizing different aging states are extracted from the measured AE data using a combination of STFT and CWT and subsequently classified by means of a multi-class SVM. First, the recorded AE signals are converted into an appropriate format and STFT is cyclic applied to the preprocessed AE data. An additional band pass filter with the range of 40 kHz to 1 MHz is applied to extract frequency of interest. The STFT result of each cycle is then investigated for its frequency content to identify relevant transient events, amplitudes, patterns, etc. Secondly, based on the fact that high AE energy are referred to significant changes in the physical properties, frequency-based AE energy is generated by calculating the root mean square of the STFT power spectrum. The next step of the processing approach consists of analyzing the AE-energy using CWT in order to extract relevant pattern. The identified patterns are then classified by applying the SVM. The analysis is mainly focused on the investigation of the frequency-based AE energy as introduced in sec. 5.2. An overview of the developed signal processing chain is shown in Fig. 6.3.

First, the recorded AE signals are preprocessed and analyzed using STFT. An additional band pass filter with the range of 40 kHz to 1 MHz is applied to extract frequencies of interest. In the next step, the STFT results are investigated for their frequency content. To identify relevant transient events, frequency-based AE energy is calculated. Furthermore, the AE energy is examined by means of CWT in order to extract significant pattern characterizing the SoH. Finally, the patterns are classified with regard to their frequency components by applying SVM.

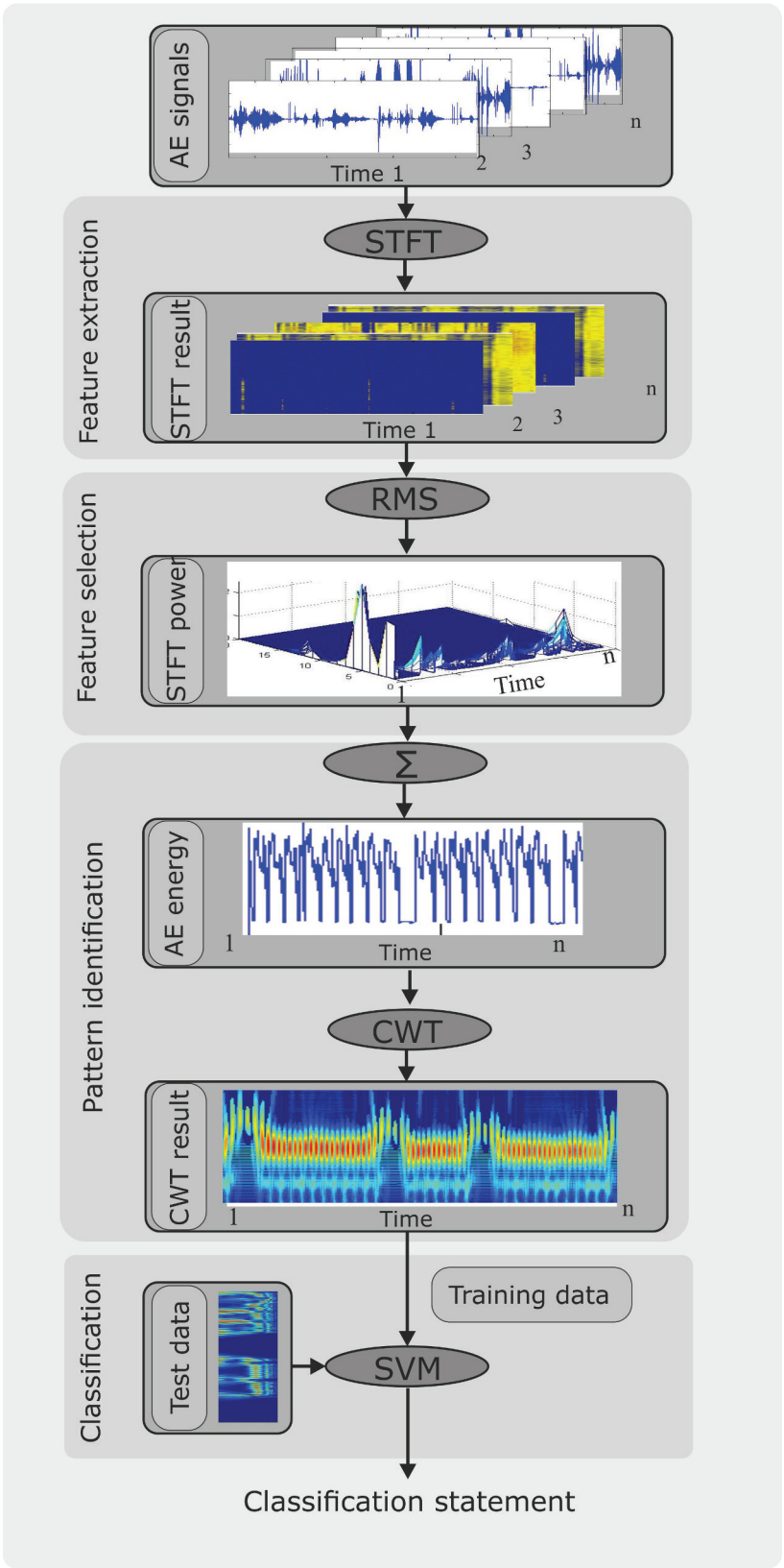

Figure 6.3: Multilevel processing approach for AE-based SoH estimation and classification [SB]

6.3 Experimental Results

6.3.1 Energy-based analysis

To investigate a correlation between SoH and the measured Acoustic Emission, the AE energy has to be calculated and analyzed. The battery degradation should be indicated by characteristics of transient events, amplitudes, and specific frequencies appearing in time and/or frequency domain. To illustrate the mentioned phenomena, aging test with the following operational parameters: $U_{EoC} = 4.3V$, $U_{EoD} = 2.7V$, $I_{EoC} = 15A$, and $I_{EoD} = -30A$ was performed at room temperature. The AE energy emitted during the initial and the last charging/discharging cycles is shown as function of time in Fig. 6.4. Significant irregularities of the energy events related to the aging process are detected. It can be observed that the initial cycle (Fig. 6.4 (a)) is characterized by high AE energy during the CC-charging, and particularly at its end. Whereas the CV-charging is characterized by a rapid decrease in the AE energy followed by a slow decrease observed during the discharging process.

In the aged state (Fig. 6.4 (b)), the AE energy appears during the CC-charging with low amplitude compared to the initial cycle. A slight decrease is also detected at the beginning of the CV-charging. Contrary to the initial cycle, here the CV-charging and the discharging process are characterized by transient events and a sudden grow of AE energy, detectable by discontinuous impulses.

The evolution of the AE energy distribution during the complete aging test (aging test 1) is shown in Fig. 6.5. On cycling, the highest AE energy amplitude is detected during the first aging cycles while the lithiation and delithiation occur. Then, the AE energy emitted during aging cycles decreases continually with cycling to reach its minimum after approximately 150 cycles (corresponding to 305 hours). This statement was also reported in [KGCT13, EIR11]. The authors attributed the observed decrease in AE activity to “the degradation of the active materials, which do not participate completely in the electrochemical reactions” [KGCT13]. It can also be observed that AE energy with low amplitude is detected during SoC-OCV tests and significant change can be noticed regarding the AE energy behavior of the individual aging cycles when the battery is in non-aged state and aged state. The results demonstrate that the AE energy present sensitivity to changes associated with the integrity degradation of lithium battery, so a correlation between the actual state of health and Acoustic Emission can be established.

6.3.2 Wavelet-based analysis

In order to extract relevant features related to SoH, the AE energy recorded during aging test 1 is examined using CWT. The result of the wavelet transform is shown in Fig. 6.6. Based on regions of high intensity, here colored in red, it can be noted that during aging cycles, AE signals occurred with specific frequency components

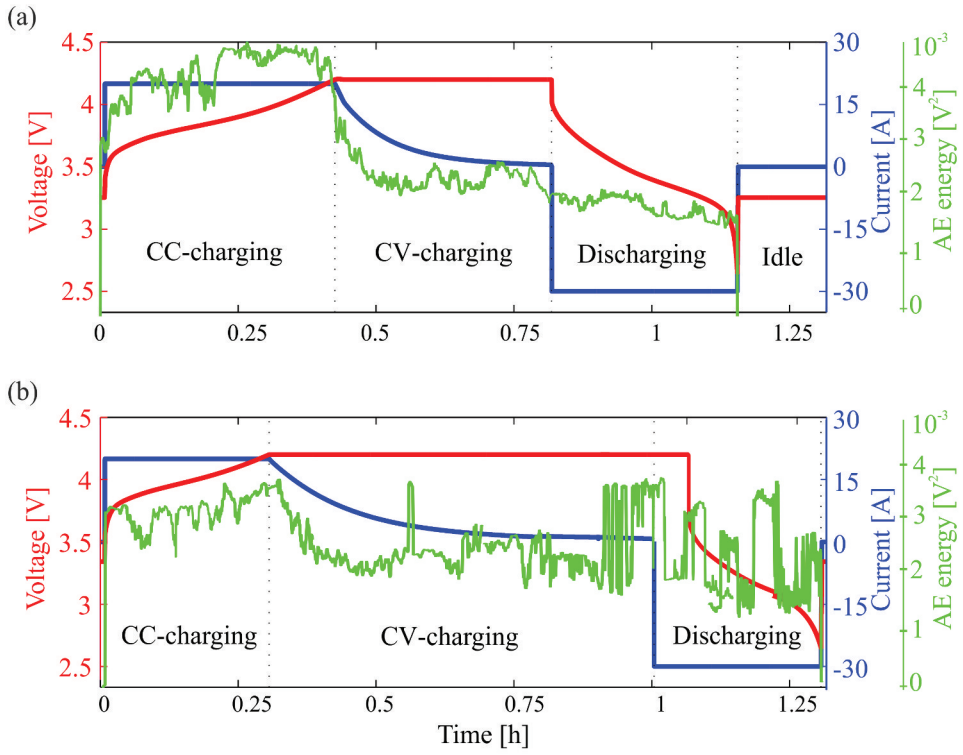

Figure 6.4: Voltage, current, and AE energy profiles during charging and discharging: (a) in non-aged state and (b) in aged state [SB]

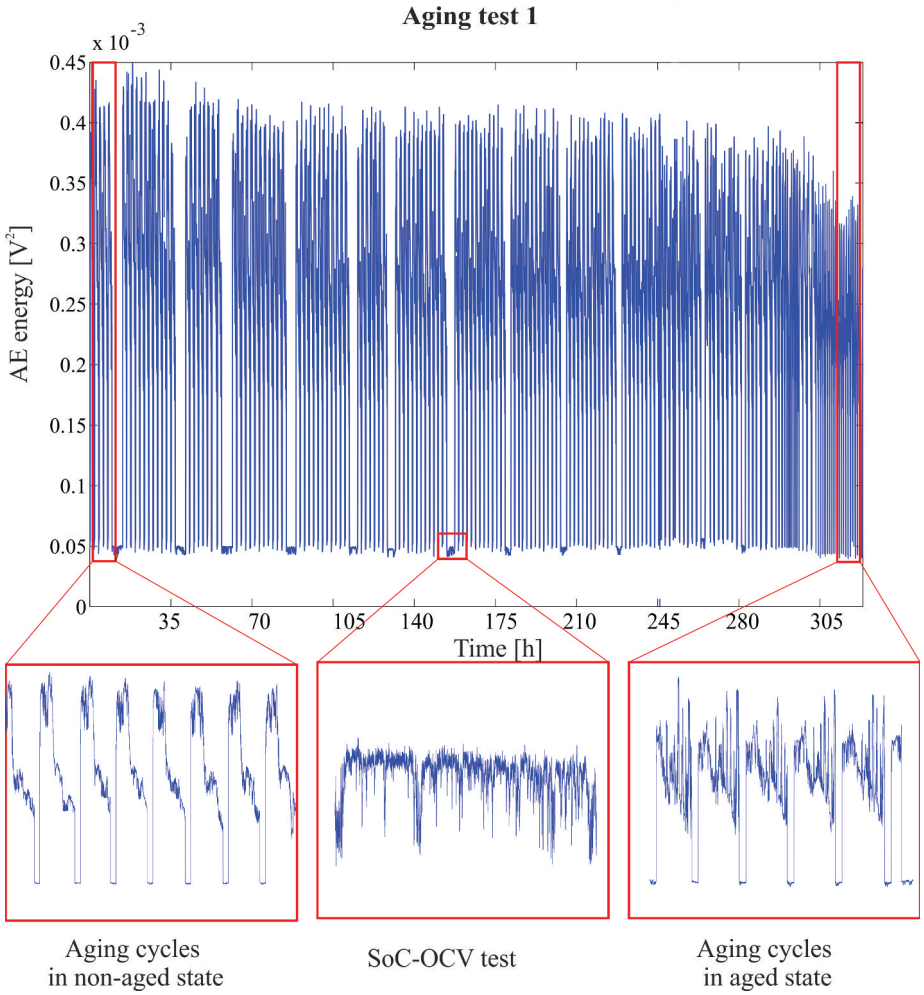

Figure 6.5: AE energy measured during the whole aging test, as function of time [SB]

Table 6.2: Operational parameters of aging test 2 and aging test 3

	Aging test 2	Aging test 3
End of charge voltage U_{EoC}	4.2V ... 4.3V	4.3V
End of discharge voltage U_{EoD}	2.7V	2.65V ... 2.7V
End of charge current I_{EoC}	10A ... 20A	15A
End of discharge current I_{EoD}	-30A	-10A ... -30A

(scale between 40 and 60). Whereas AE energy emitted during SoC-OCV tests is characterized by lower frequency components (scale > 100). The main outcomes of the CWT-based analysis are:

1. Specific patterns characterizing the aging cycles as well as the SoC-OCV tests are identified.
2. The properties of the pattern identified change in dependency on the actual state of health.

The knowledge about the obtained results allows a correlation between the SoH and the corresponding pattern and hence, based on these patterns, SoH can be automatically classified and estimated.

In order to check the repeatability of the indicated behavior of the AE energy distribution and the related CWT, two other aging tests were carried out under different operational parameters. Here, only the controllable parameters were stochastically varied. The aging profiles of the performed tests are given in Tab. 6.2.

In Fig. 6.7, the CWT analysis of AE energy measured during aging test 2 and aging test 3 is shown. Here AE has been recorded during randomly chosen periods unlike aging test 1 where AE has been recorded continuously over the whole aging process. The obtained results show similar behavior and the same patterns could be identified for both tests. The results also reveal the effects of the operational parameters on the measured AE and thus the battery integrity. It can be observed that during aging test 2, the patterns significantly change after only 140h while the same phenomena is observed after 290h during aging test 3. Consequently, it can be concluded that the aging profile plays an important role in battery lifetime, which is also known from [KGCT13, EIR11], and implicitly also observed within the reported experiments.

6.3.3 Support Vector Machine-based classification

In order to estimate and classify the SOH at different aging levels, the aging process was divided into four states (sate1: no degradation, sate 2: minimal degradation, state 3: acceptable degradation, and state 4: disproportional degradation) as shown in Fig. 6.7. Each state is characterized by specific patterns (specific CWT-coefficients) which are given as input data for the classification.

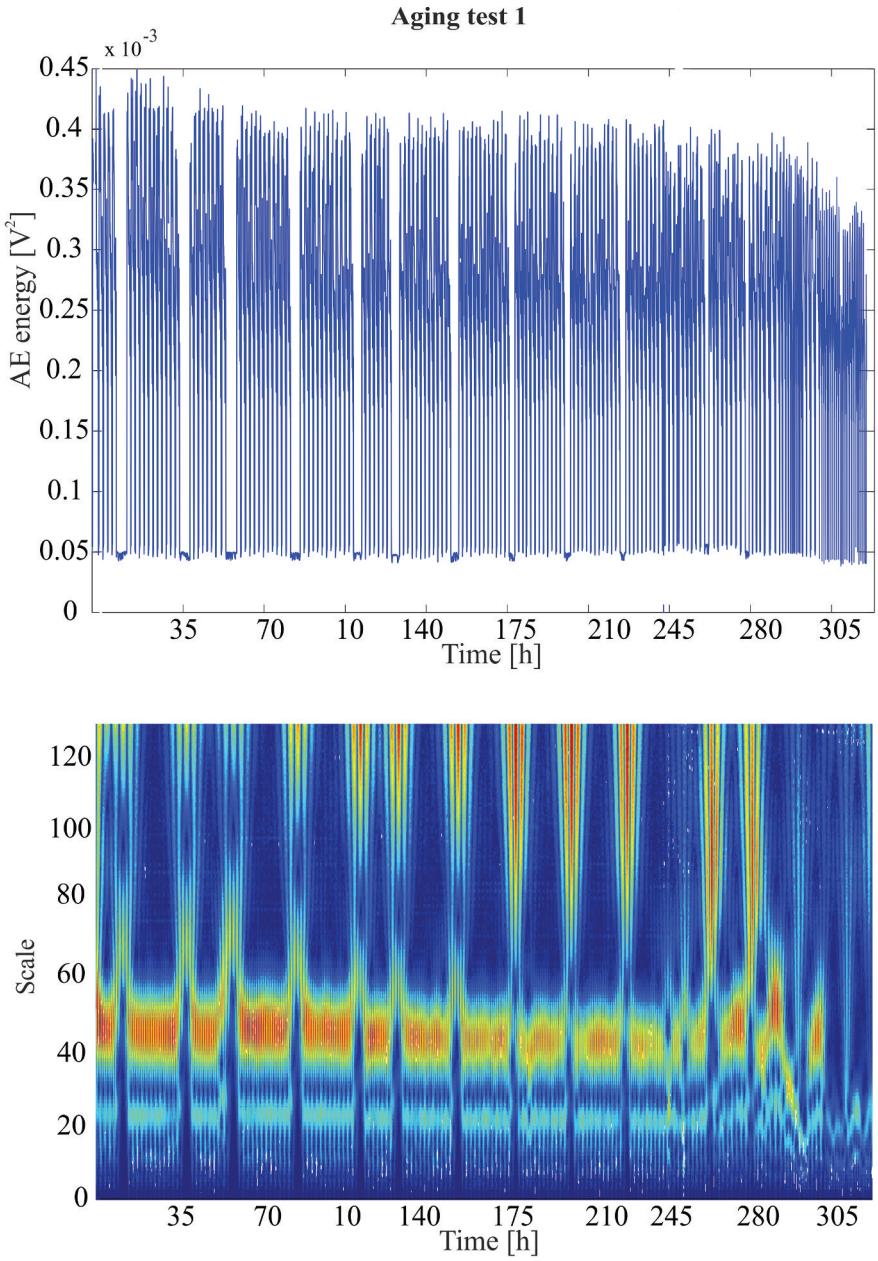

Figure 6.6: AE energy distribution and its related continuous wavelet transform [SB]

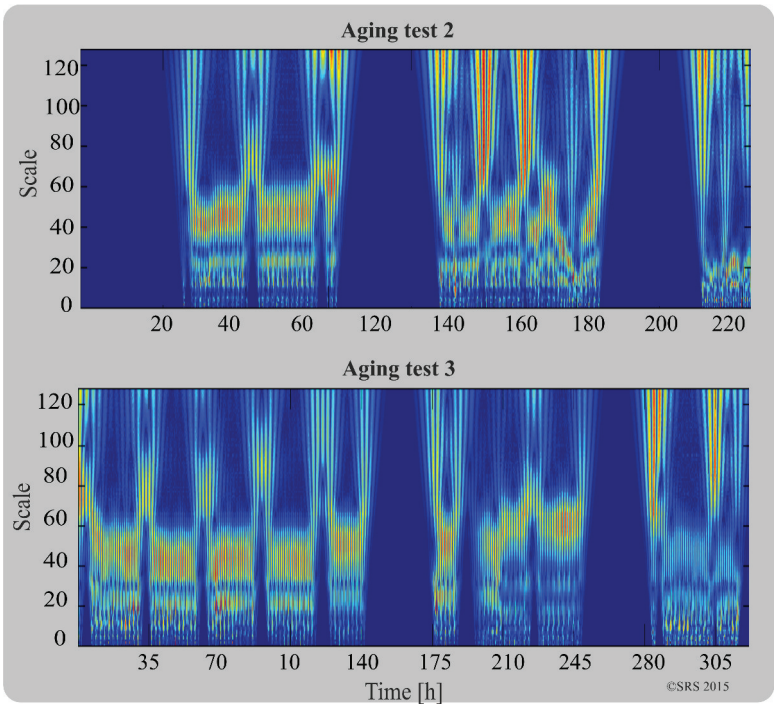

Figure 6.7: CWT analysis of AE energy measured during two aging tests with varied profiles [SB]

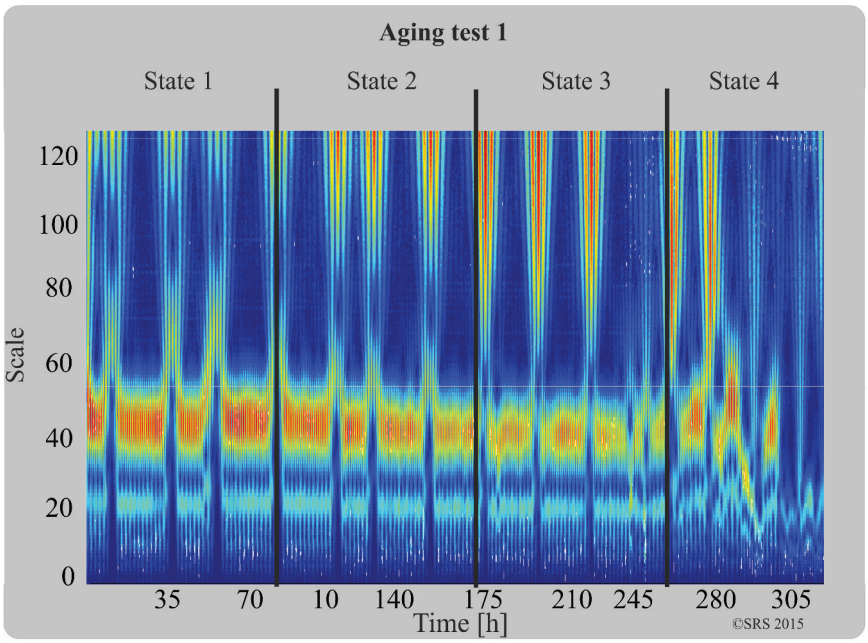

Figure 6.8: Aging process states

Table 6.3: Cross-validation accuracy and SVM classification performance

Class	CV accur.	Classification accur.
a1	99.28 %	92.94 %
b1	100 %	96.82 %
a2	92.14 %	87.12 %
b2	99.28 %	97.88 %
a3	98.57 %	94 %
b3	99.82 %	96.82 %
a4	99.28 %	95.59 %

The automated classification and recognition of the identified patterns is performed using a multi-class Support Vector Machine (SVM), see sec. 2.3.2. The data sets considered for the classification consists of samples of 128 x 100 CWT-coefficients. Since aging cycling and SoC-OCV tests are determined by two different patterns, two classes were attributed to each state except for state 4 where a distinction between classes is no longer possible. In total, seven classes (a1, a2, a3, a4, b1, b2, and b3) were defined. The procedure adopted for selecting the different classes is illustrated in Fig. 6.9.

In total, 140 samples (20 samples per class) randomly selected from CWT result of aging test 1 are used for the classification. The SVM is trained with 50 samples. In the training process, a cross-validation is performed to select accurate kernel parameters. Sequentially, the trained classifier is tested on samples extracted from CWT results of the three aging tests. The cross-validation accuracy and the performance of the classification process are summarized in Tab. 6.3. The classification accuracy demonstrates the efficiency of the classifier algorithm when dealing with samples classification.

To further investigate the performance of the designed algorithm, the training classifier is tested on all samples of aging test. The obtained result is shown in Fig. 6.10. The different colors are used to distinguish the belonging of each test sample to the correct class. A misclassification is designated by a non-matching of the blue peaks with the colored bars. From the result, it can be concluded that the algorithm can classify the systems' states quite reliable. The obtained classification rates of all classes are satisfactory. The classes b2, a3, b3, and a4 achieve the best classification accuracy. Nevertheless, the algorithm has to be improved in order to eliminate the misclassifications observed in classes a1, b1, a2.

6.4 Discussion and Conclusions

The aim of this chapter was to investigate the capability of the Acoustic Emission technique to estimate the SoH of lithium-ion battery. Therefore, a test rig was

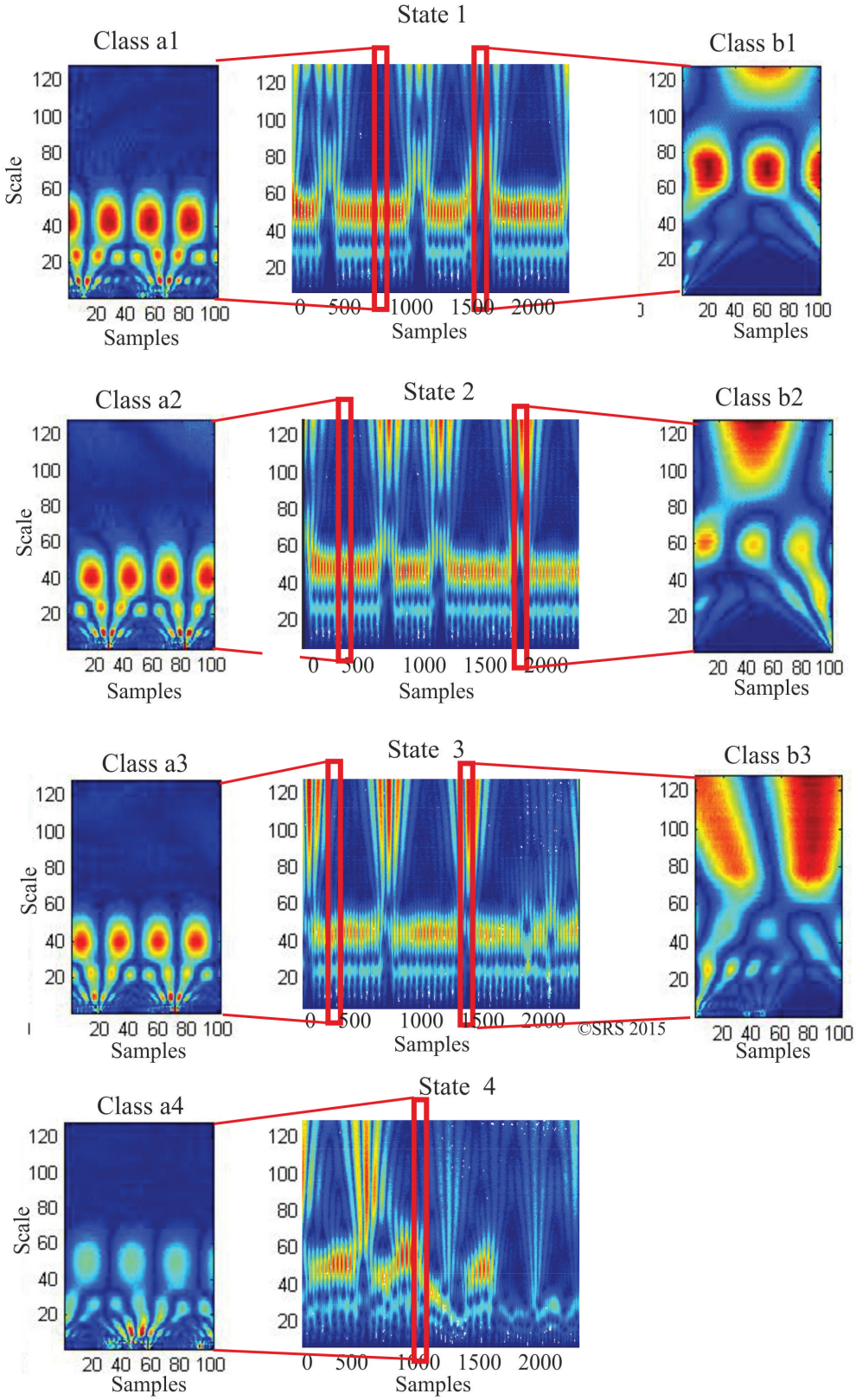

Figure 6.9: Procedure adopted for class determination [SB]

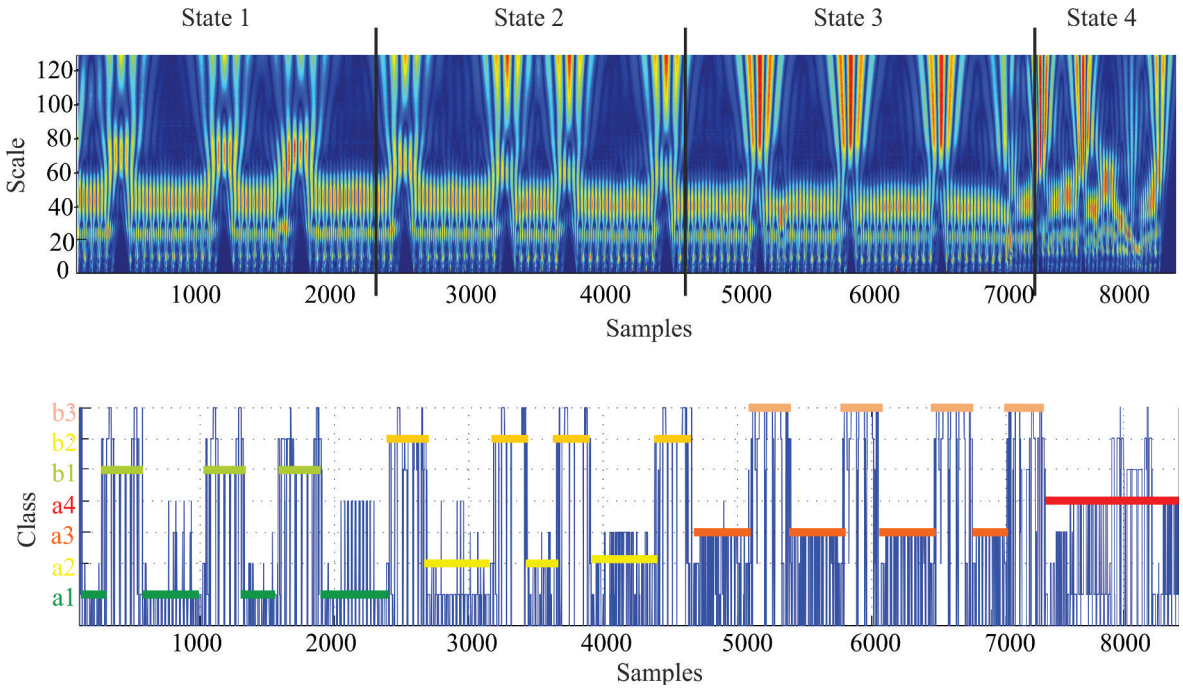

Figure 6.10: SVM classification performance on all samples of aging test 1 [SB]

designed and extended by the FPGA-measurement chain. An advanced multilevel signal processing approach comprising five processing steps was developed in order find a correlation between the emitted AE signals and the deterioration level of the battery. The validation of the new SoH estimation approach is based on battery data, collected from three aging tests performed with different aging profiles. Relevant AE-based features characterizing different aging states were extracted from the measured AE data using CWT. From the frequency-based AE energy, a distinction between a non-aged state and aged state could be detected. The AE energy showed sensitivity to changes associated with the integrity degradation of lithium battery and a strong correlation between the actual state of health and Acoustic Emission could be established. Furthermore, the application of the CWT to the AE energy allowed the identification of specific patterns characterizing the aging cycles as well as the SoC-OCV tests. It could be concluded that properties of the pattern change in dependency on the actual state of health. Subsequently, the extracted patterns were used as input data to model the multi-class SVM. The obtained classification accuracy was quite satisfactorily and reached 100% by certain classes. Compared to the model-based SoH estimation methods, the Acoustic Emission seems to be a promising SoH estimation method that can be implemented in battery management system.

7 Summary and Future Work

This thesis was essentially focused on the development, implementation, and validation of an Acoustic Emission-based structural health monitoring system capable to detect, acquire, identify, and classify several damages occurring in different materials. The Acoustic Emission technique was chosen for its ability to detect dynamic processes or changes during operation allowing an in-situ health monitoring thereby. In order to achieve the objectives of the thesis, an FPGA-based measurement chain and advanced signal processing techniques including pattern recognition approaches were developed and discussed in detail. The experimental application and validation of the developed SHM system represents the core of this work. For this purpose different test rigs were set up and series of tests were carried out in wear resistant plates, composite plates, and electrochemical components in order to identify the advantages and limitations of the proposed methodology.

Summary, resulting scientific contribution, and related benefits are summarized in the next sections. Additionally, further steps and new ideas, which were identified in conjunction with this thesis, are briefly described in the final section of this chapter

7.1 Summary

In the first Chapter, the main goals of structural health monitoring as well as the effect of the implementation of an SHM system regarding safety, economic, and commercial aspects were introduced. Additionally, the research objectives and the related challenges were presented.

In Chapter 2, theoretical background about Acoustic Emission, wave propagation, and the principle of AE data analysis were given. Since efficiency and reliability of an SHM system are strongly dependent on data processing and interpretation, fundamentals of advanced signal processing approaches with emphasis on STFT, CWT, pattern recognition, and supervised classification were introduced. In the third section, AE examination of sliding wear was discussed, starting with an introduction to wear mechanisms. Then, previous works to date of AE monitoring of sliding contact with focus on the relationship between sliding wear and Acoustic Emission were reviewed, and implications related to this study were discussed. The third section was devoted to the basic theories of Fiber Reinforced Polymer Composites. In order to thoroughly understand the potential failure mechanisms, a description of the different damage mechanisms was presented. This is followed

by an extended review on the use of AET to identify failure modes. Based on the relevance of review outcomes, guidelines for this work were determined. Finally, the application of Acoustic Emission to electrochemical cells focusing on lithium-based batteries was introduced. In order to understand the effects leading to capacity decrease and power reduction, the main aging mechanisms and the related degree of deterioration were discussed, and the challenges of this new application of Acoustic Emission were highlighted.

In Chapter 3, the development concept of the SHM system with focus on the measurement chain, used for all experimental tests, was introduced. The FPGA-based equipment and the process of recording AE signals were explained, and the effectiveness of the developed hardware with regard to the real-time implementation of advanced filtering techniques was demonstrated. In addition, preliminary tests and test setups have been carried out to investigate important effects that have a major impact on the measured AE signal. Furthermore, the influences of coupling medium, sensor arrangement and sensor location on the AE signals are discussed in detail and demonstrated through generation and analysis of artificial AE sources. The main objective of the preliminary tests was to understand the limitations and the use of the measurement chain in order to select the proper equipment that allows an exact reproducibility of the different experiments. All tests show that the amplitude is the parameter the more influenced contrary to the frequency that remains unchanged. Based on the achievement resulting from the preliminary tests, it was determined that the analysis of AE signals and hence the damage detection will be mainly performed using features extracted from the time-frequency analysis.

In Chapter 4, wear detection and classification by means of Acoustic Emission were investigated. A reliable and efficient methodology for online detection and classification of wear phenomena by means of Acoustic Emission and advanced signal processing approaches was introduced. The experiments were performed using a tribological system consisting of two martensitic plates, sliding against each other. In the first section, the developed signal processing chain was introduced. The recorded AE signals were analyzed mainly by time-frequency analysis and features extraction using a novel combination of STFT and CWT. The AE signals were examined, and the energy distribution was calculated using STFT. The third section is devoted to the experimental results. A correlation analysis between AE characteristics and the surface damage resulting from contact fatigue was investigated and three wear process stages were detected and could be distinguished. To obtain quantitative and detailed information about different wear phases, the AE energy was decomposed into a suitable number of frequency levels. The individual energy distribution and the cumulative AE energy of each frequency components were analyzed using CWT to determine different phases of the wear process. Results show that the behavior of individual frequency component changes when the wear-related effects change. Here, specific frequency ranges were attributed to the different wear-states so that a clear connection between material changes like abrasive wear, small cracks close to the surface, and surface fatigue could be determined.

In Chapter 5, an AE-based SHM system for online detection and automated classification of failure modes produced in composite structure was introduced. For this purpose, a test rig and an advanced multilevel processing approach combining CWT and multivariate statistical analysis were developed and presented in the first section. The Indentation tests were performed on CFRP plates, and the generated AE signals were recorded by the introduced measurement chain. In contrast, to the cited literature, for the pattern identification no time parameters were taken into consideration, only wavelet coefficients were used as descriptors. Continuous wavelet transform was firstly performed on preprocessed AE data to extract relevant features. Next, the dimension of the wavelet coefficient matrices was reduced using PCA. Further, KDE was used in order to restrict the zone with high feature density by smoothing the two highest principal components for better pattern identification and classification. Finally, a classification procedure was carried out for the results obtained from the KDE by using a multiclass SVM. Furthermore, waveform and frequency content of the detected AE signals were in depth examined and compared with fundamental assumptions reported in this field. The obtained frequency ranges were in accordance with those known from the literature. Specific frequency ranges could be assigned to the failure modes based on fundamental assumptions reported by various authors. It could be concluded that the selected features are effective indices of the different damage mechanisms. Signals related to delamination have the lowest frequencies while signals generated by fiber breakage have the highest frequencies. Concerning the classification, the system was trained to recognize damage represented by one pattern. The obtained classification performance reaches in same cases 94.69%.

In Chapter 6, the application of the proposed AE-based SHM system to online estimation and automated classification of State of Health (SoH) of lithium-ion battery was presented. First, the relationship between SoH and aging process was introduced. The second section was devoted to the accelerated aging test procedure including test rig and the developed signal processing approach. An advanced multilevel signal processing approach comprising five processing steps was developed in order find a correlation between the emitted AE signals and the deterioration level of the battery. The validation of the new SoH estimation approach was based on battery data collected from three aging tests performed with different aging profiles. Relevant AE-based features characterizing different aging states were extracted from the measured AE data using CWT. The third section presented the experimental results. From the frequency-based AE energy, a distinction between a non-aged state and aged state could be detected. Furthermore, the application of the CWT to the AE energy allowed the identification of specific patterns characterizing the aging cycles as well as the SoC-OCV tests. By applying the multi-class SVM, the pattern was classified with a satisfactory performance that demonstrates the effectiveness of using AE-based battery management systems to establish a direct correlation between SoH and the generated AE.

7.2 Contributions

The central scientific contributions of this thesis are summarized as follows:

- A reliable and cost efficient SHM system, able to analyze AE data in real-time, was developed. Through integration of high-speed electronic devices, continuous and real-time damage identification can be realized overcoming a fundamental challenge met by current systems. In order to test the FPGA-advantages over other technologies, regarding the real-time implementation of digital signal processing algorithms, STFT module was developed. The obtained results confirm the ability of the developed SHM system for real-time applications. In addition, the SHM system is easily adaptable to various structures and can be applied to monitor several complex systems.
- Efficiency and reliability of SHM system are strongly dependent on signal processing approaches. Unlike the measurement chain, there is no predefined processing technique able to solve all problems for all structures. The signal processing methods have to be adapted to the measured AE data that depends on experiment, test duration, and operational condition. Therefore, a combination of several damage identification techniques, pattern recognition methods, and classification approaches were developed to identify the wide variety of damage scenarios.
- The SHM system was successfully validated on a tribological system. Three wear-states could be identified. Specific frequency ranges could be attributed. A strong correlation between material changes (like abrasive wear, small cracks close to the surface, and surface fatigue) and the related Acoustic Emission could be established. The system based on time-frequency analysis showed high reliability regarding the detection and quantification of the state-of-damage and the damage progression. The study reveals that the application of the STFT- / CWT-based AE analysis is an appropriate approach to distinguish and to interpret the different damage states occurred during sliding contact. The information related to the damage accumulation and the damage assigned frequencies can be applied to obtain asset management or lifetime control of a system.
- The effectiveness of the developed SHM system to detect, identify, and classify several failure modes, occurring in CFRP plates, was investigated. The Acoustic Emission data and the related failure modes could be identified with more confidence by considering the wavelet coefficients as descriptors than by employing time-based features. The new introduced signal processing approach leads to a noticeable better identification and classification of damage mechanism and also proves the efficiency of the adopted multivariate statistical methods (PCA and KDE) and classification approaches (SVM). The presented methodology will allow an automated health monitoring of CFRP structures and, therefore, contribute increasing safety and reliability of composite-based

constructions in engineering applications like aeronautic and aerospace.

- The developed measurement chain in combination with an advanced multilevel signal processing approach were used to investigate the integrity of lithium-based battery, in terms of state of health. The recorded Acoustic Emission showed sensitivity to changes associated with the integrity degradation of lithium battery and a strong correlation between the actual state of health and Acoustic Emission could be established. The identification of specific patterns characterizing the aging cycles as well as the SoC-OCV tests demonstrate the effectiveness of using AE to SoH estimation. The potential benefits of this research have important consequences. Particularly when considering that the current methods for SoH estimation are limited to empirical models that require more information (in terms of voltage, current, impedance, ...) and, therefore, a significant computational effort. In addition, the proposed methodology can be implemented in battery management systems.

7.3 Future Work

With respect to the results presented in this thesis, further research should focus on the following aspects:

- Improvement of the measurement chain with regard to calibration and impedance in order to reduce noise and ensure better signal quality
- The development of a complete structural health monitoring solution requires the implementation of the developed algorithms in FPGA.
- The wavelet-coefficient-based approach is a novel damage identification method and obtained better results than the time-based method. The applicability of this approach should be validated on a variety of practical structures under real operating conditions to generalize it as an advanced damage detection tool for complex systems. Furthermore, more research is required on the influence of changes in the operational and environmental conditions.
- In order to suggest the Acoustic Emission as a robust battery state of health indicator, further aging tests with different profiles should be carried out. In addition, the Acoustic Emission can be used to detect and identify the individual aging mechanisms.
- The classifier revealed some difficulties when dealing with a 'continuous' classification. This can be improved by training the classification with samples extracted from different aging tests.

Bibliography

[AAF11] A. Akinwale, K. Adesina, and O. Folorunso. A framework for reducing multidimensional database to two dimensions. *Journal of Information and Computing Science*, 6:269–278, 2011.

[ABC+03] A. Affanni, A. Bellini, C. Concari, G. Franceschini, E. Lorenzani, and C. Tassoni. EV battery state of charge: neural network based estimation. In *Electric Machines and Drives Conference, 2003. IEMDC'03. IEEE International, Madison, Wisconsin USA*, volume 2, pages 684–688, June 2003.

[Abe10] S. Abe. *Support vector machines for pattern classification*. Springer-Verlag London Limited, London, England, 2010.

[ABSC11] F. Al-Badour, M. Sunar, and L. Cheded. Vibration analysis of rotating machinery using time-frequency analysis and wavelet techniques. *Mechanical Systems and Signal Processing*, 25(6):2083–2101, 2011. Interdisciplinary Aspects of Vehicle Dynamics.

[Ach73] J.D. Achenbach. *Wave Propagation in Elastic Solids*. Applied Mathematics and Mechanics Series. North-Holland Publishing Company, 1973.

[Ada07] D. Adams. *Health Monitoring of Structural Materials and Components: Methods with Applications*. Wiley, 2007.

[Add10] P.S. Addison. *The illustrated wavelet transform handbook: introductory theory and applications in science, engineering, medicine and finance*. Taylor & Francis, 2010.

[AF13] V. Agubra and J. Fergus. Lithium ion battery anode aging mechanisms. *Materials*, 6(4):1310–1325, 2013.

[AJEOT11] M. Azarbayejani, M. Jalalpour, A. El-Osery, and M. Reda Taha. Field application of smart SHM using field programmable gate array technology to monitor an RC bridge in New Mexico. *Smart Materials and Structures*, 20(8):85–105, 2011.

[AKM11] D.G. Aggelis, E.Z. Kordatos, and T.E. Matikas. Acoustic emission for fatigue damage characterization in metal plates. *Mechanics Research Communications*, 38(2):106–110, 2011.

[AKS+13] V. Arumugam, C.S. Kumar, C. Santulli, F. Sarasini, and A.J. Stanley. Identification of failure modes in composites from clustered acoustic emission data using pattern recognition and wavelet transformation. *Arabian Journal for Science and Engineering*, 38(5):1087–1102, 2013.

[AP95] A. Anastassopoulos and T.P. Philippidis. Clustering methodology for the evaluation of acoustic emission from composites. *Journal of Acoustic Emission*, 13:11–22, 1995.

[AS12] K. Asamene and M. Sundaresan. Analysis of experimentally generated friction related acoustic emission signals. *Wear*, 296(12):607–618, 2012.

[AST90] Standard Terminology for Nondestructive Examinations. E 1316-90, 1990.

[AST05] Standard Guide for Determining the Reproducibility of Acoustic Emission Sensor Response E 976-05, 2005.

[Ast06] V.P. Astakhov. *Tribology of Metal Cutting*. Tribology and Interface Engineering. Elsevier Science, 2006.

[AWD98] P. Arora, R. E. White, and M. Doyle. Capacity fade mechanisms and side reactions in lithium-ion batteries. *Journal of The Electrochemical Society*, 145(10):3647–3667, 1998.

[Bal06] D. Balageas. *Structural Health Monitoring*, chapter Introduction to Structural Health Monitoring, pages 13–44. ISTE, London, UK, 2006.

[BB94] S. Barre and M.L. Benzeggagh. On the use of acoustic emission to investigate damage mechanisms in glass-fibre-reinforced polypropylene. *Composites Science and Technology*, 52(3):369–376, 1994.

[BB06] A.J. Brunner and M. Barbezat. Acoustic Emission Monitoring of Delamination Growth in Fiber-Reinforced Polymer-Matrix Composites. In E.E. Gdoutos, editor, *Fracture of Nano and Engineering Materials and Structures*, pages 291–292. Springer Netherlands, 2006.

[BB10] K.G. Budinski and M.K. Budinski. *Engineering Materials: Properties and Selection*. Prentice Hall, 2010.

[BBB+05] M. Broussely, P. Biensan, F. Bonhomme, P. Blanchard, S. Herreyre, K. Nechev, and R.J. Staniewicz. Main aging mechanisms in Li-ion batteries. *Journal of Power Sources*, 146(1-2):90–96, 2005.

[BBHF07] M. Barbezat, A.J. Brunner, C. Huber, and P. Flüeler. Integrated active fiber composite elements: Characterization for acoustic emission and acousto-ultrasonics. *Journal of Intelligent Material Systems and Structures*, 18(5):515–525, 2007.

[BCBK01] N. Baydar, Q. Chen, A. Ball, and U. Kruger. Detection of incipient tooth defect in helical gears using multivarioate statistics. *Mechanical Systems and Signal Processing*, 15(2):303–321, 2001.

[BDS11] D. Baccar, K.U. Dettmann, and D. Söffker. FPGA-based realization of online damage state and wear detection using acoustic emission. In *Proc. 5th ECCOMAS Thematic Conference on Smart Structures and Materials SMART11, Saarbrücken, July 6-8*, pages 474–481, 2011.

[BKA14] K.M. Bak, K. Kalaichelvan, and V. Arumugam. A novel approach for classification of failure modes in single lap joints using acoustic emission data. *Journal of Composite Materials*, 48(24):3003–3017, 2014.

[BKI+08] A. Bussiba, M. Kupiec, S. Ifergane, R. Piat, and T. Böhlke. Damage evolution and fracture events sequence in various composites by acoustic emission technique. *Composites Science and Technology*, 68(5):1144–1155, 2008.

[BKKK06] S. Baby, J. Kumar, M. M. Kumar, and V. Kumar. Application of NDE techniques for damage measurements in IMI-834 titanium alloy under monotonic loading conditions. In *Proc. National Seminar on Non-Destructive Evaluation, Hyderabad , India*, 2006.

[BKSS11] V.M. Baranov, E.M. Kudryavtsev, G.A. Sarychev, and V.M. Schavelin. *Acoustic Emission in Friction*. Tribology and Interface Engineering. Elsevier Science, 2011.

[BM91] R.J. Boness and S.L. McBride. Adhesive and abrasive wear studies using acoustic emission techniques. *Wear*, 149(12):41–53, 1991.

[BMFF11] S. Bashash, S. J. Moura, J. C. Forman, and H. K. Fathy. Plug-in hybrid electric vehicle charge pattern optimization for energy cost and battery longevity. *Journal of Power Sources*, 196(1):541–549, 2011.

[Boh00] J. Bohse. Acoustic emission characteristics of micro-failure processes in polymer blends and composites. *Composites Science and Technology*, 60(8):1213–1226, 2000.

[BP06] S. Bacchelli and S. Papi. Image denoising using principal component analysis in the wavelet domain. *Journal of Computational and Applied Mathematics*, 189(1):606–621, 2006.

[BR90] J.M. Berthelot and J. Rhazi. Acoustic emission in carbon fibre composites. *Composites Science and Technology*, 37(4):411–428, 1990.

[BS] D. Baccar and D. Söffker. Identification and classification of failure modes in laminated composites by using a multivariate statistical analysis of wavelet coefficients. *Mechanical Systems and Signal Processing*, 2015, submitted.

[BS12a] D. Baccar and D. Söffker. Classification of wear by means of acoustic emission and signal processing techniques. In C. Boller, editor, *6th European Workshop on Structural Health Monitoring - We.2.D.4, Dresden, Germany*. German Society for Nondestructive Testing (DGZfP), July 2012.

[BS12b] D. Baccar and D. Söffker. Wavelet-based online evaluation and classification of wear state using acoustic emission. In *Conference on Smart Materials, Adaptive Structures and Intelligent Systems, Stone Mountain, GA, USA*, pages 609–614. ASME, 2012.

[BS13] D. Baccar and D. Söffker. Application of acoustic emission technique for online evaluation and classification of wear state. In F.K. Chang, editor, *9th International Workshop in Structural Health Monitoring, IWSHM 2013*, volume 2, pages 1218–1225. DEStech Publications, Inc., Stanford, CA, September 2013.

[BS15] D. Baccar and D. Söffker. Wear detection by means of wavelet-based acoustic emission analysis. *Mechanical Systems and Signal Processing*, 60-61:198–207, 2015.

[BSS14] D. Baccar, S. Schiffer, and D. Söffker. Acoustic emission-based identification and classification of frictional wear of metallic surfaces. In Le Cam and Mevel and Schoefs, editor, *7th European Workshop on Structural Health Monitoring, EWSHM*, pages 1178–1185, Nantes, France, July 2014.

[BTI+11] A. Bouzida, O. Touhami, R. Ibtiouen, A. Belouchrani, M. Fadel, and A. Rezzoug. Fault diagnosis in industrial induction machines through discrete wavelet transform. *IEEE Transactions on Industrial Electronics*, 58(9):4385–4395, 2011.

[Bur98] C.J. Burges. A tutorial on support vector machines for pattern recognition. *Data Mining and Knowledge Discovery*, 2:121–167, 1998.

[BV00] S.D. Brown and Z.G. Vranesic. *Fundamentals of Digital Logic with VHDL Design*. Series in Electrical and Computer Engineering. McGraw-Hill, 2000.

[Cam10] F.C. Campbell. *Structural Composite Materials*. ASM International, 2010.

[CCC+03] L.J. Cao, K.S. Chua, W.K. Chong, H.P. Lee, and Q.M. Gu. A comparison of pca, {KPCA} and {ICA} for dimensionality reduction in support vector machine. *Neurocomputing*, 55(1):321–336, 2003. Support Vector Machines.

[CCP13] L. Calabrese, G. Campanella, and E. Proverbio. Identification of corrosion mechanisms by univariate and multivariate statistical analysis during long term acoustic emission monitoring on a pre-stressed concrete beam. *Corrosion Science*, 73:161–171, 2013.

[CF10] M. Charkhgard and M. Farrokhi. State-of-Charge Estimation for Lithium-Ion Batteries Using Neural Networks and EKF. *Industrial Electronics, IEEE Transactions on*, 57(12):4178–4187, Dec 2010.

[CHWK09] H. Chang, E.H. Han, J.Q. Wang, and W. Ke. Acoustic emission study of fatigue crack closure of physical short and long cracks for aluminum alloy. *International Journal of Fatigue*, 31(3):403–407, 2009.

[CKTR92] O. Chen, P. Karandikar, N. Takeda, and T. Rcast. Acoustic emission characterization of a glass-matrix composite. *Nondestructive Testing and Evaluation*, 8(1-6):869–878, 1992.

[CLL+05] S.W. Choi, C. Lee, J.M. Lee, J.H. Park, and I.B. Lee. Fault detection and identification of nonlinear processes based on kernel PCA. *Chemometrics and Intelligent Laboratory Systems*, 75(1):55–67, 2005.

[Coh92] L. Cohen. Instantaneous scale and the short-time scale transform. In *Time-Frequency and Time-Scale Analysis. Proceedings of the IEEE-SP International Symposium, Pittsburglh, Pennsylvania, USA* , pages 383–386, Oct 1992.

[CPZ11] L. Chao, D. Peng, and C. Zhenhua. Time-frequency analysis of acoustic emission signals generated by tension damage in CFRP. *Procedia Engineering*, 23:210–215, 2011.

[CS02] K. Crammer and Y. Singer. On the algorithmic implementation of multiclass kernel-based vector machines. *Journal of Machine Learning Research*, 2:265–292, 2002.

[CSK11] Y.H. Chiang, W.Y. Sean, and J.C. Ke. Online estimation of internal resistance and open-circuit voltage of lithium-ion batteries in electric vehicles. *Journal of Power Sources*, 196(8):3921–3932, 2011.

[CSV96] O. Ceysson, M. Salvia, and L. Vincent. Damage mechanisms characterisation of carbon fibre/epoxy composite laminates by both electrical resistance measurements and acoustic emission analysis. *Scripta Materialia*, 34(8):1273–1280, 1996.

[CV95] C. Cortes and V. Vapnik. Support-vector networks. *Mach. Learn.*, 20(3):273–297, September 1995.

[CV05] M.F. Carlos and H. Vallen. *Nondestructive testing handbook: Acoustic emission testing*, volume 6, chapter Acoustic Emission Signal Processing, pages 153–154. American Society for Nondestructive Testing, ASNT, 2005.

[CWGS00] Q. Chen, R.J. Wynne, P. Goulding, and D. Sandoz. The application of principal component analysis and kernel density estimation to enhance process monitoring. *Control Engineering Practice*, 8(5):531–543, 2000.

[DC84] R. Dukes and E.A. Culpan. Acoustic emission: its techniques and applications. *IEE Proceedings on Physical Science, Measurement and Instrumentation, Management, and Education - Reviews*, 131(4):241–251, 1984.

[Det11] K.U. Dettmann. *Probalistic-based method for realizing safe and reliable mechatronic systems*. Dr.-Ing. thesis. Universität Duisburg-Essen, 2011.

[dGWJ95] P.J. de Groot, P.A.M. Wijnen, and R.B.F. Janssen. Real-time frequency determination of acoustic emission for different fracture mechanisms in carbon/epoxy composites. *Composites Science and Technology*, 55(4):405–412, 1995.

[DHC04] D.J. Dorsey, R. Hebner, and W.S. Charlton. Non-destructive evaluation of carbon fiber composite reinforcement content. *Journal of Composite Materials*, 38(17):1505–1519, 2004.

[DHPS07] G. Derrien, J. Hassoun, S. Panero, and B. Scrosati. Nanostructured sn-c composite as an advanced anode material in high-performance lithium-ion batteries. *Advanced Materials*, 19(17):2336–2340, 2007.

[DK96] K.I. Diamantaras and S.Y. Kung. *Principal Component Neural Networks: Theory and Applications*. John Wiley & Sons, Inc., New York, NY, USA, 1996.

[dOM08] R. de Oliveira and A.T. Marques. Health monitoring of FRP using acoustic emission and artificial neural networks. *Computers and Structures*, 86(3-5):367–373, 2008.

[DS11] K.U. Dettmann and D. Söffker. Adaptive modeling of reliability properties for control and supervision purposes. *Int. J. Appl. Math. Comput. Sci.*, 21(3):479–486, 2011.

[DS14] L. Debnath and F. Shah. *Wavelet Transforms and Their Applications*. Birkhäuser Boston, 2014.

[EIR11] A. Etiemble, H. Idrissi, and L. Roue. On the decrepitation mechanism of mgni and lani5-based electrodes studied by in situ acoustic emission. *Journal of Power Sources,*, 196(12):5168–5173, 2011.

[ELH+04] C. Ennaceur, A. Laksimi, C. Herve, M. Mediouni, and M. Cherfaoui. Acoustic emission technique and potential difference method for detecting the different stages of crack propagation in carbon and stainless steels. *Journal of Acoustic Emission*, 22:71–76, 2004.

[EM08] M. Elforjani and D. Mba. Detecting the onset, propagation and location of non-artificial defects in a slow rotating thrust bearing with acoustic emission. *Insight - Non-Destructive Testing and Condition Monitoring*, 50(5):264–268, 2008.

[EMF+11] M. Eaton, M. May, C. Featherston, K. Holford, S. Hallet, and R. Pullin. Characterisation of damage in composite structures using acoustic emission. *Journal of Physics: Conference Series*, 305(1):1–9, 2011.

[EPH13] H.A. Elfergani, R. Pullin, and K.M. Holford. Damage assessment of corrosion in prestressed concrete by acoustic emission. *Construction and Building Materials*, 40:925–933, 2013.

[FB94] D. Fang and A. Berkovits. Evaluation of fatigue damage accumulation by acoustic emission. *Fatigue & Fracture of Engineering Materials & Structures*, 17(9):1057–1067, 1994.

[FDN01] C.R. Farrar, S.W. Doebling, and D.A. Nix. Vibration-based structural damage identification. 359(1778):131–149, 2001.

[FK01] S. Fouvry and P.H. Kapsa. An energy description of hard coating wear mechanisms. *Surface and Coatings Technology*, 138:141–148, 2001.

[FLK+03] S. Fouvry, T. Liskiewicz, P. Kapsa, S. Hannel, and E. Sauger. An energy description of wear mechanisms and its applications to oscillating sliding contacts. *Wear*, 255(6):287–298, 2003.

[FMK11] J. Fiala, P. Mazal, and M. Kolega. Cycle induced microstructural changes. *International Journal of Microstructure and Materials Properties*, 6(3):259–272, 2011.

[FMM+14] A. Farhidzadeh, A.C. Mpalaskas, T.E. Matikas, H. Farhidzadeh, and D.G. Aggelis. Fracture mode identification in cementitious materials using supervised pattern recognition of acoustic emission features. *Construction and Building Materials*, 67:129–138, 2014.

[FW07] C.R. Farrar and K. Worden. An introduction to structural health monitoring. *Philosophical Transactions of the Royal Society A: Mathematical, Physical and Engineering Sciences*, 365(1851):303–315, 2007.

[GCE+98] M. Giordano, A. Calabro, C. Esposito, A. D'Amore, and L. Nicolais. An acoustic-emission characterization of the failure modes in polymer-composite materials. *Composites Science and Technology*, 58(12):1923–1928, 1998.

[GCS06] A.K. Ghosh, P. Chaudhuri, and D. Sengupta. Classification using kernel density estimates. *Technometrics*, 48(1):120–132, 2006.

[GDSK03] R. Ganesan, T.K. Das, A. Sikder, and A. Kumar. Wavelet based identification of delamination defect in chemical mechanical planarization using nonstationary acoustic emission signals. *IEEE Transactions on Semiconductor Manufacturingi*, 16(4):677–685, 2003.

[GGV+11] R. Gutkin, C.J. Green, S. Vangrattanachai, S.T. Pinho, P. Robinson, and P.T. Curtis. On acoustic emission for failure investigation in CFRP: Pattern recognition and peak frequency analyses . *Mechanical Systems and Signal Processing*, 25(4):1393–407, 2011.

[Gib11] R.F. Gibson. *Principles of Composite Material Mechanics, Third Edition.* Mechanical Engineering. Taylor & Francis, 2011.

[GO08] C.U. Grosse and M. Ohtsu. *Acoustic Emission Testing*. Springer, 2008.

[Gor07] A.N. Gorban. *Principal Manifolds for Data Visualization and Dimension Reduction*. Lecture Notes in Computational Science and Engineering. Springer, 2007.

[GP91] M.R. Gorman and W.H. Prosser. AE source orientation by plate wave analysis. *Journal of Acoustic Emission*, 9:283–288, 1991.

[GQH+14] Z. Guo, X. Qiu, G. Hou, B.Y. Liaw, and C. Zhang. State of health estimation for lithium ion batteries based on charging curves. *Journal of Power Sources*, 249:457–462, 2014.

[GT08] R.M. Gresham and G.E. Totten. *Lubrication and Maintenance of Industrial Machinery: Best Practices and Reliability*. Taylor & Francis, 2008.

[GY10] R.X. Gao and R. Yan. *Wavelets: Theory and Applications for Manufacturing*. Springer, 2010.

[Har05] H.R. Hardy. *Acoustic Emission/Microseismic Activity: Principles, Techniques and Geotechnical Applications*. Acoustic Emission, Microseismic Activity. Taylor & Francis, 2005.

[HBC+97] G. Housner, L. Bergman, T. Caughey, A. Chassiakos, R. Claus, S. Masri, R. Skelton, T. Soong, B. Spencer, and J. Yao. Structural control: Past, present, and future. *Journal of Engineering Mechanics*, 123(9):897–971, 1997.

[HC83] C.R. Heiple and S.H. Carpenter. *Acoustic Emission: Nondestructive testing monographs and tracts*, chapter Acoustic emission from dislocation motion, pages 33–54. Gordon and Breach Science Publishers, 1983.

[HCM04] L.C. Hollaway, K. Chryssanthopoulos, and S.S.J. Moy. *Advanced Polymer Composites for Structural Applications in Construction: ACIC 2004 : Proceedings of the Second International Conference, Held at the University of Surrey, Guildford, UK on 20-22 April 2004*. Woodhead Publishing Series in Civil and Structural Engineering Series. Woodhead Publishing, 2004.

[HCP87] C.R. Heiple, S.H. Carpenter, and Rockwell International. Rocky Flats Plant. *Acoustic Emission Produced by Deformation of Metals and Alloys*. Rockwell International, North American Space Operations, Rocky Flats Plant, 1987.

[HDS+13] S.E. Hamdi, A. Le Duff, L. Simon, G. Plantier, A. Sourice, and M. Feuilloy. Acoustic emission pattern recognition approach based on Hilbert Huang transform for structural health monitoring in polymer-composite materials. *Applied Acoustics*, 74(5):746–757, 2013.

[HGG+02] S. Huguet, N. Godin, R. Gaertner, L. Salmon, and D. Villard. Use of acoustic emission to identify damage modes in glass fibre reinforced polyester. *Composites Science and Technology*, 62(10):1433–1444, 2002.

[Hir12] I. Hiroshi. *New In-Situ Characterization Technique of Active Materials in Batteries*, chapter Electrochemical Acoustic Emission Method, Acoustic Emission, pages 133–150. 2012.

[HL02] C.W. Hsu and C.J. Lin. A comparison of methods for multiclass support vector machines. *IEEE Transactions on Neural Networks*, 13(2):415–425, 2002.

[HLCW11] Z. Han, H. Luo, J. Cao, and H. Wang. Acoustic emission during fatigue crack propagation in a micro-alloyed steel and welds. *Materials Science and Engineering*, 528(25-26):7751–7756, 2011.

[HMW12] A. Hase, H. Mishina, and M. Wada. Correlation between features of acoustic emission signals and mechanical wear mechanisms. *Wear*, 292:144–50, 2012.

[Hog07] J.A. Hogan. *Time-Frequency and Time-Scale Methods: Adaptive Decompositions, Uncertainty Principles, and Sampling*. Applied and Numerical Harmonic Analysis. Birkhäuser, 2007.

[HU05] K.S. Hemmert and K.D. Underwood. An analysis of the double-precision floating-point FFT on FPGAs. In *13th Annual IEEE Symposium on Field-Programmable Custom Computing Machines, 2005*, pages 171–180, April 2005.

[Hur72] P.L. Hurricks. Some aspects of the metallurgy and wear resistance of surface coatings. *Wear*, 22(3):291 – 320, 1972.

[HW05] T. Hansen and C.J. Wang. Support vector based battery state of charge estimator. *Journal of Power Sources*, 141(2):351–358, 2005.

[HZ13] W.Q. Han and J.Y. Zhou. Acoustic emission characterization methods of damage modes identification on carbon fiber twill weave laminate. *Science China Technological Sciences*, 56(9):228–237, 2013.

[HZZ+13] Z. Haifeng, L. Zhenlin, J. Zhongli, L. Hongxing, and L. Mingxiao. Application of acoustic emission and support vector machine to detect the leakage of pipeline valve. In *Fifth International Conference on Measuring Technology and Mechatronics Automation (ICMTMA), 2013, Hong Kong, China*, pages 283–286, Jan 2013.

[JCV98] J.W.W. Ju, J.L. Chaboche, and G.Z. Voyiadjis. *Damage Mechanics in Engineering Materials*. Studies in Applied Mechanics. Elsevier Science, 1998.

[JG00] M. Johnson and P. Gudmundson. Broad-band transient recording and characterization of acoustic emission events in composite laminates. *Composites Science and Technology*, 60(15):2803–2818, 2000.

[JGK+11] S.B. Johnson, T. Gormley, S. Kessler, C. Mott, A. Patterson-Hine, K. Reichard, and P. Scandura. *System Health Management: with Aerospace Applications*. Aerospace Series. Wiley, 2011.

[JMV+05] T. Jayakumar, C.K. Mukhopadhyay, S. Venugopal, S.L. Mannan, and B. Raj. A review of the application of acoustic emission techniques for monitoring forming and grinding processes. *Journal of Materials Processing Technology*, 159(1):48–61, 2005.

[Joh02] M. Johnson. Waveform based clustering and classification of ae transients in composite laminates using principal component analysis. *NDT & E International* , 35(6):367–376, 2002.

[Jol02] I.T. Jolliffe. *Principal Component Analysis*. Series in Statistics. Springer, 2002.

[Kai50] J. Kaiser. *Untersuchungen über das Auftreten von Geräuschen beim Zugversuch*. Dr.-Ing. thesis. Technische Hochschule München, 1950.

[KDA92] D.H. Kohn, P. Ducheyne, and J. Awerbuch. Acoustic emission during fatigue of Ti-6Al-4V: Incipient fatigue crack detection limits and generalized data analysis methodology. *Journal of Materials Science*, 27(12):3133–3142, 1992.

[KFO10] R. Khamedi, A. Fallahi, and A.R. Oskouei. Effect of martensite phase volume fraction on acoustic emission signals using wavelet packet analysis during tensile loading of dual phase steels. *Materials and Design*, 31:2752–2759, 2010.

[KGCT13] N. Kircheva, S. Genies, C. Chabrol, and P.X. Thivel. Evaluation of acoustic emission as a suitable tool for aging characterization of LiAl/LiMnO2 cell. *Electrochimica Acta*, 88:488–494, 2013.

[KHB01] G. Kamala, J. Hashemi, and A.A. Barhorst. Discrete-wavelet analysis of acoustic emissions during fatigue loading of carbon fiber reinforced composites. *Journal of Reinforced Plastics and Composites*, 20(3):222–238, 2001.

[KKB+09] C. Kaya, F. Kaya, E.G. Butler, A.R. Boccaccini, and K.K. Chawla. Development and characterisation of high-density fibre-reinforced oxide ceramic matrix composites with improved mechanical properties. *Journal of the European Ceramic Society*, 29(9):1631–1639, 2009.

[KKS10] E.A. Kolubaev, A.V. Kolubaev, and O.V. Sizova. Analysis of acoustic emission during sliding friction of manganese steel. *Technical Physics Letters*, 36(8):762–765, 2010.

[KL97a] N. Kambhatla and T.K. Leen. Dimension reduction by local principal component analysis. *Neural Computation*, 9(7):1493–1516, 1997.

[KL97b] S.T. Kim and Y.T. Lee. Characteristics of damage and fracture process of carbon fiber reinforced plastic under loading-unloading test by using AE method. *Materials Science and Engineering*, 234:322–326, 1997.

[KL14] K.R. Kim and Y.S. Lee. Acoustic emission source localization in plate-like structures using least-squares support vector machines with delta feature. *Journal of Mechanical Science and Technology*, 28(8):3013–3020, 2014.

[KSA+02] S.S. Kessler, S.M. Spearing, M.J. Atalla, C.E.S. Cesnik, and C. Soutis. Damage detection in composite materials using frequency response methods. *Composites Part B: Engineering*, 33(1):87–95, 2002.

[KSA14] M. Kempf, O. Skrabala, and V. Altstädt. Acoustic emission analysis for characterisation of damage mechanisms in fibre reinforced thermosetting polyurethane and epoxy. *Composites Part B: Engineering*, 56:477–483, 2014.

[KSTO97] T. Kinjo, H. Suzuki, M. Takemoto, and K. Ono. Fracture-mode classification in glass-fiber composites by acoustic emission source wave characterization and autoregressive coefficients. *Japanese Journal of Applied Physics*, 36(5):3281, 1997.

[LCY08] M. Lu, H. Cheng, and Y. Yang. A comparison of solid electrolyte interphase (SEI) on the artificial graphite anode of the aged and cycled commercial lithium ion cells. *Electrochimica Acta*, 53(9):3539 – 3546, 2008.

[Lee13] J.Y. Lee. Variable short-time fourier transform for vibration signals with transients. *Journal of Vibration and Control*, 2013.

[LHL+12] J. Li, Z. Han, H. Luo, J. Cao, and Y. Zhang. Investigations of the fatigue damage in 16mn steels by wavelet-based acoustic emission technique. In *IEEE Conference on Prognostics and System Health Management (PHM), Beijing, China*, pages 1–5, May 2012.

[LHOL11] D. Li, Q. Hu, J. Ou, and H. Li. Fatigue damage characterization of carbon fiber reinforced polymer bridge cables: Wavelet transform analysis for clustering acoustic emission data. *Science China Technological Sciences*, 54(2):379–387, 2011.

[Li02] X. Li. A brief review: acoustic emission method for tool wear monitoring during turning. *International Journal of Machine Tools and Manufacture*, 42(2):157–165, 2002.

[LJN+05] B.Y. Liaw, R.G. Jungst, G. Nagasubramanian, H.L. Case, and D.H. Doughty. Modeling capacity fade in lithium-ion cells. *Journal of Power Sources*, 140(1):157–161, 2005.

[LK09] T.H. Loutas and V. Kostopoulos. Health monitoring of carbon/carbon, woven reinforced composites. damage assessment by using advanced signal processing techniques. Part I: Acoustic emission monitoring and damage mechanisms evolution. *Composites Science and Technology*, 69(2):265–272, 2009.

[LKSK08] T.H. Loutas, J. Kalaitzoglou, G. Sotiriades, and V. Kostopoulos. A novel approach for continuous acoustic emission monitoring on rotating machinery without the use of slip ring. *Journal of Vibration and Acoustics*, 130(6):1–6, 2008.

[LTB+10] B. Legros, P.X. Thivel, Y. Bultel, M. Boinet, and R.P. Nogueira. Acoustic emission: Towards a real-time diagnosis technique for proton exchange membrane fuel cell operation. *Journal of Power Sources*, 195(24):8124–8133, 2010.

[LX01] G.R. Liu and C.Z. Xi. *Elastic Waves in Anisotropic Laminates*. Taylor & Francis, 2001.

[LY08] L. Liu and F.G. Yuan. Wireless sensors with dual-controller architecture for active diagnosis in structural health monitoring. *Smart Materials and Structures*, 17(2):025016, 2008.

[LZ98] G. Li and J. Zhang. Sphering and its properties. *The Indian Journal of Statistics, Series A*, 60:119–133, 1998.

[LZ12] Y. Long and S. Zhongqing. Application of kernel density estimation in lamb wave-based damage detection. *Mathematical Problems in Engineering*, 2012:1–24, 2012.

[Mal08] S. Mallat. *A Wavelet Tour of Signal Processing, Third Edition: The Sparse Way*. Academic Press, 3rd edition, 2008.

[Maz01] S. Mazumdar. *Composites Manufacturing: Materials, Product, and Process Engineering*. Taylor & Francis, 2001.

[MD01] D.B. Miracle, , and S.L. Donaldson. *Composites*. ASM handbook. ASM International. Handbook Committee, 2001.

[MDP11] P. Mazal, J. Dvoracek, and L. Pazdera. Application of acoustic emission method in contact damage identification. *International Journal of Materials and Product Technology*, 41(1):140–152, 2011.

[MF82] A. Misra and I. Finnie. A review of the abrasive wear of metals. *Journal of Engineering Materials and Technology*, 104(2):94–101, 1982.

[MHM05] R.K. Miller, E.K. Hill, and P.O. Moore. *Acoustic Emission Testing*. Nondestructive testing handbook. American Society for Nondestructive Testing, 2005.

[MK95] J.F. MacGregor and T. Kourti. Statistical process control of multivariate processes. *Control Engineering Practice*, 3(3):403–414, 1995.

[MMV+09] A. Molino, M. Martina, F. Vacca, G. Masera, A. Terreno, G. Pasquettaz, and G. Angelo. FPGA implementation of time-frequency analysis algorithms for laser welding monitoring. *Microprocessors and Microsystems*, 33(3):179–190, 2009.

[MNTO00] Y. Mizutani, K. Nagashima, M. Takemoto, and K. Ono. Fracture mechanism characterization of cross-ply carbon-fiber composites using acoustic emission analysis. *NDT & E International*, 33(2):101–110, 2000.

[MP99] J. Miettinen and P. Pataniitty. Acoustic emission in monitoring extremely slowly rotating rolling bearing. In *12th International Conference on Condition Monitoring and Diagnostic Engineering Management COMADEM 99, Sunderland, England*, pages 289–297. Oxford Coxmoor Publishing Company, 1999.

[MSS02] C.K. Mechefske, G. Sun, and J. Sheasby. Using acoustic emission to monitor sliding wear. *Insight*, 44(8):490–497, 2002.

[MTG08] A. Marec, J.H. Thomas, and R.E. Guerjouma. Damage characterization of polymer-based composite materials: Multivariable analysis and wavelet transform for clustering acoustic emission data. *Mechanical Systems and Signal Processing*, 22(6):1441–1464, 2008.

[MUC11] T. Matsuo, M. Uchida, and H. Cho. Development of acoustic emission clustering method to detect degradation of lithium ion batteries. *Journal of Solid Mechanics and Materials Engineering*, 5(12):678–689, 2011.

[MZ08] T.V. Muravaev and L.B. Zuev. Acoustic emission during the development of a luders band in a low-carbon steel. *Technical Physics*, 53(8):1094–1098, 2008.

[NI02] Q.Q. Ni and M. Iwamoto. Wavelet transform of acoustic emission signals in failure of model composites. *Engineering Fracture Mechanics*, 69(6):717–728, 2002.

[NL10] D. Nyman and J. Levitt. *Maintenance Planning, Coordination and Scheduling*. Industrial Press, Incorporated, 2010.

[OAH09] A.R. Oskouei, M. Ahmadi, and M. Hajikhani. Wavelet-based acoustic emission characterization of damage mechanism in composite materials under mode I delamination at different interfaces. *eXPRESS Polymer Letters*, 3(12):804–813, 2009.

[OGOP06] D. Ozevin, D.W. Greve, I.J. Oppenheim, and S.P. Pessiki. Resonant capacitive MEMS acoustic emission transducers. *Smart Materials and Structures*, 15(6):1863, 2006.

[OHAF12] A.R. Oskouei, H. Heidary, M. Ahmadi, and M. Farajpur. Unsupervised acoustic emission data clustering for the analysis of damage mecha-

nisms in glass/polyester composites. *Materials & Design*, 37:416–422, 2012.

[PBNR05] V. Pop, H.J. Bergveld, P.H.L. Notten, and P.P.L. Regtien. State-of-the-art of battery state-of-charge determination. *Measurement Science and Technology*, 16(12):93–110, 2005.

[PD01] W.V. Paepegem and J. Degrieck. Modelling strategies for fatigue damage behaviour of fibre-reinforced polymer composites. *European Journal of Mechanical Engineering*, 46(4):217–227, 2001.

[Pie89] A.D. Pierce. *Acoustics: An Introduction to Its Physical Principles and Applications*. Acoustical Society of America, 1989.

[PK01] Y.Z. Pappas and V. Kostopoulos. Toughness characterization and acoustic emission monitoring of a 2-D carbon/carbon composite. *Engineering Fracture Mechanics*, 68(14):1557–1573, 2001.

[PLAA14] A. Papazoglou, S. Longo, D. Auger, and F. Assadian. Nonlinear filtering techniques comparison for battery state estimation. *Journal of Sustainable Development of Energy, Water and Environment Systems*, 2(3):259–269, 2014.

[PLI09] A. Perez, P. Larranaga, and I. Inza. Bayesian classifiers based on kernel density estimation: Flexible classifiers. *International Journal of Approximate Reasoning*, 50(2):341–362, 2009.

[PPJ01] S. Piller, M. Perrin, and A. Jossen. Methods for state-of-charge determination and their applications. *Journal of Power Sources*, 96(1):113–120, 2001.

[Pro02] W.H. Prosser. *Nondestructive Evaluation: Theory, Techniques, and Applications*, chapter Acoustic emission, pages 367–446. Taylor & Francis, 2002.

[PWLZ14] L. Pei, T. Wang, R. Lu, and C. Zhu. Development of a voltage relaxation model for rapid open-circuit voltage prediction in lithium-ion batteries. *Journal of Power Sources*, 253:412–418, 2014.

[QBHK97] G. Qi, A. Barhorst, J. Hashemi, and G. Kamala. Discrete wavelet decomposition of acoustic emission signals from carbon-fiber-reinforced composites. *Composites Science and Technology*, 57(4):389–403, 1997.

[Rao13] A.K. Rao. Acoustic emission and signal analysis. *Defence Science Journal*, 40(1), 2013.

[RBKF12] A.H. Ranjbar, A. Banaei, A. Khoobroo, and B. Fahimi. Online estimation of state of charge in li-ion batteries using impulse response concept. *IEEE Transactions on Smart Grid*, 3(1):360–367, 2012.

[RBM+11] J. Remmlinger, M. Buchholz, M. Meiler, P. Bernreuter, and K. Dietmayer. State-of-health monitoring of lithium-ion batteries in electric

vehicles by on-board internal resistance estimation. *Journal of Power Sources*, 196(12):5357–5363, 2011.

[RBMK14] P. Romanowicz, M. Barski, A. Muc, and P. Kedziora. Structural health monitoring (shm) methods in machine design and operation. *Archive of Mechanical Engineering*, LXI(4):653–677, 2014.

[RCNR84] D.A. Rigney, L.H. Chen, M.G.S. Naylor, and A.R. Rosenfield. Wear processes in sliding systems. *Wear*, 100(1):195–219, 1984.

[Rei98] T.J. Reinhart. *Handbook of Composites*, chapter Overview of Composite Materials, pages 21–34. Springer US, 1998.

[RHWP02] P. Ramadass, B. Haran, R. White, and B.N. Popov. Performance study of commercial LiCoO2 and spinel-based Li-ion cells. *Journal of Power Sources*, 111(2):210 – 220, 2002.

[RJPR+04] C.R. Ramirez-Jimenez, N. Papadakis, N. Reynolds, T.H. Gan, P. Purnell, and M. Pharaoh. Identification of failure modes in glass/polypropylene composites by means of the primary frequency content of the acoustic emission event. *Composites Science and Technology*, 64(12):1819–1827, 2004.

[RLB+01] A.G. Ritchie, B. Lakeman, P. Burr, P. Carter, P.N. Bames, and P. Bowles. *Battery Degradation and Ageing*, chapter 5, pages 523–527. New York: Kluwer Academic Plenum Publishers, 2001.

[SAS03] V.R. Skalskyi, O.E. Andreikiv, and O.M. Serhienko. Investigation of the plastic deformation of materials by the acoustic emission method (review). *Materials Science*, 39(1):86–107, 2003.

[SB] D. Söffker and D. Baccar. Classification approach for evaluation of usage independent degradation processes of Li-O cells using Acoustic Emission, 2015, in preparation.

[SBB04] G. Sarre, P. Blanchard, and M. Broussely. Aging of lithium-ion batteries. *Journal of Power Sources*, 127(1-2):65–71, 2004.

[SBWDM00] M. Surgeon, C. Buelens, M. Wevers, and P. De Meester. Waveform based analysis techniques for the reliable acoustic emission testing of composite structures. *Journal of Acoustic Emission*, 18:63–68, 2000.

[SGR+12] A. Sibil, N. Godin, M. Rmili, E. Maillet, and G. Fantozzi. Optimization of acoustic emission data clustering by a genetic algorithm method. *Journal of Nondestructive Evaluation*, 31(2):169–180, 2012.

[SGUH12] M.G.R. Sause, A. Gribov, A.R. Unwin, and S. Horn. Pattern recognition approach to identify natural clusters of acoustic emission signals. *Pattern Recognition Letters*, 33(1):17–23, 2012.

[SH10] M.G.R. Sause and S. Horn. Simulation of acoustic emission in planar carbon fiber reinforced plastic specimens. *Journal of Nondestructive Evaluation*, 29(2):123–142, 2010.

[Shu02] P.J. Shull. *Nondestructive Evaluation: Theory, Techniques, and Applications*. Dekker Mechanical Engineering. Taylor & Francis, 2002.

[SIA09] M. Sifuzzaman, M.R. Islam, and M.Z. Ali. Application of wavelet transform and its advantages compared to fourier transform. *Journal of Physical Sciences*, 13:121–134, 2009.

[Sil86] B.W. Silverman. *Density Estimation for Statistics and Data Analysis*. Chapman & Hall/CRC Monographs on Statistics & Applied Probability. Taylor & Francis, 1986.

[SKH02] D.U Sung, C.G. Kim, and C.S. Hong. Monitoring of impact damages in composite laminates using wavelet transform. *Composites Part B: Engineering*, 33(1):35–43, 2002.

[SMHH12] M.G.R. Sause, T. Müller, A. Horoschenkoff, and S. Horn. Quantification of failure mechanisms in mode-I loading of fiber reinforced plastics utilizing acoustic emission analysis. *Composites Science and Technology*, 72(2):167–174, 2012.

[SP89] A.B. Strong and C.A. Ploskonka. *Fundamentals of Composites Manufacturing: Materials, Methods, and Applications*. Society of Manufacturing Engineers, 1989.

[SRB01] C. Scheer, W. Reimche, and F. Bach. Early fault detection at gear units by acoustic emission and wavelet analysis. *J. Acoustic Emission*, 25:331–340, 2001.

[Sta02] W.J. Staszewski. Intelligent signal processing for damage detection in composite materials. *Composites Science and Technology*, 62(7):941–950, 2002.

[SUS13] T. Stepinski, T. Uhl, and W. Staszewski. *Advanced Structural Damage Detection: From Theory to Engineering Applications*. Wiley, 2013.

[SVWR06] P. Singh, R. Vinjamuri, X. Wang, and D. Reisner. Design and implementation of a fuzzy logic-based state-of-charge meter for li-ion batteries used in portable defibrillators. *Journal of Power Sources*, 162:829–836, 2006.

[SW99] M. Surgeon and M. Wevers. Modal analysis of acoustic emission signals from CFRP laminates. *NDT & E International* , 32(6):311–322, 1999.

[SW04] W.J. Staszewski and K. Worden. *Signal Processing for Damage Detection*, chapter 21, pages 163–206. John Wiley & Sons, Ltd, 2004.

[SWWF10] J.J. Scholey, P.D. Wilcox, M.R. Wisnom, and M.I. Friswell. Quantitative experimental measurements of matrix cracking and delamination using acoustic emission. *Composites Part A: Applied Science and Manufacturing*, 41(5):612–623, 2010.

[SZNR10] A. Sansan, L. Zhen, Z. Nan, and W. Rui. Blind source separation based on principal component analysis-independent component analysis for acoustic signal during laser welding process. In *International Conference on Digital Manufacturing and Automation (ICDMA)*, volume 1, pages 336–339, December 2010.

[TA01] J.M. Tarascon and M. Armand. Issues and challenges facing rechargeable lithium batteries. *Nature*, 414(6861):359–367, 2001.

[Tan00] Y.Y. Tang. *Wavelet Theory and Its Application to Pattern Recognition*. Series in machine perception and artificial intelligence. World Scientific Publishing Company, 2000.

[Ten04] H.M. Tensi. The kaiser-effect and its scientific background. *Journal of Acoustic Emission*, 22:1–16, 2004.

[TOI+08] N. Taranu, G. Oprisan, D. Isopescu, I. Entuc, V. Munteanu, and C. Banu. Fibre reinforced polymer composites as internal and external reinforcements for building elements. *Bulletin of the Polytechnic Institute of Jassy-Constructions Architecture Section*, 55(1):7–20, 2008.

[Tsa95] A.H.C. Tsang. Condition-based maintenance: tools and decision making. *Journal of Quality in Maintenance Engineering*, 1(3):3–17, 1995.

[TSB03] P. Thori, P. Sharma, and M. Bhargava. An approach of composite materials in industrial machinery: advantages, disadvantages, and applications. *International Journal of Research in Engineering and Technology*, 2(12):350–355, 2003.

[TZA08] P. Theobald, B. Zeqeri, and J. Avison. Couplants and their influence on ae sensor sensitivty. *Journal of acoustic emission*, 26:91–97, 2008.

[Unn08] R. Unnporsson. *Acoustic Emission Monitoring of CFRP Laminated Composites Subjected to Multi-axial Cyclic Loading*. PhD thesis, University of Iceland, Iceland, 2008.

[Val02] H. Vallen. AE testing fundamentals, equipment, applications. *The e-Journal of Non-destructive Testing*, 7(9):1–7, 2002.

[VDE94] International electrotechnical vocabulary - chapter 191: Dependability and quality of service IEC 50(191):1990, 1994.

[VNW+05] J. Vetter, P. Novak, M.R. Wagner, C. Veit, K.C. Muller, J.O. Besenhard, M. Winter, M. Wohlfahrt-Mehrens, C. Vogler, and A. Hammouche. Ageing mechanisms in lithium-ion batteries. *Journal of Power Sources*, 147(1-2):269–281, 2005.

[VTFF14] S. Vergis, T.S. Turrentine, L. Fulton, and E. Fulton. Plug-in electric vehicles: A case study of seven markets. Technical report, Institute of Transportation Studies, University of California, Davis, 2014.

[WCM+03] R.B. Wright, J.P. Christophersen, C.G. Motloch, J.R. Belt, C.D. Ho, V.S. Battaglia, J.A. Barnes, T.Q. Duong, and R.A. Sutula. Power fade and capacity fade resulting from cycle-life testing of advanced technology development program lithium-ion batteries. *Journal of Power Sources*, 119(0):865–869, 2003.

[WJ94] P. Wand and C. Jones. *Kernel Smoothing*. CRC Monographs on Statistics & Applied Probability. Taylor & Francis, 1994.

[WKS+09] A. Widodo, E.Y. Kim, J.D. Son, B.S. Yang, A.C. Tan, D. Gu, B.K. Choi, and J. Mathew. Fault diagnosis of low speed bearing based on relevance vector machine and support vector machine. *Expert Systems with Applications*, 36(3):7252–7261, 2009.

[WM04] M. Wohlfahrt-Mehrens. Aging mechanisms of lithium cathode materials. *Journal of Power Sources*, 127(1-2):58–64, 2004.

[WMO+13] T. Wandowski, P. Malinowski, W. Ostachowicz, L. Tadeusz, G. Borowik, M. Rawski, and P. Tomaszewicz. Embedded signal processing subsystem for SHM. In *3rd International Conference of Engineering Against Failure: ICEAF III, Kos Island, Greece*, pages 694–702. The Federation of European Materials Societies, June 2013.

[WMS90] M. Wada, M. Mizuno, and T. Sasada. Study on friction and wear utilizing acoustic emission: Wear mode and AE spectrum of copper. *Journal of the Japan Society of Precision Engineering*, 56(8):1474–1479, 1990.

[WSP+06] K. Wojciechowski, B. Smolka, H. Palus, R.S. Kozera, W. Skarbek, and L. Noakes. *Computer Vision and Graphics: International Conference, ICCVG 2004, Warsaw, Poland, September 2004, Proceedings*. Computational Imaging and Vision. Springer, 2006.

[WZY11] X. Wang, H.P. Zhang, and X. Yan. Classification and identification of damage mechanisms in polyethylene self-reinforced laminates by acoustic emission technique. *Polymer Composites*, 32(6):945–959, 2011.

[XHPT14] Y. Xing, W. He, M. Pecht, and K.L. Tsui. State of charge estimation of lithium-ion batteries using the open-circuit voltage at various ambient temperatures. *Applied Energy*, 113:106–115, 2014.

[XHSZ13] R. Xiong, H. He, F. Sun, and K. Zhao. Evaluation on state of charge estimation of batteries with adaptive extended kalman filter by experiment approach. *IEEE Transactions on Vehicular Technology*, 62(1):108–117, 2013.

[Xil12] Xilinx. *System Generator for DSP. Getting Started Guide*, October 2012.

[XMTP11] Y. Xing, E.W.M. Ma, K.L. Tsui, and M. Pecht. Battery management systems in electric and hybrid vehicles. *Energies*, 4(11):1840–1857, 2011.

[YJK+00] D.J. Yoon, J.C. Jung, K.B. Kim, P. Park, and S.S. Lee. AE parameter analysis for fatigue crack monitoring. In *15th World Conference on Nondestructive Testing*. International Committee for Nondestructive Testing, 15-21 October 2000.

[ZG91] S.M. Ziola and M.R. Gorman. Source location in thin plates using cross-correlation. *The Journal of the Acoustical Society of America*, 90(5):2551–2556, 1991.

[ZH02] Z. Zhang and G. Hartwig. Relation of damping and fatigue damage of unidirectional fibre composites. *International Journal of Fatigue*, 24(7):713–718, 2002.

[ZMP06] L. Zykova, P. Mazal, and L. Pazdera. Identification of contact fatigue stages with acoustic emission method. In *9th European NDT Conference (ECNDT), Berlin, Deutschland*, 2006.

[ZPS12] D.A. Zakharov, S.N. Ptichkov, and V.V. Shemyakin. Acoustic emission signal attenuation in the waveguides used in underwater AE testing. In *10th European Conference on Non-Destructive Testing, Moscow 2010, June 7-11*, 2012.

[ZW08] Q. Zhang and R. E. White. Capacity fade analysis of a lithium ion cell. *Journal of Power Sources*, 179(2):793–798, 2008.

Publications

This thesis is based on the results and development steps published in the following publications and/or presented on the corresponding conferences.

Journal articles

1. D. Baccar and D. Söffker, Wear detection by means of wavelet-based acoustic emission analysis. *Mechanical Systems and Signal Processing*, 60-61:198-207, 2015.
2. D. Baccar and D. Söffker, Identification and Classification of Failure Modes in Laminated Composites by using a Multivariate Statistical Analysis of Wavelet Coefficients, *Mechanical Systems and Signal Processing,* (2015), submitted.
3. D. Söffker and D. Baccar, Classification approach for evaluation of usage independent degradation processes of Li-O cells using Acoustic Emission, in preparation for *Journal of Power Sources*.

Conference papers

1. Baccar, D.; Schiffer, S.; Söffker, D: Acoustic Emission-based Identification and Classification of Frictional Wear of Metallic Surfaces. Proc. Le Cam, Vincent and Mevel, Laurent and Schoefs, Franck. EWSHM -7th European Workshop on Structural Health Monitoring, Nantes, France, July 8-11, 2014.
2. Schiffer, S.; Rothe, S.; Baccar, D.; Söffker, D.: Classification of system's health condition using the new Adaptive Fuzzy-based Feature Classification Approach AFFCA in comparison to a macro-data-based approach. Proc. Le Cam, Vincent and Mevel, Laurent and Schoefs, Franck. EWSHM -7th European Workshop on Structural Health Monitoring, Nantes, France, July 8-11, 2014.
3. Baccar, D.; Söffker, D.: Application of acoustic emission Technique for online evaluation and classification of wear state. In: Chang, F.K. (Ed.): Structural Health Monitoring 2013, 2013, pp. 1218-1225.
4. Söffker, D.; Rothe, S.; Schiffer, S.; Aljoumaa, H.; Baccar, D.: Smart, tough, and successful: Three new innovative approaches for diagnosis and prognosis of technical systems. In: Chang, F.K. (Ed.): Structural Health Monitoring 2013, 2013, pp. 81-88.
5. Baccar, D.; Söffker, D.: Classification of wear by means of acoustic emission and signal processing techniques. In: Boller, Christian (Ed.); Deutsche Gesellschaft fuer Zerstoerungsfreie Pruefung e.V. (DGZfP), 6th European Workshop on Structural Health Monitoring - We.2.D.4, Dresden, Germany, July3-6, 2012.

6. Baccar, D.; Söffker, D.: Wavelet-based online evaluation and classification of wear state using acoustic emission. ASME 2012 Conference on Smart Materials, Adaptive Structures and Intelligent Systems, Stone Mountain, GA, USA, 2012.

7. Söffker, D.; Aljoumaa, H.; Baccar, D.; Rothe, S.: Smart, robust und einfach: Drei innovative Konzepte zur Maschinendiagnose. 9. Aachener Kolloquium für Instandhaltung, Diagnose und Anlagenüberwachung AKIDA, Aachen, 2012.

8. Baccar, D.; Dettmann, K.-U.; Söffker, D.: FPGA-based realization of online damage state and wear detection using acoustic emission. Proc. 5th ECCOMAS Thematic Conference on Smart Structures and Materials SMART'11, Saarbrücken, July 6-8, 2011, pp. 474-481.

9. Dettmann, K.-U.; Baccar, D.; Söffker, D.: Examination of wear phenomena by using filtering techniques for FDI purposes. In: Chang, F.K. (Ed.): Structural Health Monitoring 2011, 2011, pp. 1037-1044.

Student theses

In the context of the research projects at the Chair of Dynamics and Control the following student theses have been supervised by Dipl.-Ing. (FH) Dorra Baccar, M.Sc. and Univ.- Prof. Dr.-Ing. Dirk Söffker. Development steps and results of the research projects and the student theses are integrated to each other and hence are also part of this thesis.

1. Ben Nablia, S.: Schädigungsanalyse an Faserverbundwerkstoffen mittels Schallemission. Studienarbeit. University of Duisburg-Essen, Chair of Dynamics and Control (SRS), 2011.

2. Susan, G.: Moderne Energiespeicher und aktuelle Entwicklungen. Bachelor thesis. University of Duisburg-Essen, Chair of Dynamics and Control (SRS), 2012.

3. Chao, H.: Modern Motors and Generators. Bachelor thesis. University of Duisburg-Essen, Chair of Dynamics and Control (SRS), 2013.

4. Way, H.K.: Seismic Measurement Approaches used for Diagnostic and Prognostic. Bachelor thesis. University of Duisburg-Essen, Chair of Dynamics and Control (SRS), 2014.

5. Tagoe, F.: State-of-the-Art of Aging Tests on Lithium Batteries University of Duisburg-Essen, Chair of Dynamics and Control (SRS), 2014.

.

Appendix

This appendix presents all the results obtained by the examination of AE signals generated in CFRP laminates.

AE events generated in CFRP laminates generated during indentation tests

To investigate the AE signals generated in CFRP laminates, many indention tests were carried out under the same laboratory conditions. The results show that the obtained result is not restricted to the four examined AE events studied in chapter 5. The same outcomes are observed for more than 36 AE events measured during four tests. The AE events, CWT-, PCA-, and KDE- results of the 36 selected AE events are shown in the following subsections.

The following figures represent the preprocessed AE events as a function of time.

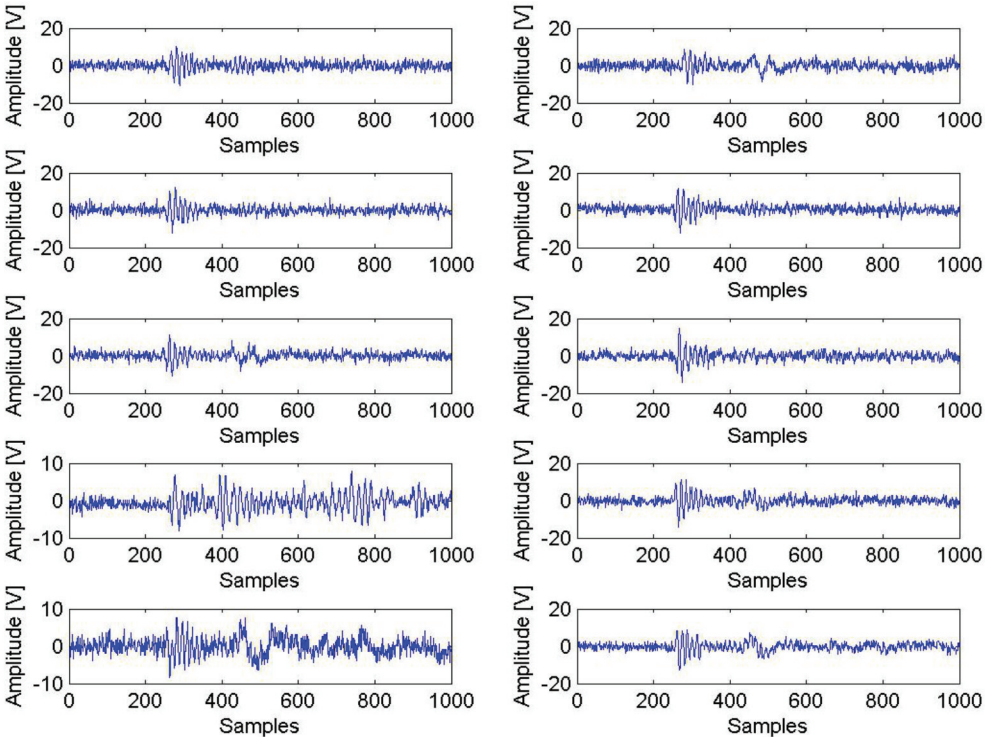

Figure A.1: Preprocessed AE events (indentation test 1)

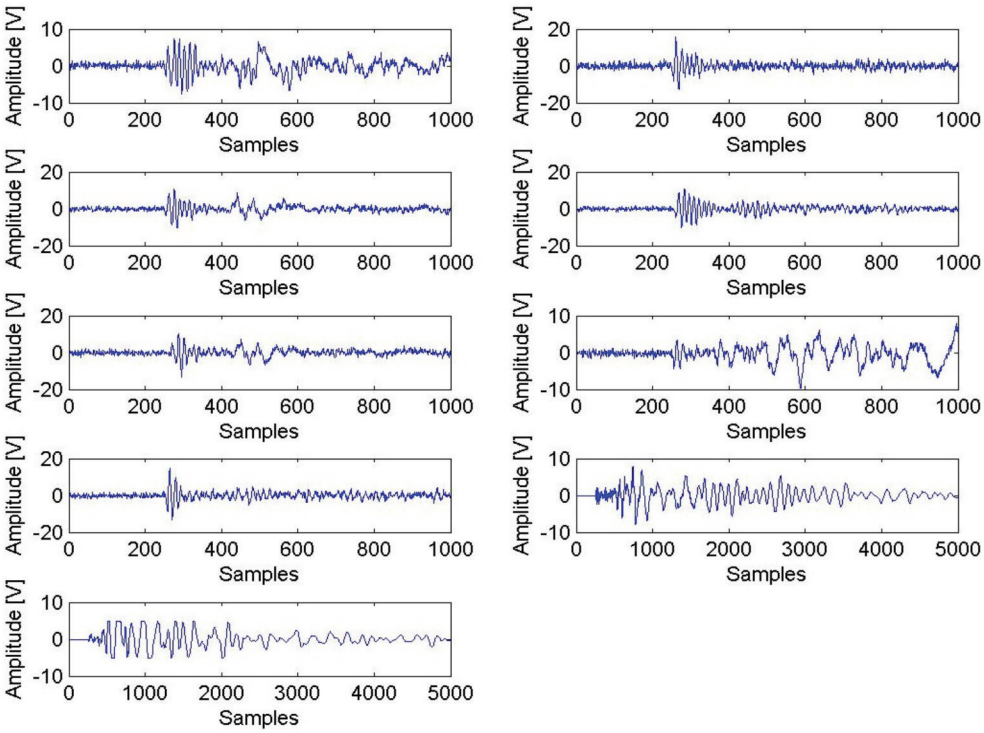

Figure A.2: Preprocessed AE events (indentation test 2)

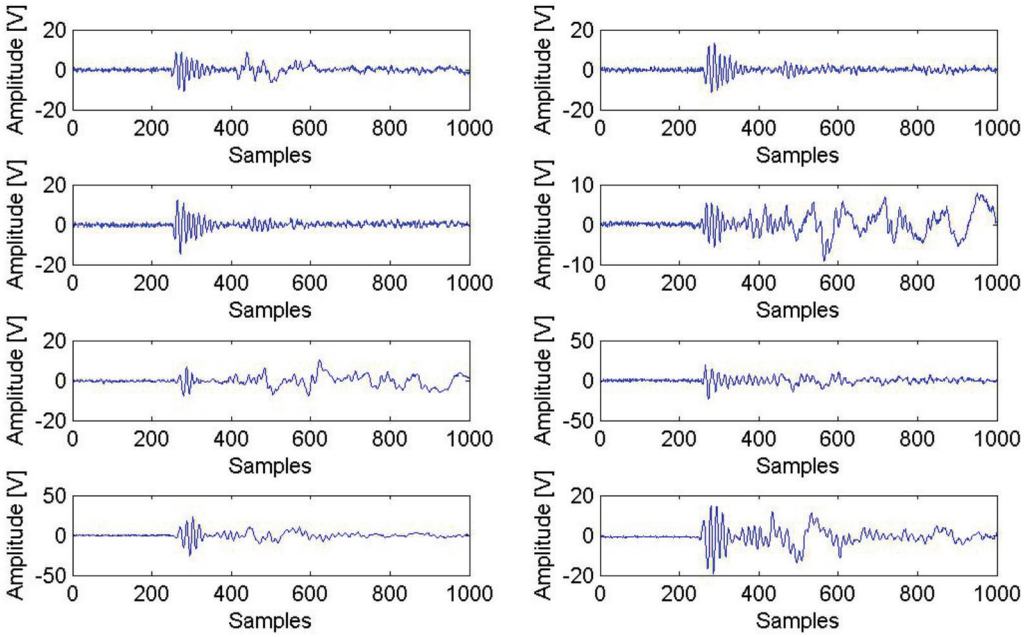

Figure A.3: Preprocessed AE events (indentation test 3)

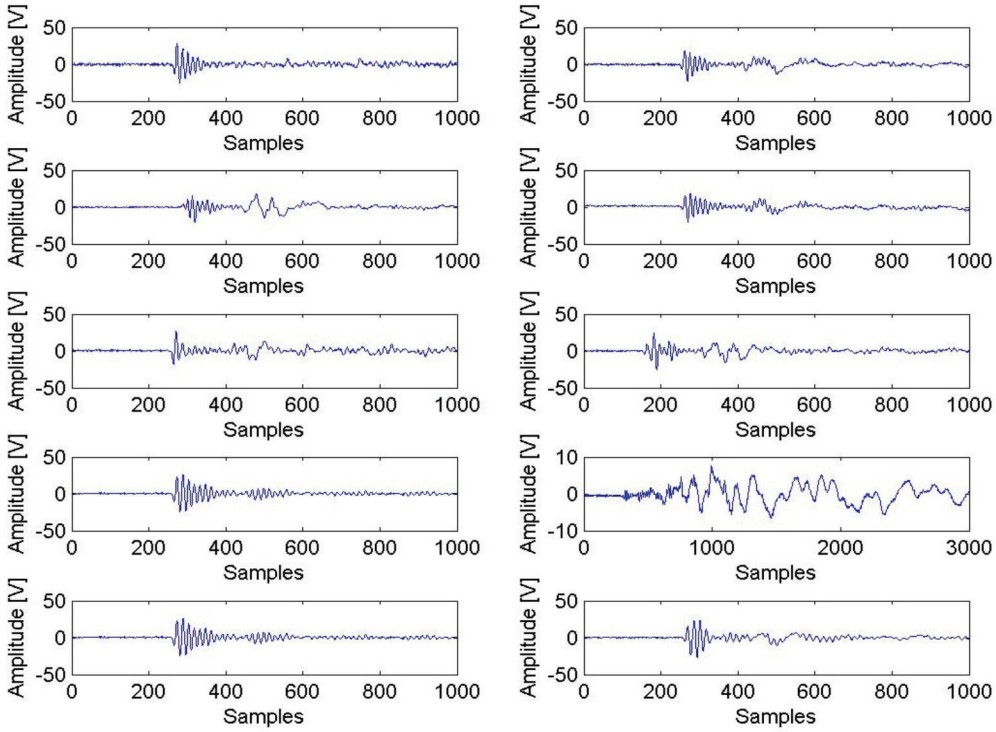

Figure A.4: Preprocessed AE events (indentation test 4)

The results show that the measured AE events are repeatable and are characterized by the same behaviors.

Continuous Wavelet Transform analysis

The following figures show the time-frequency representation of the 36 AE events.

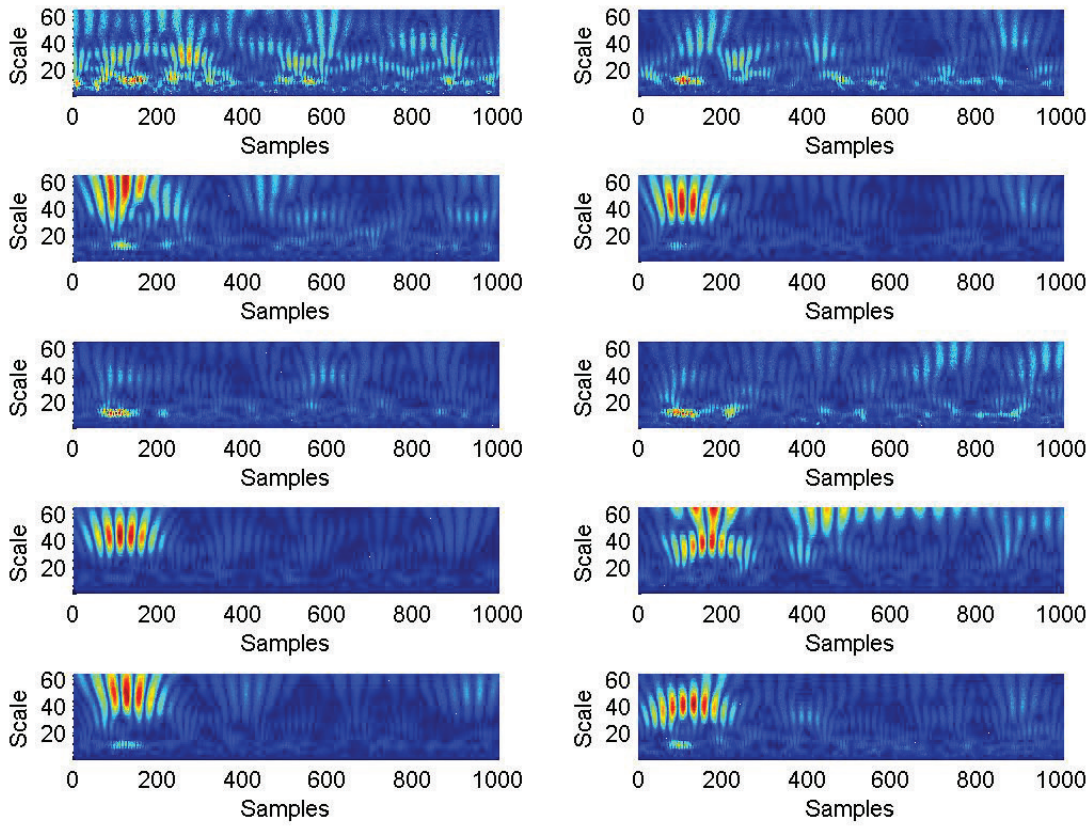

Figure A.5: Time and time-frequency representations of AE events (indentation test 1)

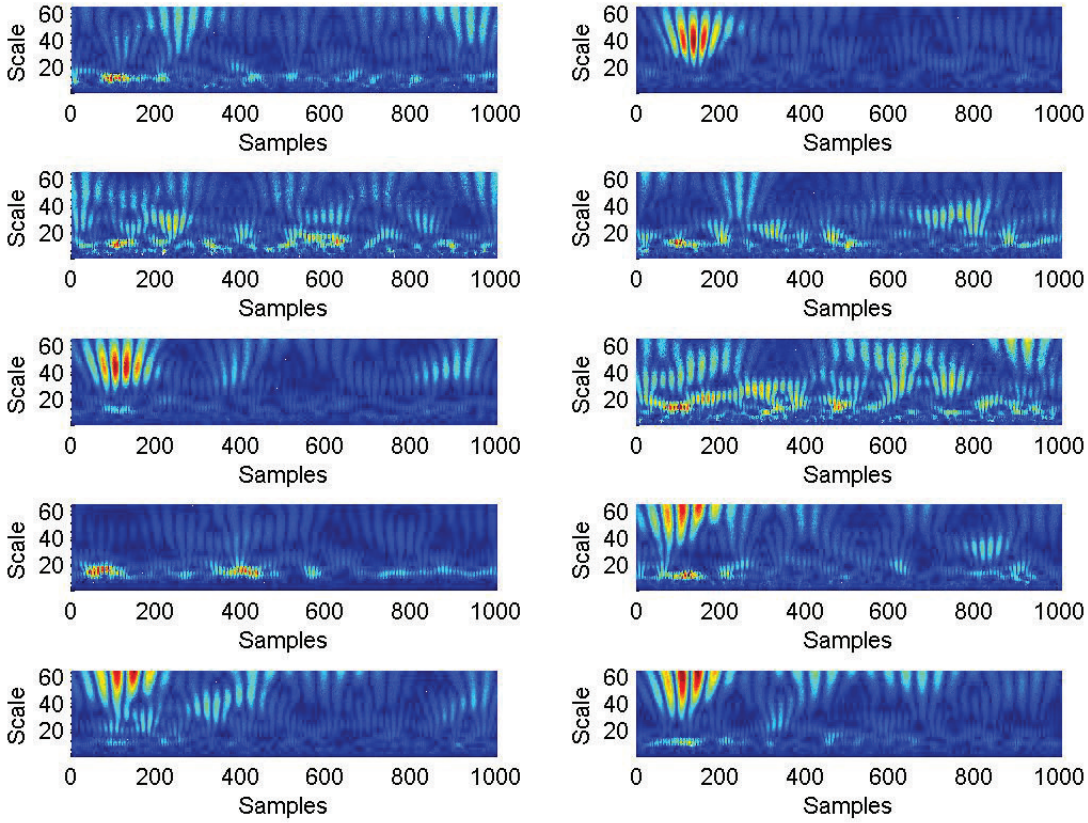

Figure A.6: Time and time-frequency representations of AE events (indentation test 2)

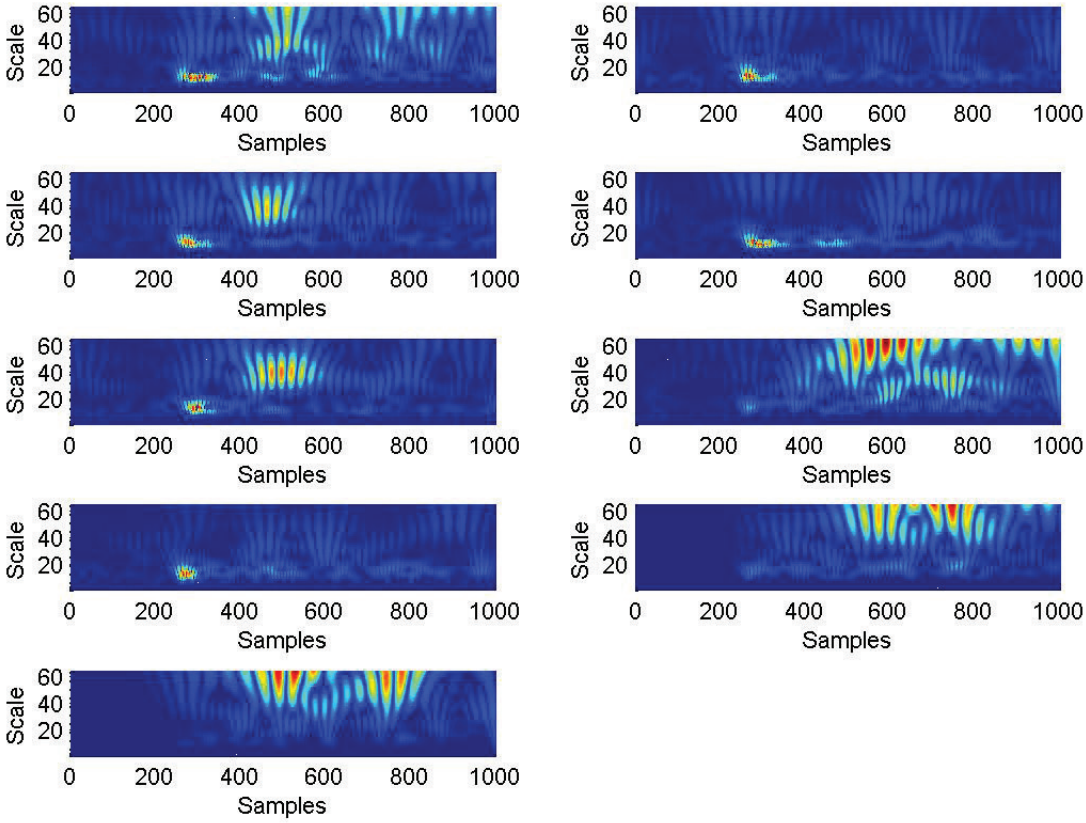

Figure A.7: Time and time-frequency representations of AE events (indentation test 3)

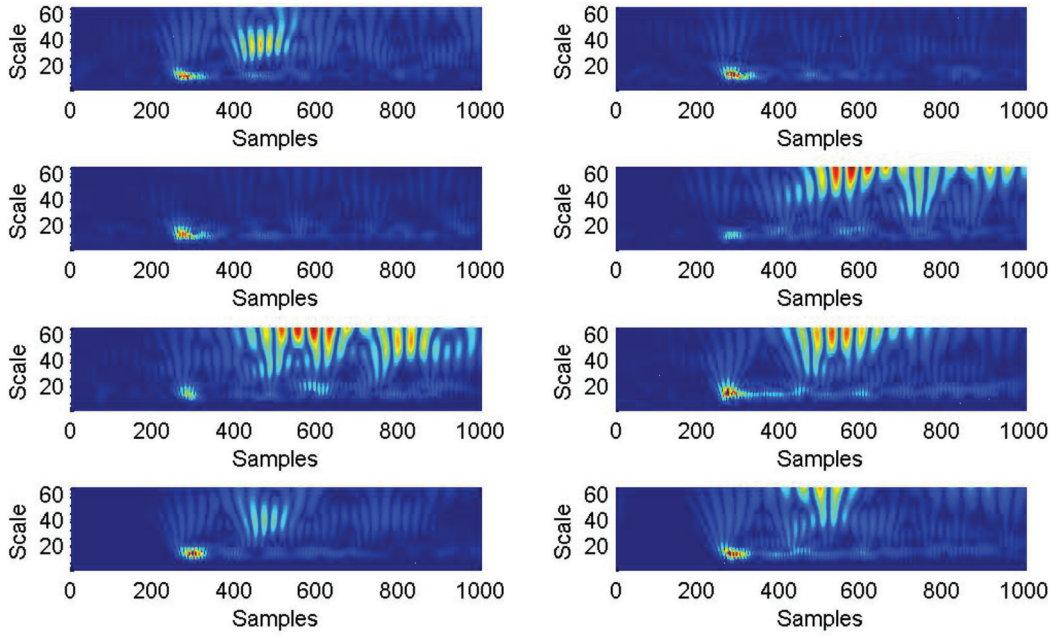

Figure A.8: Time and time-frequency representations of AE (indentation test 4)

From the CWT results it can be concluded that the frequencies of all AE events are mainly situated in four frequency ranges: >100 kHz (relatively low number of AE events), 100-150 kHz, 150-250 kHz, and 350-500 kHz (high number of AE events).

Results of Principal Component Analysis

The PCA visualization of the CWT coefficients is illustrated on the following figures. Here the PCA results are illustrated based on the frequency content of the AE events.

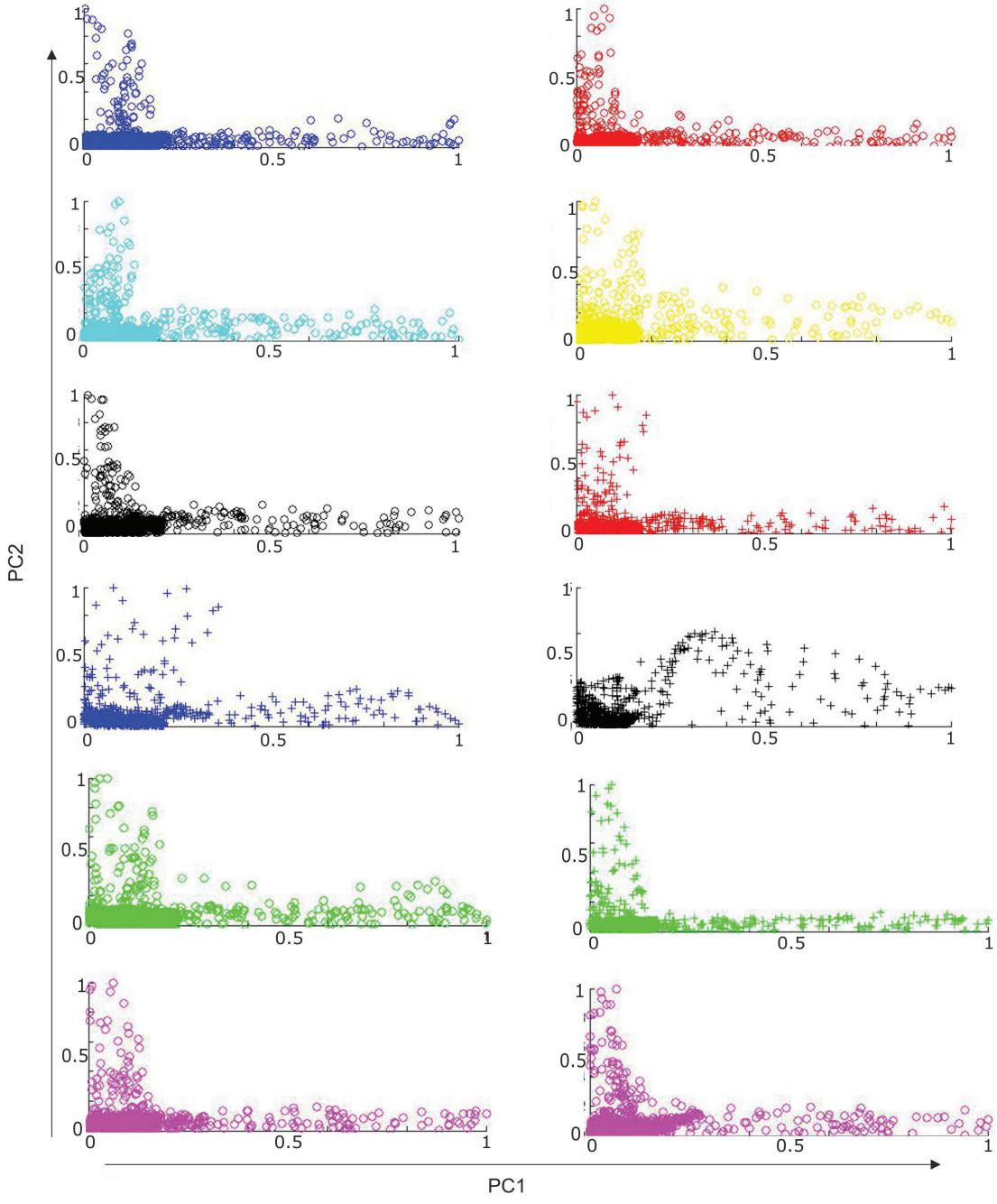

Figure A.9: PCA visualization of AE events with the frequency content in the range of 100-150 kHz

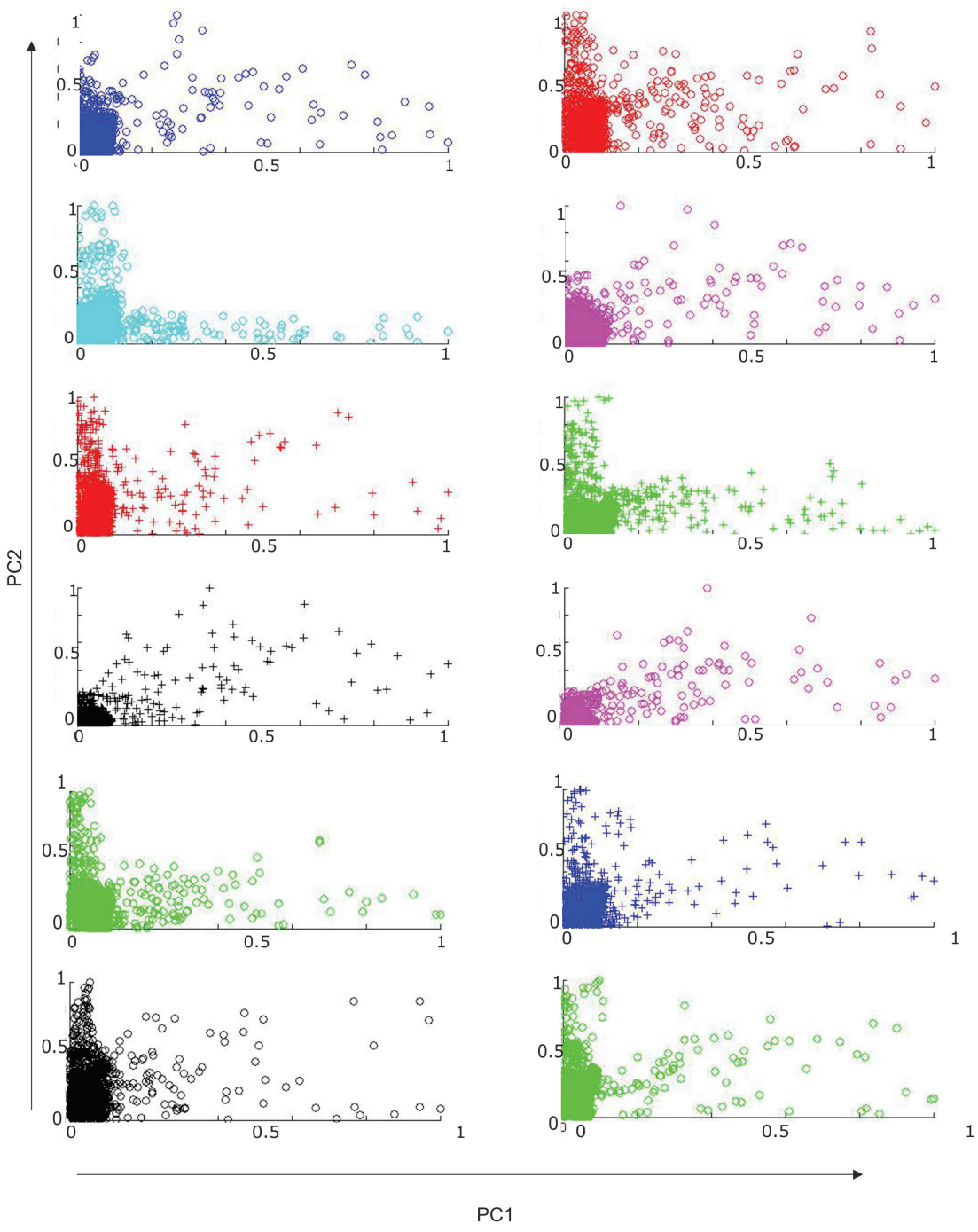

Figure A.10: PCA visualization of AE events with the frequency content in the range of 350-500 kHz

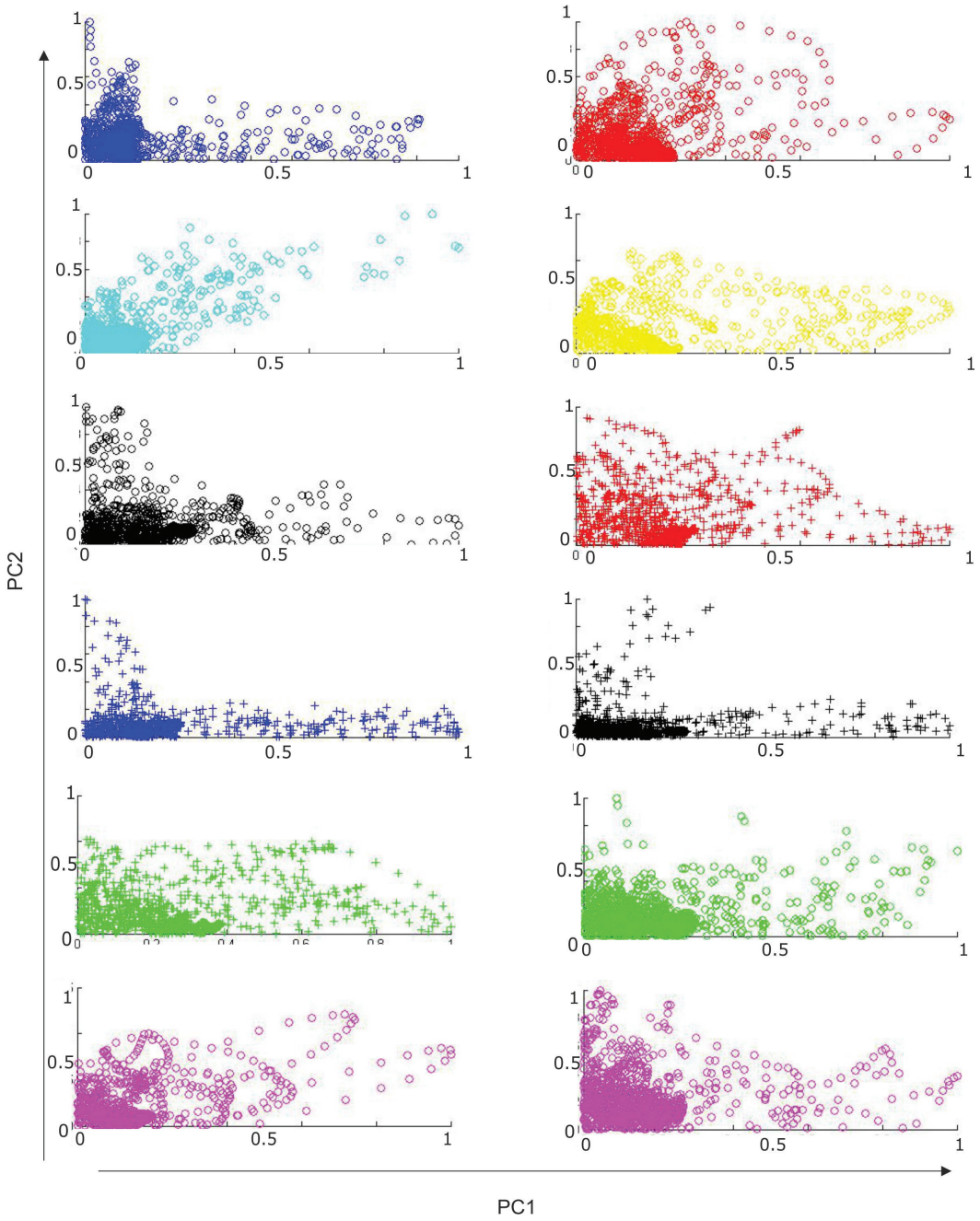

Figure A.11: PCA visualization of AE events with the frequency content in the ranges of 50-100 kHz and 150-200 kHz

The results show that AE events containing the same frequency contents are characterized by the same PCA distribution.

Result of Kernel Density Estimation

The KDE results of the first and second component of the 36 AE events are shown in the following figures.

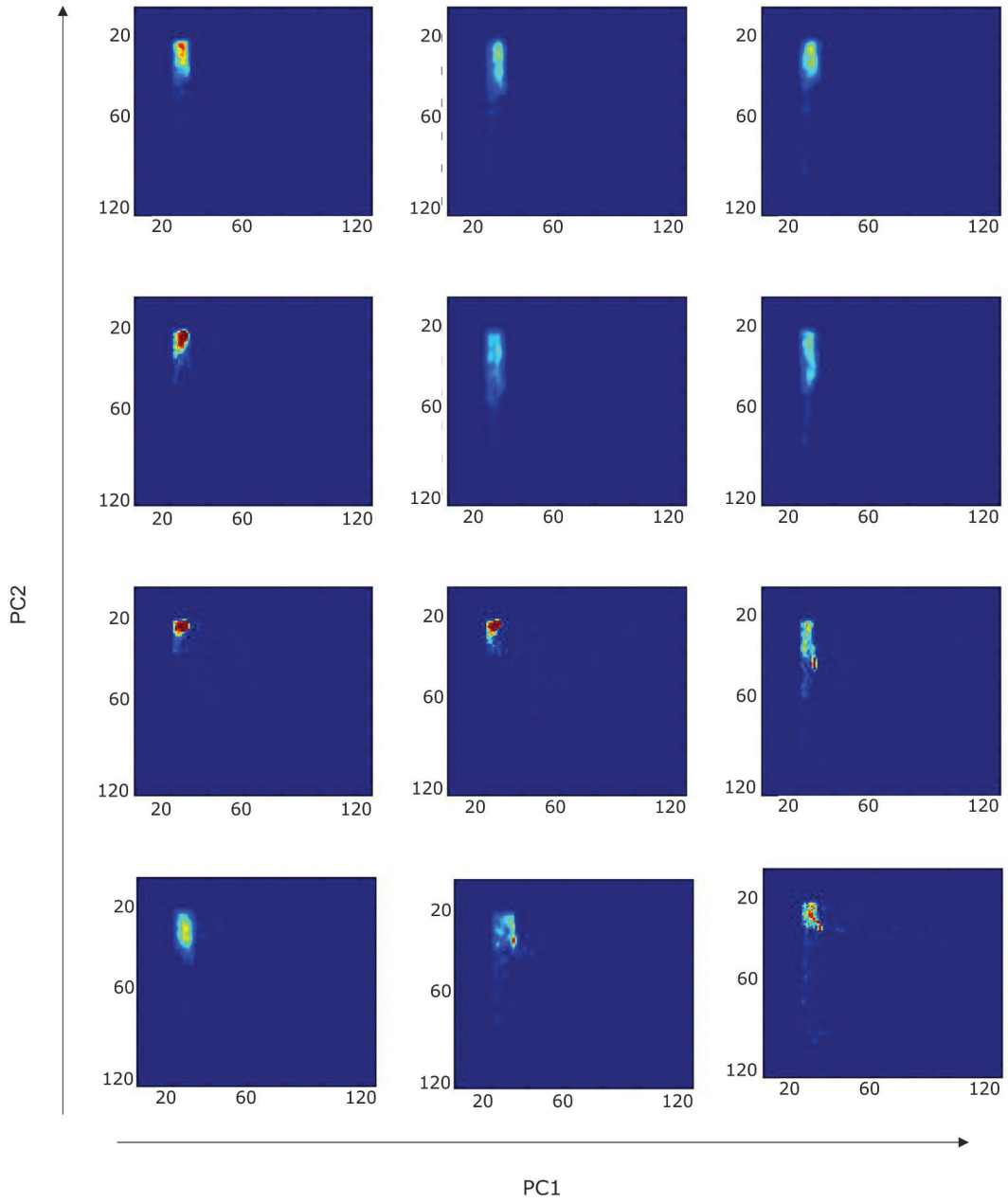

Figure A.12: Kernel density estimation of AE events with the frequency content in the range of 100-150 kHz

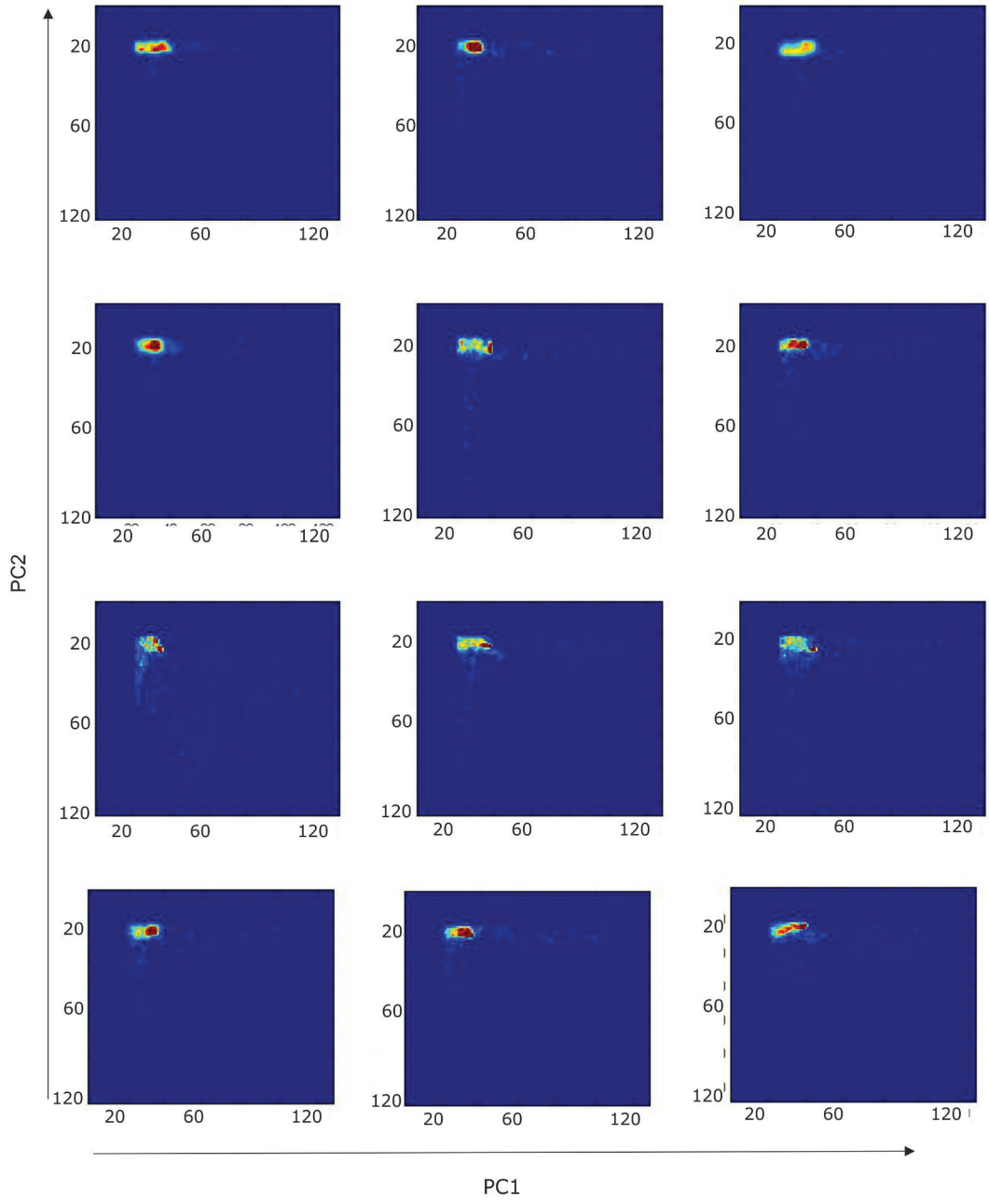

Figure A.13: Kernel density estimation of AE events with the frequency content in the range of 350-500 kHz

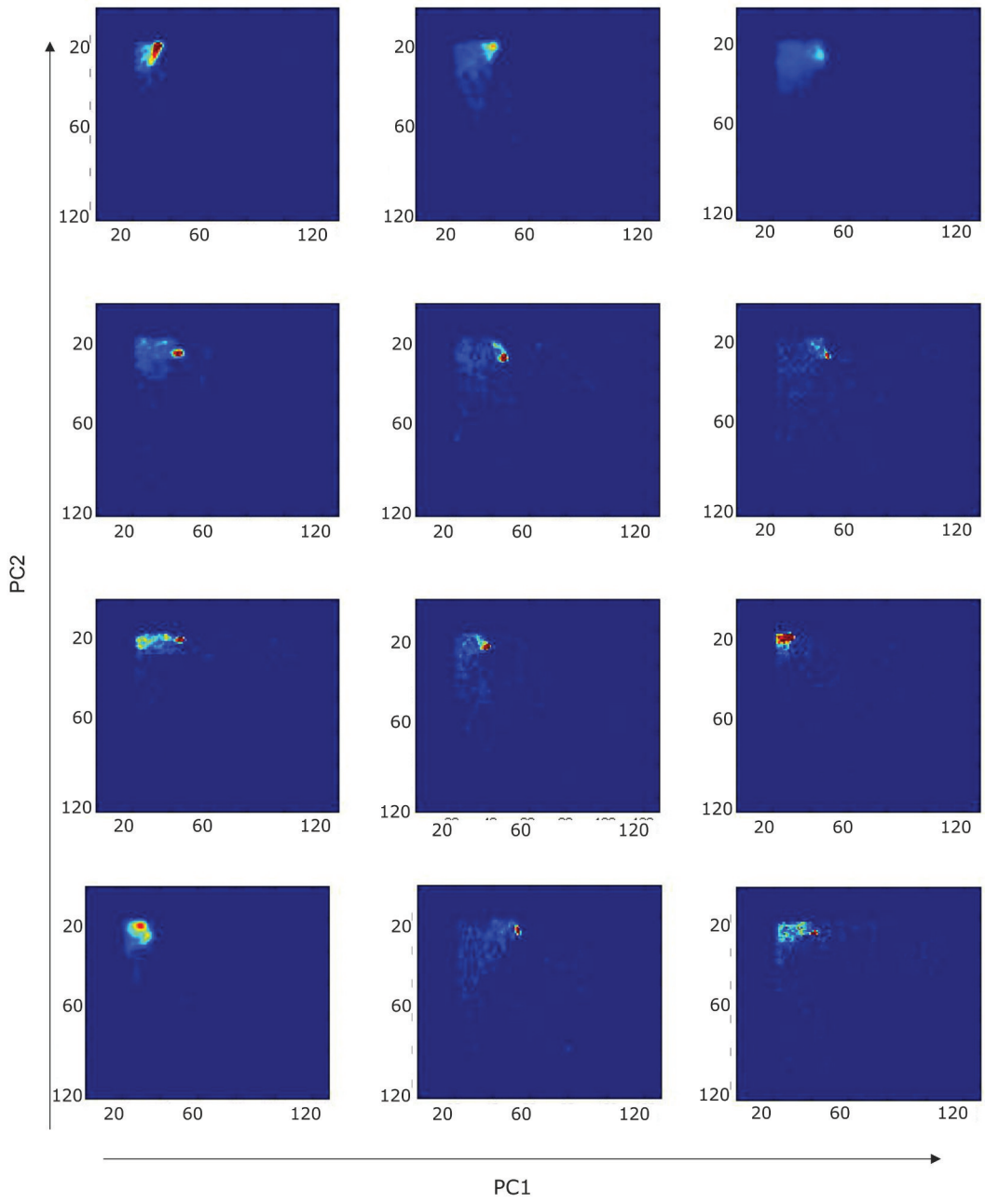

Figure A.14: PCA visualization of AE events with the frequency content in the ranges of 50-100 kHz and 150-200 kHz